1985

VLSI IMPLEMENTATON OF RESIDUE NUMBER SYSTEM ARCHITECTURES.

MAGDY ABD EL-AZIZ. BAYOUMI
University of Windsor

CANADIAN THESES ON MICROFICHE

I.S.B.N.

THESES CANADIENNES SUR MICROFICHE

National Library of Canada
Collections Development Branch

Canadian Theses on
Microfiche Service

Ottawa, Canada
K1A 0N4

Bibliothèque nationale du Canada
Direction du développement des collections

Service des thèses canadiennes
sur microfiche

NOTICE

The quality of this microfiche is heavily dependent upon the quality of the original thesis submitted for microfilming. Every effort has been made to ensure the highest quality of reproduction possible.

If pages are missing, contact the university which granted the degree.

Some pages may have indistinct print especially if the original pages were typed with a poor typewriter ribbon or if the university sent us a poor photocopy.

Previously copyrighted materials (journal articles, published tests, etc.) are not filmed.

Reproduction in full or in part of this film is governed by the Canadian Copyright Act, R.S.C. 1970, c. C-30. Please read the authorization forms which accompany this thesis.

AVIS

La qualité de cette microfiche dépend grandement de la qualité de la thèse soumise au microfilmage. Nous avons tout fait pour assurer une qualité supérieure de reproduction.

S'il manque des pages, veuillez communiquer avec l'université qui a conféré le grade.

La qualité d'impression de certaines pages peut laisser à désirer, surtout si les pages originales ont été dactylographiées à l'aide d'un ruban usé ou si l'université nous a fait parvenir une photocopie de mauvaise qualité.

Les documents qui font déjà l'objet d'un droit d'auteur (articles de revue, examens publiés, etc.) ne sont pas microfilmés.

La reproduction, même partielle, de ce microfilm est soumise à la Loi canadienne sur le droit d'auteur, SRC 1970, c. C-30. Veuillez prendre connaissance des formules d'autorisation qui accompagnent cette thèse.

THIS DISSERTATION
HAS BEEN MICROFILMED
EXACTLY AS RECEIVED

LA THÈSE A ÉTÉ
MICROFILMÉE TELLE QUE
NOUS L'AVONS REÇUE

NL-339 (r. 82/08)

Canada

I. ADDUCTS OF METHYLATED ARSINES WITH BORON TRIHALIDES AND SILICON TETRAFLUORIDE WITH AMMONIA

II. METHYL AND PHENYLSELENO DERIVATIVES OF SILICON, GERMANIUM AND TIN

by

Jaafar M. Chehayber

A Dissertation
submitted to the Faculty of Graduate Studies through
the Department of Chemistry in Partial Fulfillment
of the requirements for the degree of
Doctor of Philosophy at
The University of Windsor

Windsor, Ontario, Canada

1984

Dedicated to the memories of my father and brother.

ABSTRACT

Nine adducts of the type $Me_nAsH_{3-n}.BX_3$ and several mixed halide derivatives of the general formulae $Me_nAsH_{3-n}.BX_2Y$ and $Me_nAsH_{3-n}.BXYZ$ (n=1,2,3; X,Y,Z = Cl,Br,I) have been prepared. Their i.r. and Raman spectra have been recorded and normal coordinate analysis utilized as a confirmation of the vibrational assignments of $MeAsH_2$ and Me_2AsH adducts. The crystal structures of the three $Me_3As.BX_3$ (x = Cl,Br,I) adducts have been determined and a comparison drawn with many conclusions based on the vibrational analysis. The molecules are shown to possess an As-B coordinate bond and to have C_{3v} symmetry with staggered conformation. The ^1H and ^{11}B chemical shifts have been recorded and used to indicate relative acidity and basicity of the acceptor and donor species.

The synthesis and characterization of some selenium ligands of the type Me_3MCH_2SeR where M = Si,Ge,Sn; R = Me,Ph, are reported. I.r., Raman, ^1H and ^{13}C n.m.r. spectra are employed to characterize these ligands. Selected reactions of these compounds with Na_2PdCl_4, and K_2PtCl_4 have produced a series of new coloured Pd(II) and Pt(II) complexes. The crystal structure of dichloro-bis (methyl trimethylsilylmethyl selenide) palladium (II), $(Me_3SiCH_2SeMe)_2PdCl_2$, shows the molecule to be square

planar with the ligands in the trans arrangement at palladium bonded by selenium.

Ab initio molecular orbital calculations were performed on axial-, equatorial-, and square pyramidal $SiF_4.NH_3$ and also on cis- and trans-$SiF_4.2NH_3$ complexes. The electronic structures of these five isomers were determined and their relative stabilities discussed.

TABLE OF CONTENTS

ACKNOWLEDGEMENTS v

ABSTRACT vi

LIST OF TABLES xi

LIST OF FIGURES xiv

LIST OF ABBREVIATIONS xvii

PART ONE

GENERAL INTRODUCTION

CHAPTER

I. EXPERIMENTAL TECHNIQUES 2

I.1 The Vacuum Line 3
I.2 The Starting Materials 8
1.3 Instrumental Techniques 12

II. VIBRATIONAL SPECTROSCOPY AND NORMAL COORDINATE ANALYSIS 16

II.1 Vibrational Spectroscopy 17
II.2 Normal Coordinate Analysis 19
References - Part One 26

PART TWO

A SPECTROSCOPIC AND CRYSTALLOGRAPHIC INVESTIGATION OF METHYLATED ARSINE ADDUCTS WITH BORON TRIHALIDES

INTRODUCTION 30
PREPARATION 32
PHYSICAL PROPERTIES 36
^{1}H N.M.R. SPECTROSCOPY 38

III. VIBRATIONAL AND NORMAL COORDINATE ANALYSIS OF $MeAsH_2.BX_3$ (X=Cl,Br,I) 46

III.1 The Methylarsine Frequencies . . . 47
III.2 The AsB Donor-Acceptor Frequency . 50

III.3 The BX_3 Frequencies. 50
III.4 Normal Coordinate Analysis 59

IV. VIBRATIONAL AND NORMAL COORDINATE ANALYSIS OF $Me_2AsH.BX_3$ (X=Cl,Br,I). 65

IV.1 The Dimethylarsine Frequencies. . . . 66
IV.2 The As-B Stretching Frequency 68
IV.3 The BX_3 Frequencies 68
IV.4 Normal Coordinate Analysis. 77

V. A ^{11}B N.M.R. SPECTROSCOPIC INVESTIGATION OF Me_nAsH_{3-n} ADDUCTS OF BORON TRIHALIDES (n=1,2,3). 82

V.1 Introduction. 83
V.2 Experimental. 86
V.3 Results and Discussion. 87

VI. THE CRYSTAL STRUCTURES OF $Me_3As.BX_3$ ADDUCTS (X=Cl,Br,I). 95

VI.1 Introduction. 96
VI.2 Experimental. 96
VI.3 Discussion. 104
References - Part Two 107

PART THREE

SYNTHESIS, CHARACTERIZATION AND SELECTED REACTIONS OF SELENIUM-GROUP IV LIGANDS

VII. SYNTHESIS, CHARACTERIZATION AND SELECTED REACTIONS OF SELENIUM-GROUP IV LIGANDS 115

VII.1 Introduction 116
VII.2 Preparation. 118
VII.3 Characterization 119
VII.4 Preparation of some Pd (II) and Pt (II) Complexes 141
VII.5 Crystal Structure of $(Me_3SiCH_2SeMe)_2PdCl_2$. 143
References - Part Three 155

PART FOUR

AB INITIO STUDIES OF COMPLEXES BETWEEN SiF_4 AND NH_3

VIII. AB INITIO STUDIES OF COMPLEXES BETWEEN SiF_4 AND NH_3 161

VIII.1 Molecular orbital Calculations. 162
VIII.2 Introduction 163
VIII.3 Calculations and Results 165
VIII.4 Discussion 166
References - Part Four 178

VITA AUCTORIS 180

LIST OF TABLES

Table		Page
I.1	Low-temperature baths (±5°C)	5
(a)	Melting points (°C) of $Me_nAsH_{3-n}.BX_3$ (n=1,2,3,; X=Cl,Br,I)	37
(b)	^1H n.m.r. chemical shifts for $Me_nAsH_{3-n}.BX_3$ (n=1,2,3; X=Cl,Br,I).	42
III.1	The approximate description and symmetry species of the fundamental vibrations of $MeAsH_2.BX_3$ (X=Cl,Br,I).	55
III.2	Observed I.R. and Raman frequencies (cm^{-1}), ± 3 cm^{-1} for $MeAsH_2.BCl_3$ with potential energy distributions	56
III.3	Observed I.R. and Raman frequencies (cm^{-1}), ± 3 cm^{-1} for $MeAsH_2.BBr_3$ with potential energy distributions.	57
III.4	Observed I.R. and Raman frequencies (cm^{-1}), ± 3 cm^{-1} for $MeAsH_2.BI_3$ with potential energy distributions.	58
III.5	Modified Urey-Bradley force fields of $MeAsH_2.BX_3$.	62
III.6	Geometric parameters of $MeAsH_2.BX_3$.	63
IV.1	The approximate description and symmetry species of the fundamental vibrations of $Me_2AsH.BX_3$ (X=Cl,Br,I).	73
IV.2	Observed I.R. and Raman frequencies (cm^{-1}), ± 3 cm^{-1}, for $Me_2AsH.BCl_3$ with potential energy distributions.	74
IV.3	Observed I.R. and Raman frequencies (cm^{-1}), ± 3 cm^{-1}, for $Me_2AsH.BBr_3$ with potential energy distributions.	75
IV.4	Observed I.R. and Raman frequencies (cm^{-1}), ± 3 cm^{-1}, for $Me_2AsH.BI_3$ with potential energy distributions.	76

Table		Page
IV.5	Modified Urey-Bradley force fields of $Me_2AsH.BX_3$.	79
IV.6	Geometric parameters of $Me_2AsH.BX_3$. . . .	80
V.1	^{11}B chemical shifts of unmixed and mixed boron halides adducts of Me_nAsH_{3-n} (n = 1,2,3)	88
VI.1	Crystallographic and refinement data. . .	99
VI.2	Final fractional coordinates and thermal parameters of non-hydrogen atoms of $Me_3As.BX_3$ (X=Cl,Br,I)	100
VI.3	Bond lengths (Å) and angles (°)	101
VII.1	The vibrational spectra and the tentative assignments of the series Me_3MCH_2SeMe (M=Si,Ge,Sn).	126
VII.2	The vibrational spectra and the tentative assignments of the series Me_3MCH_2SePh (M=Si,Ge,Sn).	134
VII.3	^1H n.m.r. chemical shifts of Me_3MCH_2X (X=H,Cl,I, SeMe, SePh; M = Si,Ge,Sn) . .	136
VII.4	The ^{13}C chemical shifts of Me_3MCH_2X and Me_3MCH_2SePh; X=Cl,I; M=Si,Ge,Sn.	138
VII.5	Pd(II) and Pt(II) complexes of Me_3MCH_2SeR	142
VII.6	Crystallographic Data	145
VII.7	Final fractional coordinates and isotropic thermal parameters for non-hydrogen atoms of $(Me_3SiCH_2SeMe)_2PdCl_2$ with standard deviations in parentheses	146
VII.8	Final fractional coordinates and thermal parameters for hydrogen atoms of $(Me_3SiCH_2SeMe)_2PdCl_2$.	147
VII.9	Bond lengths (Å) and angles (°) for $(Me_3SiCH_2SeMe)_2PdCl_2$ with standard deviations in parentheses	148

Table		Page
VIII.1	Calculated total energy, dissociation energy, charge distributions, charge transfer, and dipole moment of $SiF_4.nNH_3$, n = 1,2.	168

LIST OF FIGURES

Figure		Page
I.1	The vacuum line.	4
I.2	Reaction and storage vessels	7
(a)	The AsH stretching modes of $MeAsH_2.BCl_3$ (ca 2254 cm^{-1}) in the Raman spectrum at different times from preparation	39
(b)	Selected regions of the i.r. spectra of the volatile materials above $MeAsH_2.BCl_3$(A) and $MeAsH_2.BBr_3$(B)	40
(c)	^1H n.m.r. spectrum of $Me_2AsH.BI_3$	44
(d)	^1H n.m.r. spectrum of $MeAsH_2.BBr_3$.	45
III.1	Far i.r. spectra of $MeAsH_2.BCl_3$ (A), $MeAsH_2.BBr_3$(B) and $MeAsH_2.BI_3$ (C).	51
III.2	Selected regions of the solid Raman spectrum of $MeAsH_2.BCl_3$	52
III.3	Selected regions of the solid Raman spectrum of $MeAsH_2.BBr_3$	53
III.4	Selected regions of the solid Raman spectrum of $MeAsH_2.BI_3$.	54
IV.1	Far i.r. spectra of $Me_2AsH.BCl_3$ (A), $Me_2AsH.BBr_3$ (B), and $Me_2AsH.BI_3$ (C).	69
IV.2	Selected regions of the solid Raman spectrum of $Me_2AsH.BCl_3$	70
IV.3	Selected regions of the solid Raman spectrum of $Me_2AsH.BBr_3$	71
IV.4	Selected regions of the solid Raman spectrum of $Me_2AsH.BI_3$.	72
V.1	Changes in ^{11}B chemical shifts across the series BCl_nBr_{3-n} and BBr_nI_{3-n} (n=1,2,3) for the $MeAsH_2$, Me_2AsH, and Me_3As adducts and free boron halides	89

Figure		Page
V.2	The ^{11}B n.m.r. spectrum of $MeAsH_2/BCl_3/BBr_3$ system.	91
V.3	The ^{11}B n.m.r. spectrum of $Me_2AsH/BBr_3/BI_3$ system	92
V.4	The ^{11}B n.m.r. spectrum of $Me_3As/BCl_3/BI_3$ system	93
V.5	The ^{11}B n.m.r. spectrum of $Me_3As/BCl_3/BBr_3/BI_3$ system.	94
VI.1	Unit cell packing of $Me_3As.BCl_3$ and $Me_3As.BBr_3$	102
VI.2	Unit cell packing of $Me_3As.BI_3$	103
VII.1	The i.r. spectrum of Me_3SiCH_2SeMe.	120
VII.2	The i.r. spectrum of Me_3GeCH_2SeMe.	121
VII.3	The i.r. spectrum of Me_3SnCH_2SeMe.	122
VII.4	The Raman spectrum of Me_3SiCH_2SeMe	123
VII.5	The Raman spectrum of Me_3GeCH_2SeMe	124
VII.6	The Raman spectrum of Me_3SnCH_2SeMe	125
VII.7	The i.r. spectrum of Me_3SiCH_2SePh.	128
VII.8	The i.r. spectrum of Me_3GeCH_2SePh.	129
VII.9	The i.r. spectrum of Me_3SnCH_2SePh.	130
VII.10	The Raman spectrum of Me_3SiCH_2SePh	131
VII.11	The Raman spectrum of Me_3GeCH_2SePh	132
VII.12	The Raman spectrum of Me_3SnCH_2SePh	133
VII.13	The ^1H n.m.r. spectrum of Me_3GeCH_2SeMe (A), and Me_3GeCH_2SePh (B)	139
VII.14	The ^{13}C n.m.r. spectrum of Me_3SiCH_2SePh with $CDCl_3$ as an external standard	140

Figure		Page
VII.15	View of $(Me_3SiCH_2SeMe)_2PdCl_2$. Unlabeled atoms are related to labeled one by the Pd center of inversion	149
VII.16	Contents of one unit cell of $(Me_3SiCH_2SeMe)_2PdCl_2$. The cell shown extends along a, b and c from -1/4 to 3/4. H atoms are not included for clarity	150
VIII.1	Schematic view of SiF_4 and NH_3 adducts with structural parameters	167

LIST OF ABBREVIATIONS

Å	angstrom
(a)	asymmetric
br	broad
ca	about
cm	centimetre
cm^{-1}	wave number
def	deformation
dp	depolarized
Et	ethyl
Hz	Hertz
i.r.	infrared
L	litre
m	medium
mdyn	millidyne
Me	methyl
MHz	Megahertz
mL	millilitre
mm	millimetre
mmole	millimole
n.m.r.	nuclear magnetic resonance
o.d.	outside diameter
p	polarized
Ph	phenyl
ppm	parts per million
rad	radian
(s)	symmetric
sh	shoulder
str	stretch
s,vs	strong, very strong
TMS	tetramethylsilane
w	weak

PART ONE

GENERAL INTRODUCTION

CHAPTER I

EXPERIMENTAL TECHNIQUES

I.1 The Vacuum Line

The general principles of vacuum line techniques are discussed in detail in several books.[1-3] Air or moisture sensitive compounds are handled most conveniently on the vacuum line provided that they are sufficiently volatile. A nitrogen-filled glove bag was used to complement the usage of the line.

The vacuum line used in this work (Figure I.1) was built from Pyrex glass and consists of one major and three minor manifolds M1, M2 and M3 (volume ca 100 mL each). All manifolds are similar, with M1 and M2 being used more frequently and are connected by a series of four U-traps. M3 is on the other side of the rack and mostly used for overnight pumping. The major manifold M is connected to the pumping system and to the minor manifolds via Teflon-Viton stopcocks (ACE Glass Inc., Vineland, N.J.). M1 and M2 were equipped with simple manometers. A Pirani gauge was used to monitor the vacuum in the system and its head connected at PG to the major manifold. The pumping system consisted of a mechanical rotary pump (Edwards High vacuum, Crawley, U.K.) and a glass mercury diffusion pump (D) with two liquid nitrogen backing traps T. Removal of the cold traps and switching the pump "on" or "off" was undertaken by the manipulations of the high-vacuum silicone-greased stopcocks (1,2,3).

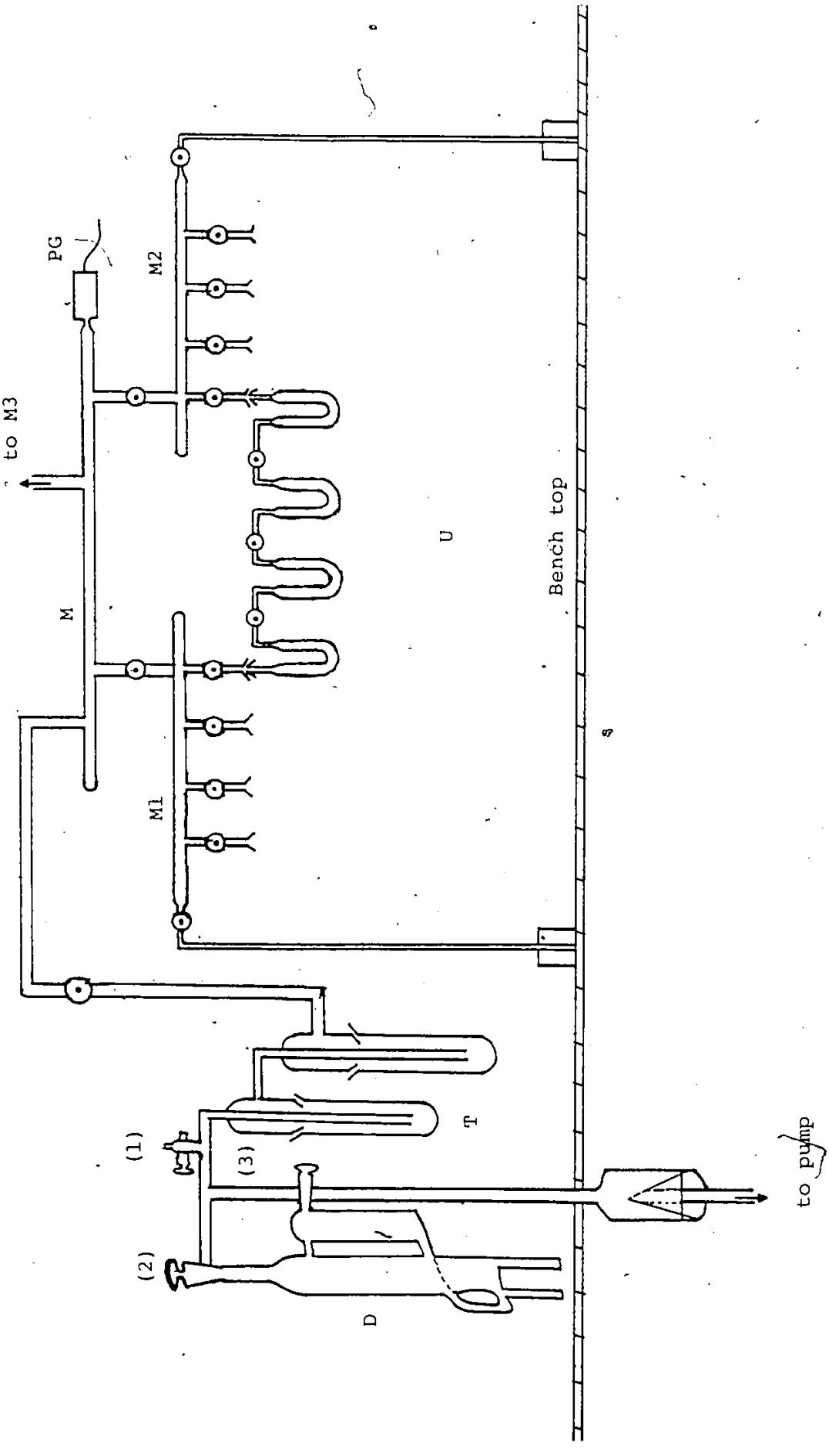

Fig. I.1. The vacuum line.

I.1.1 Separation of Volatile Materials

Low-temperature slush baths were used to effect separation of volatile materials. Table I.1 contains those baths frequently used along with their temperatures. These baths were prepared by mixing the material with a refrigerant such as dry ice or liquid nitrogen. The efficiency of separation is dependent on the surface area of the trap, the quantity of sample, and the relative vapour pressures of the constituents making up the mixture. When low volatility liquids or non-condensable gases were involved, the system was opened to the pump.

Table I.1 Low-temperature baths (±5°C)

Material	Temperature (°C)
Ice/water	0
Ice/salt water	0 to -12
Carbon tetrachloride	-23
Chlorobenzene	-45
Chloroform	-63
Dry ice/acetone	-78
Toluene	-96
1-bromobutane	-112
Methyl cyclohexane	-126
n-pentane	-132
Iso-pentane	-160
Liquid N_2	-196

I.1.2 Storage and Reaction Vessels

Stability, volatility and quantity of compounds in question dictated the shapes of the storage and reaction vessels. They were constructed of Pyrex glass and all were fitted with Teflon-Viton stopcocks except in those few cases where a greased ground glass stopcock was more practical (e.g., tube breakers). The following description of these vessels and their schematic drawings (Fig. I.2) are intended to clarify their usage and shapes.

A. Storage vessel for gases ($MeAsH_2$, Me_2AsH) fitted with a Teflon-Viton stopcock and a MS19 ball joint (volume 1L).

B. Used to store dry solvents (benzene, ether, THF), to be used on the line, fitted as A (volume 100-200 mL).

C. Used for selenium reactions, equipped with a septum inlet, fitted as A (volume 100 mL).

D. Reaction vessel with two or three necks, equipped with a dropping funnel and used for the preparations of $MeAsH_2$ and Me_2AsH (volume 250-500 mL).

E. Storage vessel used mainly to store BCl_3 and BBr_3, fitted as A (volume 25 mL).

F. Same as E except for the graduation. Used to store compounds with low volatility. Knowing the density of the stored compound, it is easy to calculate the number of moles transferred into a reaction vessel.

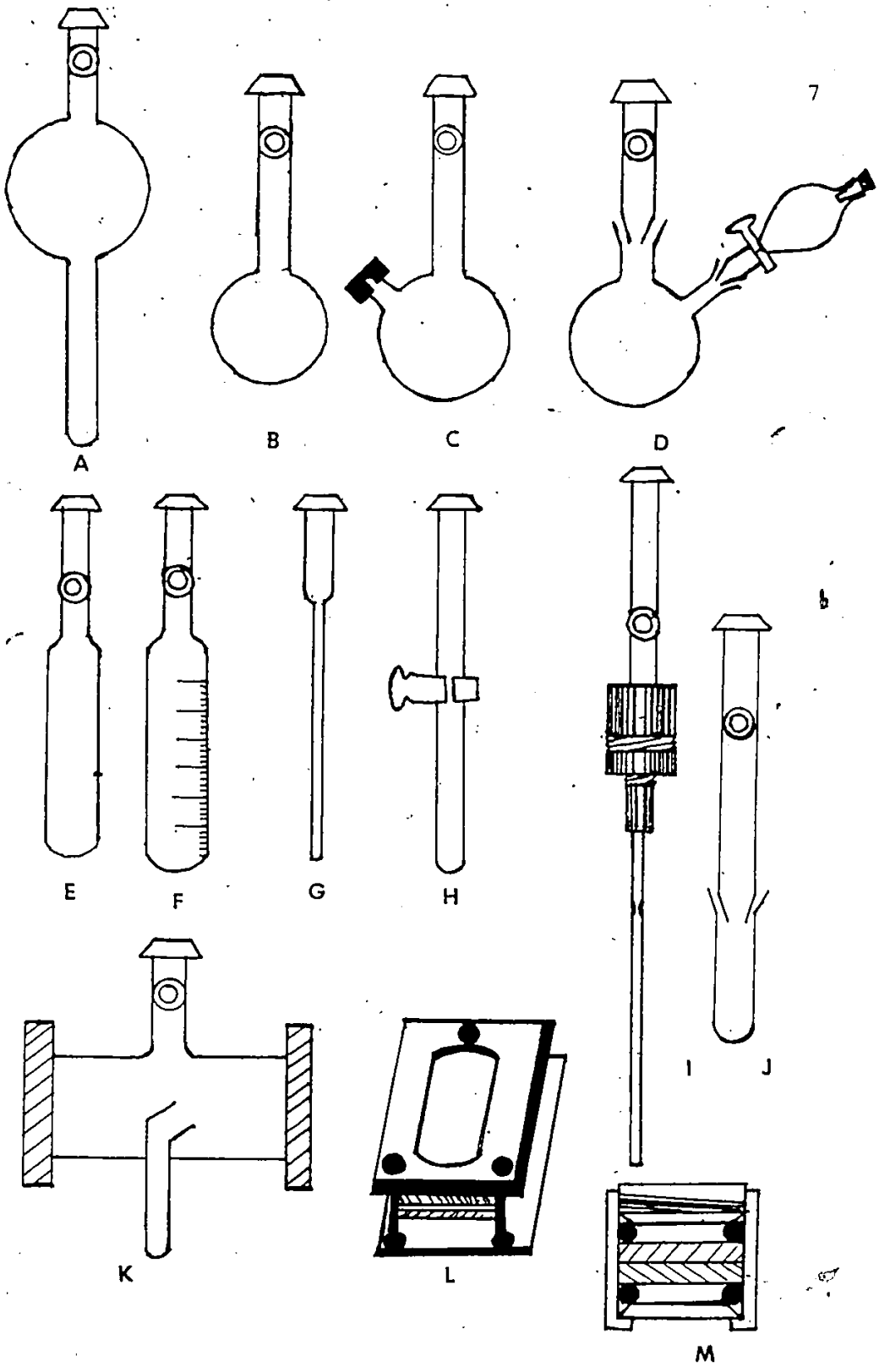

Fig. I.2. Reaction and storage vessels.

G. Hand-drawn semimicro tube, used to collect samples for ^{1}H n.m.r. and Raman analysis, fitted with a MS19 ball joint.

H. Tube breaker, equipped with a greased ground-glass stopcock. Ideal for recovering samples already sealed in the semimicro tubes described above, fitted as G.

I. N.m.r. vacuum connector (Kontes Scientific Glassware/ Instruments, Vineland, N.J.) one end connects to 10 mm o.d. tubing, the other end connects to n.m.r. tubes or to 5 mm Pyrex tubes for Raman studies, fitted as A.

J. Used to prepare samples of methylated arsine adducts to be transferred to the dry box where a pellet or a mull is prepared. It has a detachable 14/23 ground joint and fitted as A.

K. I.r. gas cell with KBr windows fitted as A.

L. I.r. solution cell with polyethylene plates used to record far i.r. spectra in nujol.

M. Air-tight holder with CsI plates and O-rings used to record i.r. spectra of heavy liquids.

I.2 The Starting Materials

The compounds listed under this title were either commercially available with suppliers listed at the end, or were prepared by known synthetic methods. Purity was checked by ^{1}H n.m.r., i.r., Raman spectroscopy or by a combination of the above.

Boron tribromide: BBr_3[a]; stored in an E-type vessel and degassed at -78°C prior to use. Purity checked by i.r. and Raman.[4]

Boron trichloride: BCl_3[b]; stored in an E-type vessel and degassed at -112°C prior to use. Purity checked by i.r.[5]

Boron triiodide: BI_3[a]; stored in a tightly capped jar under refrigeration, handled in the nitrogen-filled glove bag and used as a solution in benzene. A trace of mercury was added to eliminate free iodine. i.r.[4]

Chloromethyl(trimethyl)germane: Me_3GeCH_2Cl; stored in a F-type vessel and prepared by chlorination of tetramethyl germane.[6] The product was distilled into a trap held at -78°C. Purity was checked by b.p.[6] and i.r.[7]

Chloromethyl(trimethyl)silane: Me_3SiCH_2Cl[c]; stored in a F-type vessel and used as supplied. Purity checked by i.r.[7] and ^1H n.m.r.[8]

Chloro(trimethyl)stannane: Me_3SnCl[a]; used as supplied. Purity checked by i.r.[9] and ^1H n.m.r.[10]

Cupric acetate monohydrate: $Cu(C_2H_3O_2)_2.H_2O$[d]; used as supplied.

Dimethylarsine: Me_2AsH; prepared in vessel D by the reduction[11] of sodium dimethylarsonate with zinc dust and HCl and stored in vessel A. Purity checked by i.r. and ^1H n.m.r.[12]

Iodomethyl(trimethyl)stannane: Me_3SnCH_2I; stored in vessel F and prepared by the reaction of methylene iodide and a zinc-copper couple followed by addition of chloro(trimethyl)stannane.[13] The collected mixture was distilled on the vacuum line into traps held at 0°C, -63°C and -196°C. The portion at -63°C was kept and the rest discarded. This portion was purified further by successive trap to trap distillation. Purity checked by refractive index and ^1H n.m.r.[13]

Methylarsine: $MeAsH_2$; stored in an A-type vessel and prepared in vessel D by the reduction of sodium methylarsonate with zinc dust and HCl[14]. The volatile products were collected in traps held at -45°C, -95°C and -196°C. $MeAsH_2$ condensed in the -196°C trap and later purified by successive trap to trap distillation to remove last traces of water and ethanol. Purity checked by i.r. and Raman.[15]

Methyllithium: $MeLi^a$; used as supplied in an ethereal solution and stored in the refrigerator in the original container.

Methylene iodide: $CH_2I_2^a$; used as supplied and kept in the dark when not in use. Purity checked by ^1H n.m.r., i.r.[16,17] and Raman.[18]

Phenyllithium: $C_6H_5Li^a$; used as supplied in benzene-ether or cyclohexane solutions and stored in the refrigerator in the original containter.

Selenium: Se_8[e]; used as supplied.

Sodium dimethylarsonate: $Me_2As(O)ONa.3H_2O$[d,e]; stored and used as supplied.

Sodium methylarsonate: $MeAs(ONa)_2.6H_2O$[a]; stored and used as supplied.

Sodium tetrachloropalladate (II): Na_2PdCl_4[a]; kindly donated by Dr. W. J. Holland.

Potassium tetrachloroplatinate (II): K_2PtCl_4; kindly donated by Dr. D. W. Stephan.

Tetramethylsilane: Me_4Si[f]; stored in vessel A, n.m.r. grade.

Tetramethylgermane: Me_4Ge[c]; stored in an E-type vessel and purity checked by ^1H n.m.r.[19]

Trimethylarsine: Me_3As[g,h]; stored in E-type vessel and purity verified by i.r.[20] and ^1H n.m.r.[21]

Zinc: Zn[d]; used as dust in the synthesis of methylated arsines and also as granular 20 mesh to prepare the Zn/Cu couple.

Solvents: methyl iodide[i], carbon tetrachloride[j], methylene chloride[i], deuterated methylene chloride[k] were of spectral grade. Diethyl ether and THF were dried by distillation over $LiAlH_4$[a]. Benzene was dried by distilling slowly until the distillate was no longer cloudy and then stored over sodium wire.

Commercial Suppliers

a. Alfa Division, Ventron Corp., Beverley, Mass.
b. Matheson Gas Products, East Rutherford, N.J.
c. Laramie Chemical Co., Laramie, Wy.
d. Fisher Scientific Co., Fairlawn, N.J.
e. The British Drug Houses Ltd., Poole, Dorset, Eng.
f. J. T. Baker Chemical Co., Phillipsburg, N.J.
g. Organometallics Inc., East Hampstead, N.H.
h. Strem Chemicals, Newburyport, Ma.
i. Aldrich Chemical Co., Milwaukee, Wisc.
j. NMR Specialties Inc., New Kensington, Pa.
k. Stohler Isotope Chemicals, Montreal, P.Q.

I.3 Instrumental Techniques

a. N.m.r. Spectroscopy

Three different instruments were used for n.m.r. studies. A Varian EM-360 permanent magnet instrument operating at 60 MHz was used for fast routine checks. A more sophisticated Bruker WP80 spectrometer operating at 80 MHz was also used. The ^{11}B and ^{13}C n.m.r. spectra were recorded on a Bruker CPX100 multinuclear pulsed Fourier transform spectrometer operating at 28.88 and 22.63 MHz respectively. Samples were either neat or in a deuterated solvent sealed in hand-drawn semi-microtubes or in 5 mm n.m.r. tubes (Wilmad Glass Co., Buena, N.J.). Semi-micro tubes could then be placed in 5 mm n.m.r. tubes and surrounded by 10% solution of TMS/CCl_4. This solution kept the semi-micro tubes in a vertical position while spinning and acted as an external standard. Boron trifluoride etherate $Et_2O.BF_3$ was used as an external reference for the ^{11}B n.m.r. spectra. TMS was used as an external reference

for all ^{1}H n.m.r. spectra. For ^{13}C n.m.r. spectra, deuterochloroform $CDCl_3$ was used as a deuterium lock signal and external standard. The instrument's data processing system then corrected all chemical shifts to the TMS scale.

b. I.r. Spectroscopy

Almost all mid- and far-i.r. spectra were recorded on a Perkin-Elmer 180 spectrometer, operating with an Interdata Model 6/16 computer. Some routine mid-i.r. scans were recorded on a Beckman IR-12 spectrometer operating from 200 cm^{-1} to 4000 cm^{-1}. Calibration was effected against known bands of polystyrene. Solid samples were run as KBr or CsI pellets, and/or mulls of Nujol between polyethylene plates (Fig. I.2.L). Liquid samples were run as a thin film between CsI plates in an air-tight device (Fig. I.2.M). The cell depicted in Fig. I.2.k was used for gas samples (pressure 5-10 cm Hg, path length 9 cm). The KBr windows were polished by cesium oxide powder/ethanol on silk, then attached to the main body of the cell using a thin even layer of Apiezon A40 wax while continually pumping on the vacuum line.

c. Raman Spectroscopy

Two spectrometers were used, a Spex and a Spectra-physics 700. Both were equipped with an argon ion laser and model 265 exciter. The strongest exciting line at

488.0 nm (20492 cm^{-1}) was employed. Spectra were usually run at a slit width of 8 cm^{-1} and a power of 300-600 mw. Periodical calibration was checked using liquid CCl_4. Samples were sealed as solids, liquids or in solutions under vacuum in thin-walled glass tubing (2-5 mm o.d. and 5-10 cm long). First, the tube was aligned in the sample compartment by eye, then a strong peak was found and the pen stopped at the maximum. By using fine controls to adjust the sample in three directions, the signal was optimized. Spectra were then obtained with the polarizer-analyzer in the parallel position. Without changing any control and on the same chart, with the polarizer in the perpendicular position, the polarized spectra were obtained.

d. X-Ray Crystallography

Data were collected on a Syntex $P2_1$ four-cycle automated diffractometer operating in conjunction with a Nova 1200 computer. The diffractometer was equipped with a molybdenum tube and a highly oriented graphite monochromator (λ = 0.71069Å, $2\theta_m$ = 12.2°) operating at 50 kV and 20 mA. The crystals were either sealed in capillary tubes or mounted on glass fibers depending on their air and moisture sensitivities.

A random orientation photograph was taken with $2\theta = \omega = \chi = 0°$ and the ϕ axis rotating at 234°/min. 7-10 reflections from the x, y film were used for a center-

ing reflection program. Assuming $\omega = 0$, the program looks for a particular reflection by calculating 2θ and χ. The refined values of 2θ, χ and ω were used in the autoindexing program, thus producing a list of axial vectors with angles between them. Standard symmetry rules took over then to select the unit cell dimensions and axial photographs were taken to check mirror symmetry. Rough data were then collected when $15° < 2\theta < 25°$ from which ca 15 well separated reflections were chosen to give the final cell dimensions and the orientation matrix for data collection. Solution and refinement of structures, and programs used will be discussed later in this manuscript.

CHAPTER II

VIBRATIONAL SPECTROSCOPY AND NORMAL COORDINATE ANALYSIS

II.1 Vibrational Spectroscopy

I.r. and Raman spectroscopy have been widely used for the study of molecular vibrations of inorganic and organometallic compounds. I.r. spectroscopy was developed and used much earlier than Raman spectroscopy, but now they are frequently used in conjunction to explain and assign molecular vibrations. A molecular vibration that results in a change in dipole moment or polarizability gives rise to activity in the i.r. or Raman effect respectively. This difference leads to differences in relative intensities and in certain cases normal modes may be active in the i.r. and inactive in the Raman or vice versa. The wide use and understanding of these techniques have been furthered by some well written books and many reviews on the subject. Herzberg,[22] Woodward,[23,24], Wilson, Decius and Cross[25] are just a few names worth mentioning.

The molecules studied in this thesis belong to the C_s point group which produces a' and a" vibrational modes which are active in both effects. To help identify the totally symmetric modes, the polarized (perpendicular) spectrum is also recorded and appears below the normal (parallel) spectrum. The terms "perpendicular" and "parallel" denote the alignment of the polarizer-analyzer in front of the collimator. The bands which are reduced by more than 6/7 in intensity are called polarized bands The totally symmetric modes a' in the point group normally

appear as polarized bands while the asymmetric a" modes appear as depolarized bands in the Raman spectrum.

Theoretically, since all vibrational modes are allowed, 3N-6 (N = number of atoms) fundamentals should be observed. In practice, the number of observed bands is different from that of those expected. Therefore, the first obstacle is to identify the fundamentals in the spectra, considering degeneracies arising from local symmetry (such as the C_{3v} symmetry of the CH_3 group). In fact, there is no guarantee that each fundamental corresponds to a band even if the numbers are the same. Additional bands often indicate the presence of impurities. However, even with pure and stable samples, it is common to be left with unassigned bands. These excess bands may be the result of overtones ($2\nu_j$), combination or difference bands ($\nu_j + \nu_k$ or $\nu_j - \nu_k$) and Fermi resonance. The latter involves a situation where an overtone or combination having the same symmetry and frequency as a fundamental are mixed together giving two new modes with different frequencies.[25,26] Higher forms of combination could also exist but are not expected to be observed under the experimental conditions used in this work. However, binary combinations are common especially in the i.r. spectra although they appear with low intensity. The opposite of the above could also happen. When fewer bands than expected are observed this could be the result

of the inactivity of some bands or the non-appearance of allowed bands because of low intensity. In the C_s point group, inactivity can be ruled out since all bands are i.r. and Raman active. The use of both the i.r. and Raman spectra usually solves any problem arising from low intensities because a vibration is unlikely to have a low intensity in both spectra. Band overlapping and accidental degeneracies may also contribute to a lessening in the number of observed bands. The combination of several of the above can lead to a misinterpretation of the data especially more so if only one compound rather than a series is studied. When a series of related compounds are investigated, many of the obscurities and much of the guess work can be eliminated. In this work, there was no attempt to assign overtones or combination bands since it was not found helpful or necessary in assigning fundamentals.

II.2 Normal Coordinate Analysis

Normal coordinate analysis (NCA) is a method for explaining molecular vibrations in terms of individual motions of each atom in the molecule which can be described by convenient mathematical terms. Classical texts[22,23,25] contain the full accounts of the well developed method. Normal coordinates are calculated by equation (II.1) derived by Hencher.[27]

$$[Y]^t[D]^t[F][D][Y] = [\Lambda] \qquad \text{(II.1)}$$

t denotes the matrix transpose and the matrices are defined as follows:

[Y]: is a transformation matrix from mass-weighted Cartesian coordinates [η] to normal coordinates (Q] such that

$$[\eta] = [Y][Q] \qquad \text{(II.2)}$$

The elements of [η] have the form $m_i^{1/2}X_i$ where m is the mass and X_i is the displacement from the equilibrium position.

[D]: is a transformation matrix from internal coordinates [S] to mass-weighted Cartesian coordinates such that

$$[S] = [D][\eta] \qquad \text{(II.3)}$$

The [D] matrix can be calculated from molecular geometry.[25]

[F]: is the potential energy coefficient (force constants) matrix, defined by equation (II.4):

$$2V = \sum_{i,j} \frac{\partial^2 V}{\partial S_i \partial S_j} S_i S_j = [S]^t[F][S] \qquad \text{(II.4)}$$

[Λ]: is a diagonal matrix comprising of the λ roots of the determinant (II.5).

$$| [D]^t [F] [D] - \lambda [I] | = 0 \qquad \text{(II.5)}$$

which satisfy the following equations:

$$\eta_i = \overset{o}{\eta}_i \cos [\lambda . t^{1/2} + \theta]$$

$$= \overset{o}{\eta}_i \cos (\omega t + \theta]$$

$$\text{where } \omega (\text{rad } S^{-1}) = 2\pi\nu (S^{-1}) = \lambda^{1/2} \qquad \text{(II.6)}$$

For in-phase motions of all atoms θ can be considered 0. Equation (II.1) is obtained in terms of 3N mass-weighted Cartesian coordinates. Then the determinant is 3N by 3N and has 3N roots. Six roots correspond to translational and rotational motions and have $\lambda = 0$, which produces 3N-6 non-zero molecular vibrational roots. The calculated root (frequency) does not always agree with the observed one, i.e.,

$$\lambda = 4\pi^2\nu^2 = 4\pi^2 C^2 \sigma^2 \qquad \text{(II.7)}$$

What is required is an acceptable agreement between λ and $\sigma (cm^{-1})$, and for that the assumed force constants are systematically adjusted. In practice, the force constants are determined in order to test predicted assignments of experimentally measured frequencies. For N internal coordinates there are $N(N+1)/2$ force constants to be calculated which is always larger than the 3N-6 vibrational

frequencies. Therefore, the determination of the GVFF (general valence force field) is impossible with this little information. The solution to this problem lies in increasing the number of observables by isotopic substitutions (deuteration), or in decreasing the number of force constants by adopting one of the force field models which will be discussed later, or in both. Additional data can be obtained from Coriolis coefficients, centrifugal distortion constants[22,28] which can be calculated, and mean amplitudes of vibration measured by electron diffraction.[29] Even with all this extra information, it has been impossible to determine the GVFF except for simple molecules such as MH_3, MH_4 (M = C,Si,Ge,N,P,As).[30] While isotopic substitution by deuteration was found helpful in the 1400 cm^{-1} region of methylated phosphine adducts of boron trihalides, it was complicating the situation in the 700-800 cm^{-1} region of the spectra where the CD_3 rocking modes and the P-B stretching mode lie. Consequently, it becomes necessary to reduce the number of force constants.

a) Force Fields

One of the common practices is to limit the number of force constants such that they are less than or equal to the number of frequencies observed. This can be accomplished in many ways. One is to neglect all interaction terms completely which means that all off-diagonal terms in the F

matrix are set to zero. This, in turn, produces a simple valence force field (SVFF). This force field can be uniquely determined without difficulties since the number of force constants is at most equal to that of the observed frequencies. However, it does not normally produce a good agreement between observed and calculated frequencies. Other force fields that have been utilized include the orbital valency force field[31,32] (OVFF) and hybrid orbital force field[33] (HOFF). A different but very realistic model has been used by H. C. Urey and C. A. Bradley.[34] In this force field, the interactions are supposed to be caused by repulsions between non-bonded atoms. Thus, the internal coordinates are defined in such a way that the number of interaction terms is reduced. Each force field has its advantages and disadvantages. The choice of the model depends on the molecules investigated and partially on personal preferences. The Urey-Bradley force field has been successfully applied to molecules such as CCl_4, $SiCl_4$, $TiCl_4$, $SnCl_4$ and $SnBr_4$.[35,36] A modified Urey-Bradley force field has been applied to molecules of the type $Me_nMH_{3-n}.BX_3$ (n = 0,1,2,3; M = P,As; X = Cl, Br, I)[37-40] where the non-bonded interactions between halogens, and between halogens and the donor atom are considered. All molecules studied in this work by normal coordinate analysis are treated by the modified Urey-Bradley model.

In this force field the potential energy of the vibration of each valence coordinate r_1 and r_2 is

$$2V = K'_{r_1} r_1 \Delta r_1 + K'_{r_2} r_2 \Delta r_2 + H' r_1 (r_1 \Delta\theta) + F' \rho \Delta\rho + \ldots \quad \text{(II.8)}$$

where F is a repulsion force constant between terminal atoms, and ρ is the non-bonded distance between them. ρ is related to r_1, r_2 and θ by the cosine law so that it is a redundant coordinate. The potential is expressed in terms of distances, Δr_1^2, Δr_2^2, $\Delta\theta^2$, $\Delta r_1\Delta\theta$, $\Delta r_2\Delta\theta$, and $\Delta r_1 \Delta r_2$ after the redundancy is eliminated, with four force constants (in UBFF) K_{r_1}, K_{r_2}, H_θ, F instead of six constants (in GVFF) $f_{\Delta r_1^2}$, $f_{\Delta r_2^2}$, $f_{\Delta\theta^2}$, $f_{\Delta r_1/\Delta r_2}$, $f_{\Delta r_1/\Delta\theta}$, $f_{\Delta r_2/\Delta\theta}$.[23]

b) Force Constant Calculation

The calculation of force constants was performed with a program written by Dr. J. L. Hencher[27] (Larmol). The normal coordinates were expressed in mass-weighted Cartesian coordinates by a method similar to Gwinn's.[41] The atoms and their connections to other atoms in a dummy atoms framework are defined using an algorithm by Hilderbrandt.[42] The secular equations were solved and refinement to a set of trial force constants was performed by the least-squares method to give the best agreement

between observed and calculated frequencies.

Several iterations are needed with successive adjustments to obtain the "best fit", and then convergence of the solution is said to be achieved. It is worth mentioning at this point that a good fit and convergence do not necessarily mean a favourable solution by physical standards. Based on the order of varying force constants and interaction terms used, many solutions can be obtained which yield a good fit. The final aim is to produce an internally consistent set of force constants which makes physical sense and which can be used on similar molecules to also calculate their frequencies.

A set of force constants must support the vibrational assignments in terms of a reasonable potential energy distribution otherwise, even an excellent fit between observed and calculated frequencies cannot be indicative of a good approximation to the real force field.

REFERENCES

PART ONE

1. D. F. Shriver, The Manipulation of Air-Sensitive Compounds, McGraw-Hill, New York, N.Y. (1969).

2. R. T. Sanderson, Vacuum Manipulation of Volatile Compounds, J. Wiley, New York, N.Y. (1948).

3. W. L. Jolly, The Synthesis and Characterization of Inroganic Compounds, Prentice-Hall, Englewood Cliffs, N.J. (1970).

4. T. Wentink and V. H. Tiensuu, J. Chem. Phys. 28, 826 (1958).

5. R. E. Scruby, J. R. Lacher and J. D. Park. J. Chem. Phys. 19, 386 (1951).

6. V. F. Mironov, S. A. Mikhailyants and T. K. Gai. Zh. Obshch. Khim. 39, 397 (1969).

7. M. Jakoubková, Z. Papousková and V. Chvalovský. Collect. Czech. Chem. Commun. 45, 854 (1980).

8. A. N. Egorochkin, V. F. Mironov and M. G. Voronkov. Zh. Struck. Khim. 7, 450 (1966).

9. F. K. Butcher, W. Gerrard, F. F. Mooney, R. G. Rees, H. A. Willis, A. Anderson and H. A. Gebbie. J. Organomet. Chem. 1, 431 (1964).

10. H. C. Clark, J. T. Kwon, L. W. Reeves and E. J. Wells, Inorg. Chem. 3, 907 (1964).

11. W. H. Dehn. Am. Chem. J. 40, 88 (1908): CA 2; 2793.

12. A.J.F. Clark. Ph.D. Thesis, University of Windsor (1979).

13. D. Seyferth and S. B. Andrews. J. Organomet. Chem. 30, 151 (1971).

14. R. C. Cookson and F. G. Mann. J. Chem. Soc. 67 (1949).

15. A. Harvey and K. Wilson. J. Chem. Phys. 44, 3535 (1966).

16. J. Pierre. Ann. Phys. 1, 127 (1966).

17. K. Nukuda, O. Yamamoto, T. Suzuki, M. Takeuchi and M. Ohnishi. Ann. Chem. 35, 1892 (1963).

18. M. Ito. J. Chem. Phys. 42, 391 (1965).

19. H. Schmidbaur, Chem. Ber., 97, 1639 (1964).

20. H. Siebert, Z. Anorg. Allg. Chem. 273, 161 (1953).

21. R. G. Kostganouskii, I. I. Chervin, V. V. Yaskshin, and A. U. Stepanyants, Izv. Akad. Nauk SSSR, Ser. Khim., 162 (1967); Chem. Abstr., 68, 75338 (1968).

22. G. Herzberg. Molecular Spectra and Molecular Structure II. Infra-red and Raman Spectra of Polyatomic molecules, Van Nostrand, Princeton, N. J. (1945).

23. L. A. Woodward, Introduction to the Theory of Molecular Vibrations and Vibrational Spectroscopy, Clarendon Press, Oxford (1972).

24. L. A. Woodward, in Raman Spectroscopy: Theory and Practice, Vol. 1, ed. H. A. Szymanski, Plenum Press, New York, N.Y. (1970).

25. E. B. Wilson, J. C. Decius and P. C. Cross, Molecular Vibrations, McGraw Hill, New York, N.Y. (1955).

26. E. Fermi, Z. Physik, 71, 250 (1931).

27. J. L. Hencher, Ph.D. Thesis, McMaster University (1964).

28. I. M. Mills, J. Mol. Spectr. 5, 334 (1960).

29. S. J. Cyvin Molecular Vibrations and Mean Square Amplitudes, Elsevier, Amsterdam (1968).

30. J. L. Duncan and I. M. Mills, Spectrochim. Acta 20, 523 (1964).

31. D. F. Heath and J. W. Linnett, Trans. Far. Soc. 54, 264 (1949).

32. J. W. Linnett and P. J. Wheatley. Trans. Far. Soc. 54, 39 (1949).

33. I. M. Mills, Spectrochim. Acta 19, 1585 (1963).

34. H. C. Urey and C. A. Bradley, Phys. Rev. 38, 1969 (1931).

35. J. W. Linnett. Quart. Rev. 1, 947 (1973).

36. T. Shimanouchi, I. Nakagawa, J. Hiraishi and M. Ishii. J. Mol. Spectr. 19, 78 (1966).

37. J. E. Drake, J. L. Hencher and B. Rapp. J. Chem. Soc. Dalton, 595 (1974).

38. J. E. Drake, J. L. Hencher and B. Rapp. Inorg. Chem. 16, 2289 (1977).

39. J. E. Drake, L. N. Khasrou and A. Majid. Can. J. Chem. 59, 2417 (1981).

40. J. E. Drake, J. L. Hencher and L. N. Khasrou. Can. J. Chem. 59, 2898 (1981).

41. W. D. Gwinn, J. Chem. Phys. 55, 477 (1977).

42. R. L. Hilderbrandt, J. Chem. Phys. 51, 1654 (1969).

PART TWO

A SPECTROSCOPIC AND CRYSTALLOGRAPHIC INVESTIGATION OF METHYLATED ARSINE ADDUCTS WITH BORON TRIHALIDES

INTRODUCTION

The bonds formed between elements of Group IIIA and Group VA, especially those of boron compounds with nitrogen and phosphorus donors, have been studied extensively.[1-5] The structures of adducts of ammonia or its methylated analogs with boron trifluoride have been determined by single crystal X-ray structure analysis.[6-8] The $Me_3N.BX_3$ adducts, where X = Cl, Br, I, were also studied by X-ray crystallography.[9] Other investigations of amine adducts of boron trihalides and borane include vibrational and microwave studies,[10,11] the ^{11}B and ^{13}C n.m.r. and mass spectra of trimethylamine adducts of mixed boron trihalides,[12-14] and the examination of the relative acceptor power of boron trihalides towards trimethylamine.[15,16] The phosphorus analogs have drawn even more attention. Phosphine borane, $PH_3.BH_3$ for example, has been studied by X-ray crystallography[17], microwave,[18] i.r. and Raman spectroscopy.[19-22] The vibrational spectra and normal coordinate analysis have been reported for $Me_2PH.BH_3$[23] $Me_2PH.BX_3$[24] and $Me_3P.BX_3$.[25] The crystal structures of $Me_3P.BX_3$ have also been determined.[26] In addition, the ^1H and ^{11}B n.m.r. spectra of several alkyl and arylphosphine adducts[27,28] and the characterization of $Ph_3P.BI_3$ have been reported.[29,30]

Relatively less attention has been devoted to the

study of similar species with an As-B bond. The As-B bonds in arsine-boron polymers of the form $[(CH_3)_2AsBH_2]_n$[31] and $[(CF_3)_2AsBH_2]_n$[32] where n = 3,4 have been found to be weaker than the corresponding P-B bonds in the analogous trimers and tetramers.[33] Thus, it is conceivable that the relatively less stable As-B bond is responsible for the quantity of work done on these species. Among studies reported are the microwave study of $Me_3As.BH_3$,[34] the preparation of $Me_3As.BCl_3$,[35,36] the ^1H and ^{11}B n.m.r. spectra of $Me_3As.BX_3$ where X = Br,I,[37] and the vibrational spectra and normal coordinate analysis of $Me_3As.BX_3$[38,39] and $Ph_3As.BX_3$[38] where X = Cl,Br,I.

This work is a continuation of the many published investigations of compounds having a M-B bond where M = N,P,As. No study has been dedicated so far to the methyl- and dimethylarsine adducts of boron trihalides. In this section the vibrational spectra and normal coordinate analysis of methyl- and dimethylarsine adducts will be discussed along with the ^{11}B n.m.r. spectra of the mixed halide adducts and finally, the crystal structures of trimethyl arsine adducts. Comparisons are made between compounds studied herein and analogous ones studied by other workers. Included in these comparisons is the examination of the variation of vibrational spectra

features and calculated force constants with bond lengths and angles determined by X-ray diffraction. Also, the ^{11}B and ^{1}H n.m.r. chemical shifts changes, arising from changing the halogen on boron or the group on arsenic, were employed as alternative ways of assessing relative strengths of the donor-acceptor bonds.

PREPARATION

All $Me_nAsH_{3-n}.BX_3$, $Me_nAsH_{3-n}.BX_2Y$ and $Me_nAsH_{3-n}.BXYZ$ adducts (n = 1,2,3,; X,Y,Z = Cl,Br,I) were prepared by the direct combination of the reactants at room temperature in reaction vessels I and J on the vacuum line. The boron trihalide adducts were prepared as in the following equation:

$$Me_nAsH_{3-n} + BX_3 \rightarrow Me_nAsH_{3-n}.BX_3$$

The adducts of binary mixtures of boron trihalides were prepared as in the following equation:

$$BX_3 + BY_3 \rightleftharpoons BX_2Y + BXY_2$$

$$+$$

$$2Me_nAsH_{3-n}$$

$$\downarrow$$

$$Me_nAsH_{3-n}.BX_3 + Me_nAsH_{3-n}.BY_3 + Me_nAsH_{3-n}.BX_2Y + Me_nAsH_{3-n}.BXY_2$$

The tertiary mixtures were prepared in a similar fashion

where ten boron trihalides are expected to result from an equimolar mixture of BCl_3, BBr_3 and BI_3. To this equilibrium mixture, the arsine donor was then added in three times the number of moles of each BX_3.

A. Formation of the adducts $Me_nAsH_{3-n}.BX_3$ (n=1,2,3; X=Cl,Br).

The arsine Lewis base and the boron trihalide Lewis acid were condensed in an approximately 1:1 molar ratio (ca 0.5 mmole) in vessels I or J which were held at -196°C. The reaction vessel was then isolated on the vacuum line and the reactants were warmed slowly to room temperature by using a series of baths (-126°C, -95°C, -78°C, -12°C and 0°C). After 0.5 h at room temperature the vessel was momentarily opened to the pump to remove any excess of reactants. The product was then either removed from the vacuum line to the glove bag where a CsI pellet and a Nujol mull were prepared for i.r. spectra, or an appropriate solvent was distilled in so that the n.m.r. or Raman spectra could be recorded.

B. Formation of the $Me_nAsH_{3-n}.BI_3$ adducts

Boron triiodide is a solid and, therefore, was manipulated in the glove bag BI_3 (0.2 g; 0.5 mmole) was purified by agitation with dry benzene (0.5 ml) and a

trace of elemental mercury in the nitrogen-filled glove bag. The reaction vessel was then transferred to the vacuum line, held at -196°C and opened to the line to pump away nitrogen. A slight excess of the arsine was then distilled in. The reaction then proceeded under the same conditions mentioned for the preparation of the chlorides and bromides. Benzene was removed by vacuum distillation and the last traces were removed by pumping on the product for ca 20 min. The adduct was then treated as above for spectroscopic examination.

C. Formation of the mixed adducts $Me_nAsH_{3-n}.BX_2Y$ and $Me_nAsH_{3-n}.BXY_2$ (n=1,2,3; X,Y=Cl,Br)

Equimolar quantities (0.5 mmole) of BX_3 and BY_3 were distilled into the evacuated tube I on the vacuum line. The contents were then allowed to equilibrate and after 1 h at room temperature, the reactants were held at -196°C and a slight excess of the appropriate arsine was distilled into the vessel. Gradual warming by using a series of slush baths as described above resulted in reaction as indicated by the formation of a white solid. After 30 minutes at room temperature, the tube was momentarily opened to the vacuum line, deuterated methylene chloride distilled in and the tube torch-sealed.

D. Formation of the mixed adducts $Me_nAsH_{3-n}.BX_2I$ and $Me_nAsH_{3-n}.BXI_2$ (n=1,2,3; X=Cl,Br)

Boron triiodide was handled as in section B. The tube was then attached to the line and nitrogen pumped away. An equimolar amount of BX_3(X=Cl,Br) was then distilled in and the contents were left to equilibrate. After 1 h at ambient temperature, the appropriate arsine was distilled in and the reaction allowed to proceed as in (C). Benzene was then carefully removed by vacuum distillation followed by 30 minutes of pumping. CD_2Cl_2 was then distilled in and the tube torch-sealed.

E: Formation of $Me_nAsH_{3-n}.BClBrI$

A predetermined amount of purified BI_3(ca 0.2 g in 0.5 mL of C_6H_6) was placed in the tube I in the glove bag. The tube was transferred to the vacuum line and equimolar amounts of BCl_3 (0.5 mmole) and BBr_3 (0.5 mmole) were distilled into the tube at -196°C. After 1 h at room temperature, the arsine (ca 0.15 mmole) was distilled in and then the reaction allowed to proceed and the product treated as in sections C and D above.

F. Spectroscopic Techniques

I.r. spectra were recorded on solid samples of each adduct. The reaction vessel J with the freshly prepared

adduct was transferred to the glove bag where a CsI pellet for mid-i.r. and a Nujol mull for far i.r. were prepared. Solid and solution Raman spectra were also recorded for each adduct in sealed 5 mm thin-walled glass tubes (reaction vessel I in Fig. I.2). Two solvents, CH_3I and CH_2Cl_2 were chosen for polarization studies in order to eliminate problems arising from masked adduct peaks by bands of one solvent. All spectra were recorded on freshly prepared samples.

For ^{1}H and ^{11}B n.m.r. spectra, CD_2Cl_2 solutions of the adducts were sealed in n.m.r. tubes (vessel I in Fig. I.2). All n.m.r. samples were kept at -78°C when not in use to prevent dissociation. TMS was found to react with free boron trihalides and thus it was used as an external standard. All spectra were recorded on freshly prepared samples.

PHYSICAL PROPERTIES

The adducts which are the subject of this investigation, are white, moisture sensitive solids as reported earlier for similar compounds.[35-40] These adducts were found to be soluble in polar solvents such as chloroform and methyl iodide. Methylene chloride is a relatively better solvent and the deuterated solvent was used to prevent masking of the AsH protons by the more intense

CH_2 peak of the undeuterated solvent. The methyl- and dimethylarsine adducts were found to be much more soluble than the trimethylarsine adducts thus suggesting some degree of dissociation in CD_2Cl_2 at room temperature. The BI_3 compounds tend to darken on extended exposure to light, indicative of the photosensitivity often associated with iodides. The melting points of these adducts are displayed in Table (a).

Table (a). Melting points (°C) of Me_nAsH_{3-n}·BX_3 (n=1,2,3,; X=Cl,Br,I)

Me_nAsH_{3-n}	BCl_3	BBr_3	BI_3
Me_3As	310[a]	245[a]	275[a]
Me_2AsH	104	122	130[b]
$MeAsH_2$	46	68	78[b]

[a]ref. 5; [b]turns yellow.

The methylarsine adducts are less stable than their respective dimethyl- and trimethylarsine analogs. A glance at Table (a) suggests the trend of stability which is established for the phosphine analogs, although melting points are, of course, not necessarily a direct indication of stability. $MeAsH_2.BCl_3$, the least stable compound, turns completely to pale white polymeric liquid in a few

hours. After formation, this adduct continues to exert a positive pressure which is indicative of HCl elimination similar to H_2 elimination in $MeAsH_2.BH_3$.[31] A monitoring of the As-H symmetric and asymmetric stretching frequencies at ca 2254 cm^{-1} in the Raman spectrum clearly shows decomposition with time (Fig. (a)) indicating a continuous breaking of the As-H bond. A sampling of the volatile materials above $MeAsH_2.BCl_3$ and $MeAsH_2.BBr_3$ showed the existence of HCl and HBr from the band with characteristic P and R branches of the two diatomic molecules in the i.r. spectra (Fig. (b)). Presumably, HX elimination proceeds in accord with the following equation:

$$n\ MeAsH_2.BCl_3 \rightarrow [MeAsH.BCl_2]_n + n\ HCl$$

Trimers and tetramers of this type were identified in the polymerization of $Me_2AsH.BH_3$ but the products of polymerization of $MeAsH_2.BH_3$ were also hard to precisely identify.[31]

^1H N.M.R. SPECTROSCOPY

The amount of data on the ^1H n.m.r. spectra of arsine adducts is relatively scarce compared with amine or phosphine chemistry. The properties of amine adducts have been widely studied by n.m.r. spectroscopy.[41-46]

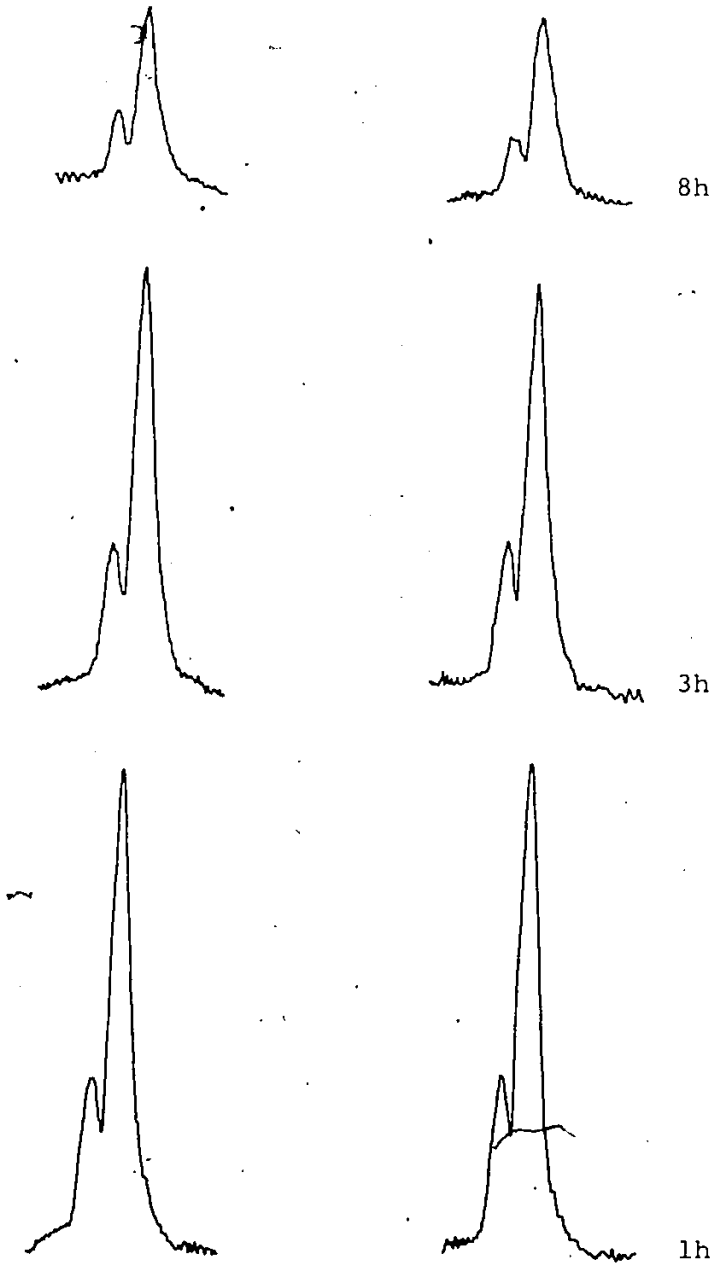

Fig. (a). The AsH stretching modes of $MeAsH_2.BCl_3$ (ca 2254 cm^{-1}) in the Raman spectrum at different times from preparation.

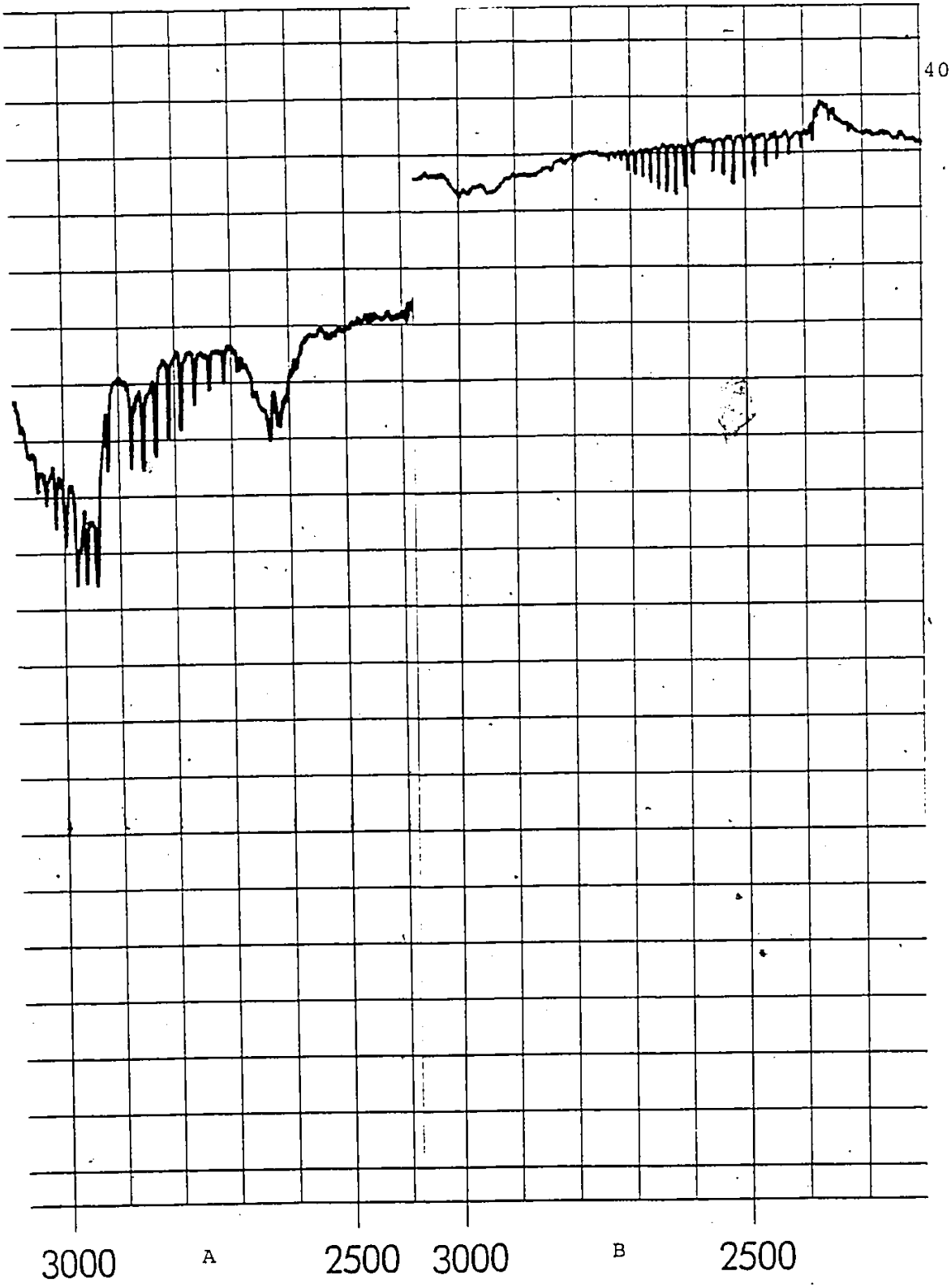

Fig. (b). Selected regions of the i.r. spectra of the volatile materials above $MeAsH_2.BCl_3$ (A) and $MeAsH_2.BBr_3$ (B).

These reports discuss a variety of topics including studies of exchange reactions of trimethylamine with its borane adduct, long range B-H coupling and quadrupole relaxation, and the evaluation of relative acid strengths of several boron Lewis acids using trimethylamine as a standard Lewis base. Investigations of phosphine adducts [47-50] have been centered on correlations between chemical shifts and coupling constants with bond strength and adduct stability and on variable temperature studies.[45,51,52]

The few reports that have appeared on the ^1H n.m.r. spectra of trimethylarsine boron trihalide adducts have produced conflicting results.[38,53] Our results for the methyl- and dimethylarsine analogs agree with one study[38] in the sense that both investigations show a down field trend in the chemical shift upon adduct formation and in the order that lends support to the already established order of Lewis acidity $BI_3 > BBr_3 > BCl_3$. The unusual chemical shifts in the other report[53] have been explained in terms of anisotropic solvent effects. The chemical shifts are listed in Table (b). The spectra and chemical shifts of $Me_3As.BX_3$ agree very well with those reported earlier.[38] The ^1H n.m.r. signal of the methyl group in $Me_2AsH.BX_3$ is broadened considerably in the adducts relative to the free arsine as reported earlier.[38,53]

Table (b). ^{1}H n.m.r. chemical shifts for $Me_nAsH_{3-n}.BX_3$ (n=1,2,3; X=Cl,Br,I)[a,b,c]

Compound	δMe	δAsH
Me_3As	0.95	
$Me_3As.BCl_3$	1.50 (0.55)	
$Me_3As.BBr_3$	1.60 (0.65	
$Me_3As.BI_3$	1.69 (0.74	
Me_2AsH	0.97	2.39
$Me_2AsH.BCl_3$	1.63 (0.66)	4.61 (2.22)
$Me_2AsH.BBr_3$	1.76 (0.79)	5.00 (2.61)
$Me_2AsH.BI_3$	1.83 (0.86)	5.10 (2.71)
$MeAsH_2$	0.975	1.46
$MeAsH_2.BCl_3$	1.65 (0.67)	6.13 (4.67)
$MeAsH_2.BBr_3$	2.30 (1.32)	6.83 (5.37)
$MeAsH_2.BI_3$	2.38 (1.4)	6.9 (5.44)

[a] All spectra recorded in CD_2Cl_2 solutions

[b] In ppm downfield relative to external TMS

[c] Coordination chemical shifts are given in brackets where $\Delta\delta = \delta$ (adduct) - δ (free base)

In $Me_3As.BX_3$, the broad singlets appear as distorted quartets arising from the overlapping of the 1:1:1:1 quartet arising from coupling with the ^{11}B nucleus (I = 3/2; 81.2%) with the 1:1:1:1:1:1:1 septet arising from coupling with the ^{10}B nucleus (I = 3; 18.8%). In $Me_2AsH.BX_3$, the methyl protons are first split by the protons on As into a doublet and each line of the doublet

is further split into a distorted quartet by ^{11}B and ^{10}B nuclei. The overall signal should look like two closely placed distorted quartets with the separation depending on J_{HH} coupling which is ca 6.95 Hz in the free Me_2AsH base. The As-H signal is split into a septet by the methyl protons and each line of this septet is split into a distorted quartet by coupling with boron. Thus the overall appearance is that of a hump in the spectrum. Figure (c) shows the ^1H n.m.r. spectrum of $Me_2AsH.BI_3$. No coupling is observed for the methyl protons of $MeAsH_2.BX_3$ with the boron nucleus. The absence of coupling may result from an increase in the electric field gradient around boron which in turn would increase the quadrupole interaction and decrease the likelihood of observing small hyperfine splitting due to boron. The electric field gradient would be zero for a true symmetrical tetrahedral environment around boron. This suggests that with the stronger As-B bonds associated with $Me_3As.BX_3$ and $Me_2AsH.BX_3$, the electric field gradient is sufficiently close to zero to allow the observation of hyperfine splitting. The weakest As-B bond is $MeAsH_2.BX_3$ lead to the greatest distortion around boron and hence the least likely situation in which to observe splitting. The two As-H protons appear as a hump in the spectrum similar to that in $Me_2AsH.BX_3$. The ^1H n.m.r. spectrum of $MeAsH_2.BBr_3$ is depicted in Fig. (d).

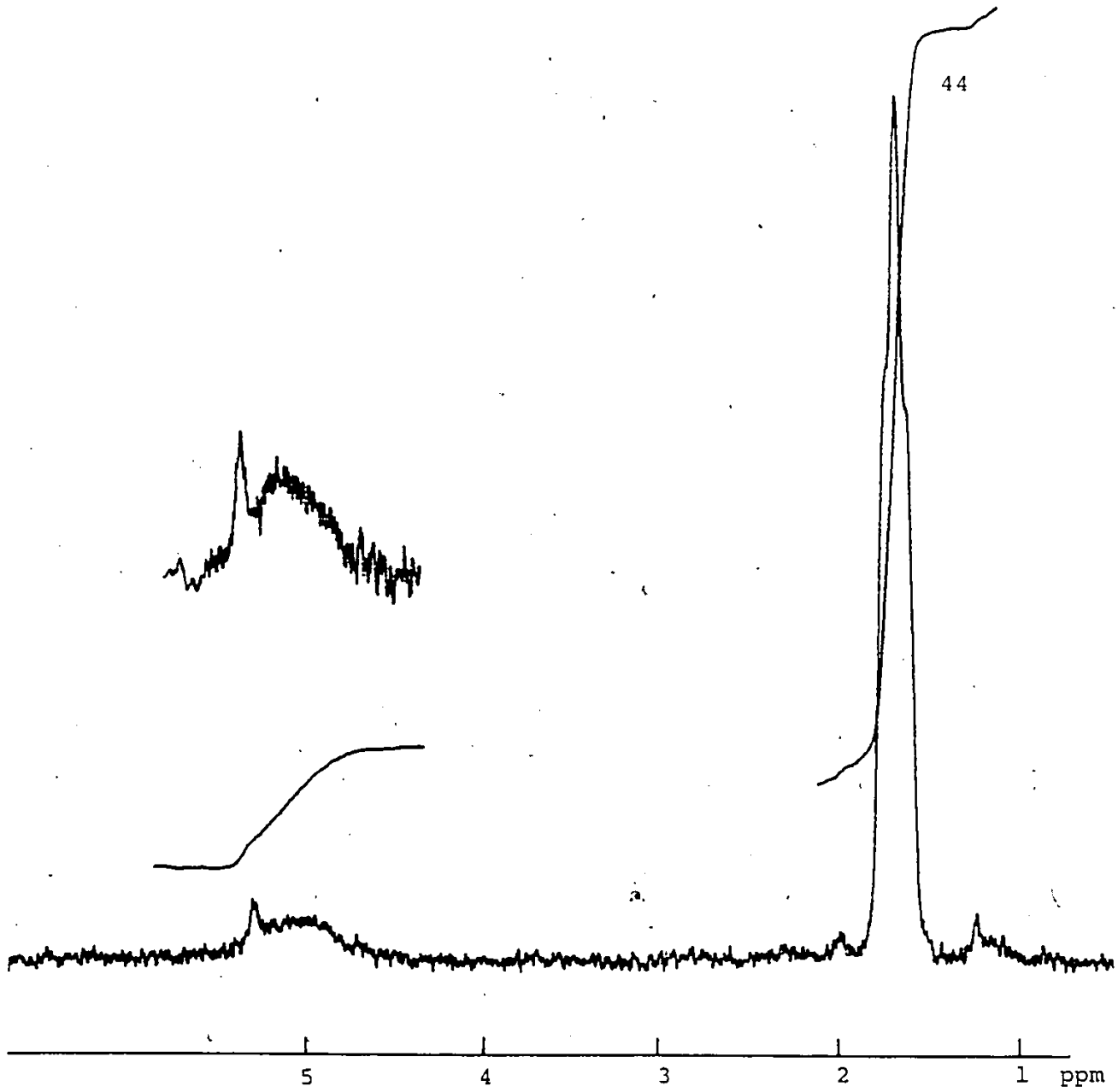

Fig. (c). ^{1}H n.m.r. spectrum of $Me_2AsH.BI_3$.

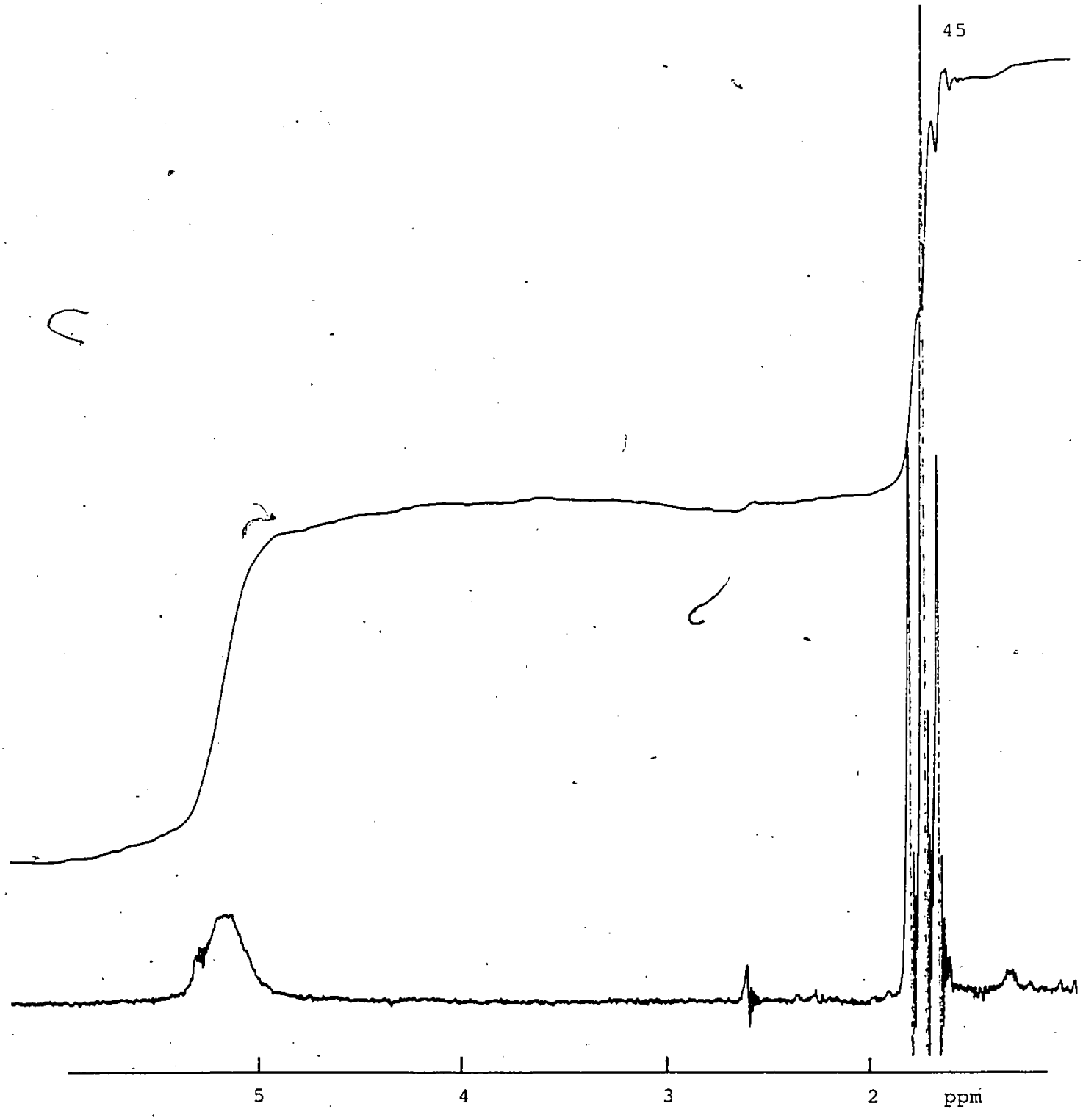

Fig. (d). ^{1}H n.m.r. spectrum of $MeAsH_2.BBr_3$.

CHAPTER III

VIBRATIONAL AND NORMAL COORDINATE ANALYSIS OF $MeAsH_2.BX_3$ (X = Cl,Br,I)

The eleven-atom molecules $MeAsH_2.BX_3$ were assumed to have a staggered configuration with a C_s point group symmetry. The vibrational representation is $\Gamma_v = 16a' + 11a''$ with all modes active in both i.r. and Raman effects. The in plane (a') and out of plane (a") modes were expected to give rise to polarized and depolarized Raman bands respectively. To make matters simpler, the CH_3 and BX_3 vibrations were considered degenerate and symmetric in terms of the local group symmetry even though these modes were split into a' and a" modes. The description of normal modes and the numbering of the frequencies are shown in Table III.1 and the i.r. and Raman spectra in Figs. III.1 - III.4. Tables III.2 - III.4 contain the full spectroscopic information on each adduct along with calculated frequencies and potential energy distributions.

III.1 The Methylarsine Frequencies

The methyl group stretching modes occur in the same region as in the free donor,[54] with two asymmetric CH_3 stretches (ν_1, ν_{17}) appearing in the Raman spectra in the range 3020-3000 cm^{-1}. One symmetric (ν_2) CH_3 stretch is assigned to an intense band in the Raman spectra at 2936, 2921 and 2930 cm^{-1} in $MeAsH_2.BCl_3$, $MeAsH_2.BBr_3$ and $MeAsH_2.BI_3$ respectively. The CH_3 symmetric (ν_5) and asymmetric (ν_4, ν_{19}) deformation modes are assigned to

relatively weak bands in the ranges 1230-1260 cm^{-1} and 1400-1430 cm^{-1} respectively. These vibrations appear to be shifted slightly to lower frequencies relative to the free base and have been assigned in the same region as in related molecules.[38,39,54-56] The two rocking modes (ν_7,ν_{20}) are considered degenerate although they are split into an a' and an a" modes. The region 930-950 cm^{-1} is assigned to these vibrations and there is no particular trend along the adduct series although these modes seem to be shifted slightly to higher frequencies upon formation of the adducts. These results are in agreement with the corresponding region in the spectra of $MePH_2.BX_3$ adducts.[57]

The various AsH fundamentals in the adducts were assigned by comparison with respective modes in free $MeAsH_2$. The symmetric (ν_3) and asymmetric (ν_{18}) AsH stretching modes are readily distinguished in the Raman spectra. They occur at prominently higher wavenumber values than in the free base, and this behavior was observed for the PH stretching modes in the $PH_3.BX_3$ adducts.[58] This effect is consistent with an increase in the AsH bond strength attributable to an increase in the s-character contribution as the environment around As approaches a tetrahedron upon adduct formation.[33] The definite trend toward lower AsH stretching

frequencies as the acceptor ability of the Lewis acid increases may suggest an increase in the drift of charge away from the AsH bonds without a further large change in the hybridization on arsenic.[27,57,58] The AsH_2 scissoring mode (ν_6) appears as a medium weak band in the i.r. spectrum at ca 1050-1100 cm^{-1} which is higher than the corresponding motion in the free base. The AsH_2 rocking frequency (ν_{22}) appears as a weak vibration in the 400 cm^{-1} region in the i.r. and Raman spectra, lower than the corresponding mode in the free base by ca 250 cm^{-1}. The very weak and difficult to assign bands in the 850-900 cm^{-1} region have been associated with the twist (ν_{21}) and wagging (ν_8) motions of AsH_2. The CAs stretching frequency (ν_{10}) appears as a strong polarized band in the Raman spectra at ca 600 cm^{-1}, compared with 563 cm^{-1} in $MeAsH_2$.[54] This vibration has been assigned at 610 cm^{-1} in $Me_3As.BH_3$,[59] and 575-618 cm^{-1} in $Me_3As.BX_3$.[38,39] Upon formation of the adducts, the strengthening of the CAs bond is consistent with the rehybridization argument presented above for the AsH bonds. The CAsB bonding mode (ν_{13}) is associated with medium to strong polarized bands at 200, 190 and 189 cm^{-1} for $MeAsH_2.BCl_3$, $MeAsH_2.BBr_3$ and $MeAsH_2.BI_3$ respectively. Extensive mixing of these modes with those of BX_3 is indicated in the potential energy distribution.

III.2 The AsB Donor-Acceptor Frequency

The AsB stretching frequency (ν_9) varies slightly from 653 cm^{-1} for $MeAsH_2.BCl_3$ to 640 cm^{-1} in $MeAsH_2.BI_3$. It appears as a strong and polarized band in the Raman spectra. This vibration appears at 500 cm^{-1} in $Me_3As.BH_3$,[59] 670-720 cm^{-1} in $Me_3As.BX_3$[39] and 650-670 cm^{-1} in $Me_3As.BX_3$.[38] It is interesting to note that the PB stretching frequency in the analogous $MePH_3.BX_3$[57] has been assigned at 762, 767 and 759 cm^{-1} for the BCl_3, BBr_3 and BI_3 adducts respectively. If the M-B bond (M=P, As) is treated as a pseudo-diatomic molecule then the ratio $(\bar{\nu}_{PB}^2 \times \mu_{PB} / \bar{\nu}_{AsB}^2 \times \mu_{AsB} = f_{PB}/f_{AsB})$ is equal to ca 1.1 suggesting that the PB bond is stronger than the AsB bond.[31]

III.3 The BX_3 Frequencies

The assignment of the BX_3 fundamentals was best achieved by comparison with studies undertaken for other BX_3 compounds [24,25,38,39,58,60] The polarized, intense bands at 373, 238 and 175 cm^{-1} are assigned to the symmetric BX_3 stretch (ν_{12}) and are shifted to lower wavenumbers in comparison with those assigned at 471, 278 and 190 cm^{-1} for planar BCl_3, BBr_3 and BI_3 respectively.[61,62] These shifts can be related to the rearrangement of the Lewis acid from the planar (sp^2) to the approximate tetrahedral (sp^3) configuration on coordination with

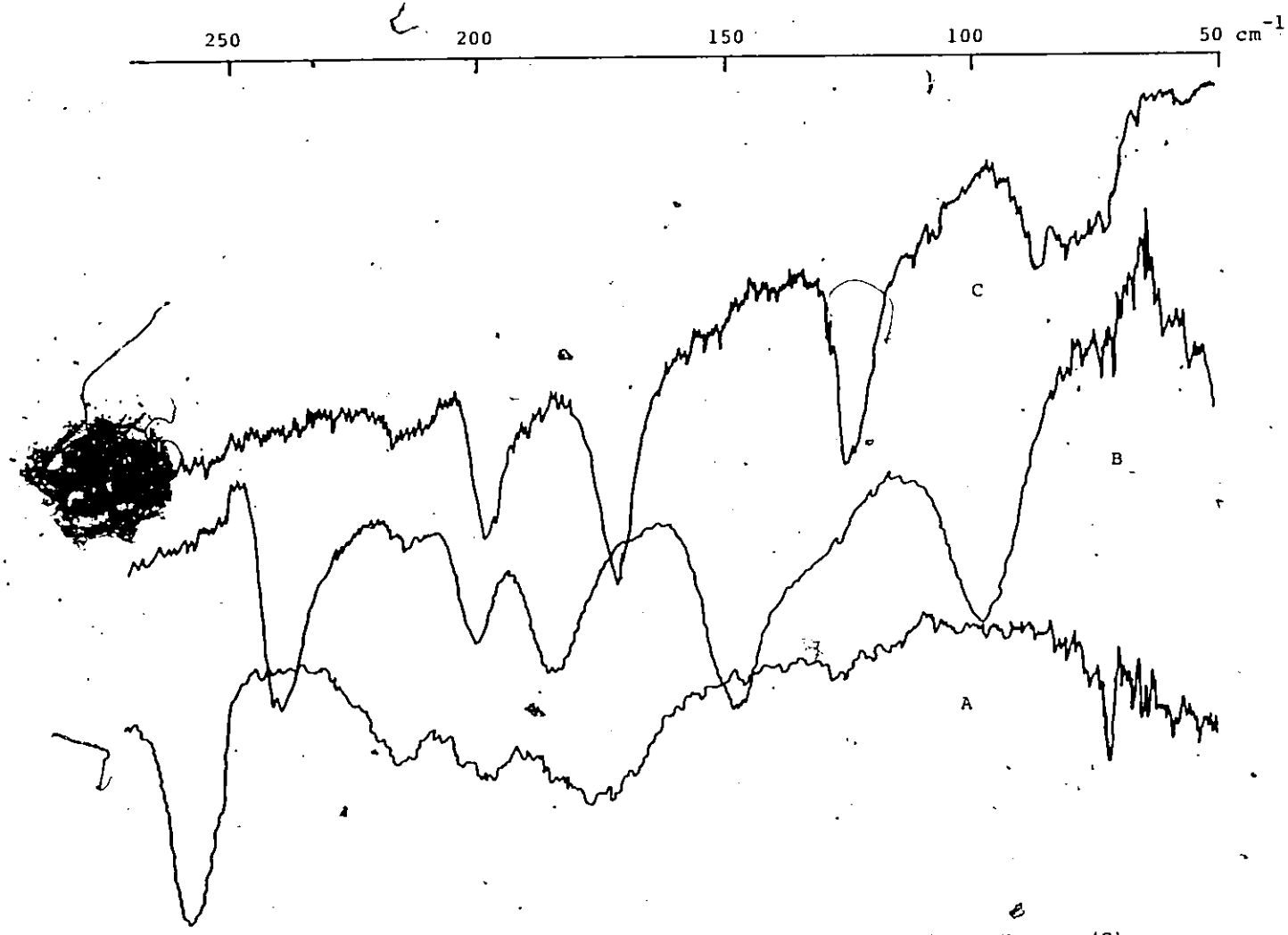

Fig. III.1 Far i.r. spectra of $MeAsH_2.BCl_3$ (A), $MeAsH_2.BBr_3$ (B) and $MeAsH_2.BI_3$ (C)

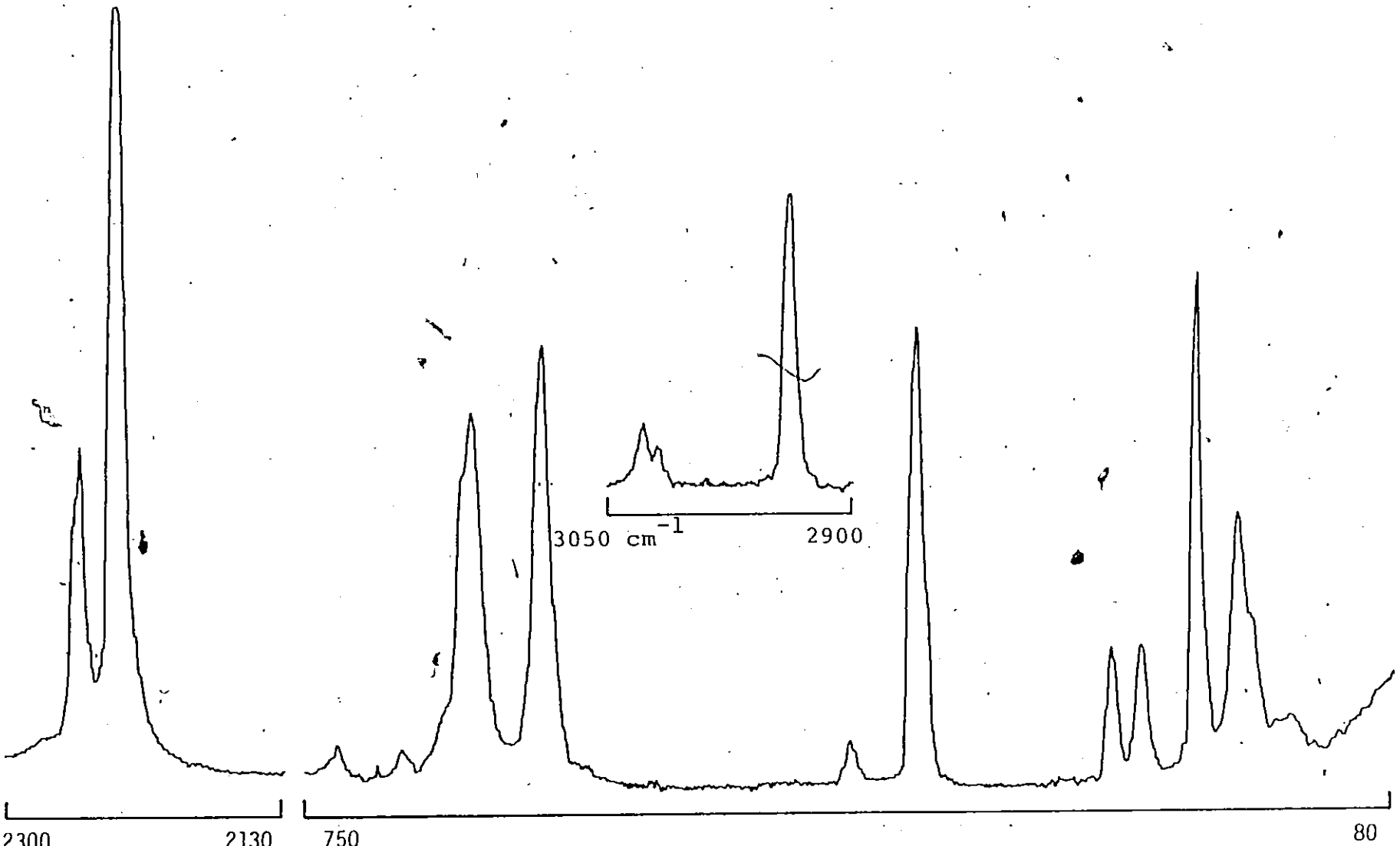

Fig. III.2. Selected regions of the solid Raman spectrum of $MeAsH_2.BCl_3$.

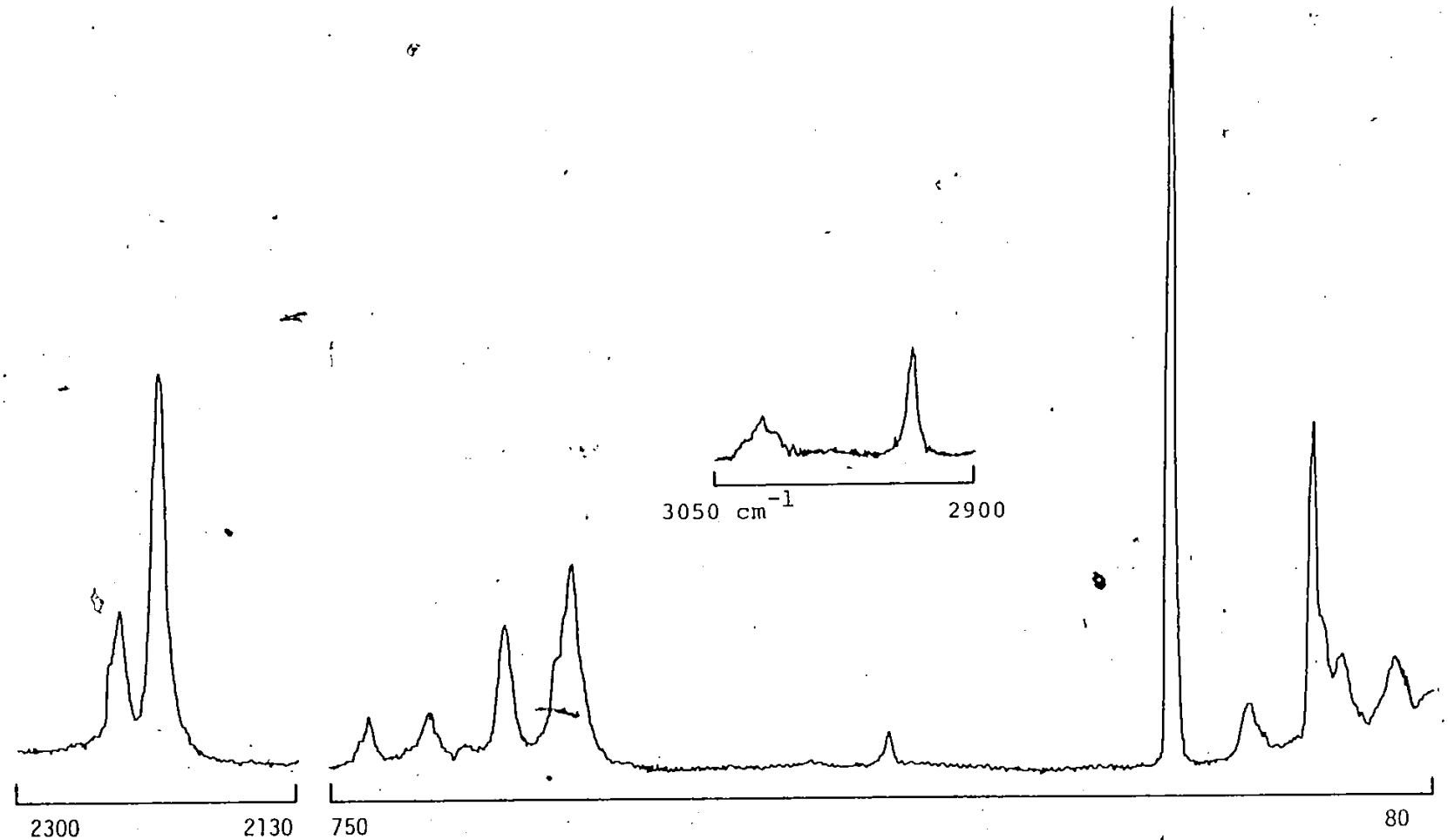

Fig. III.3. Selected regions of the solid Raman spectrum of $MeAsH_2.BBr_3$.

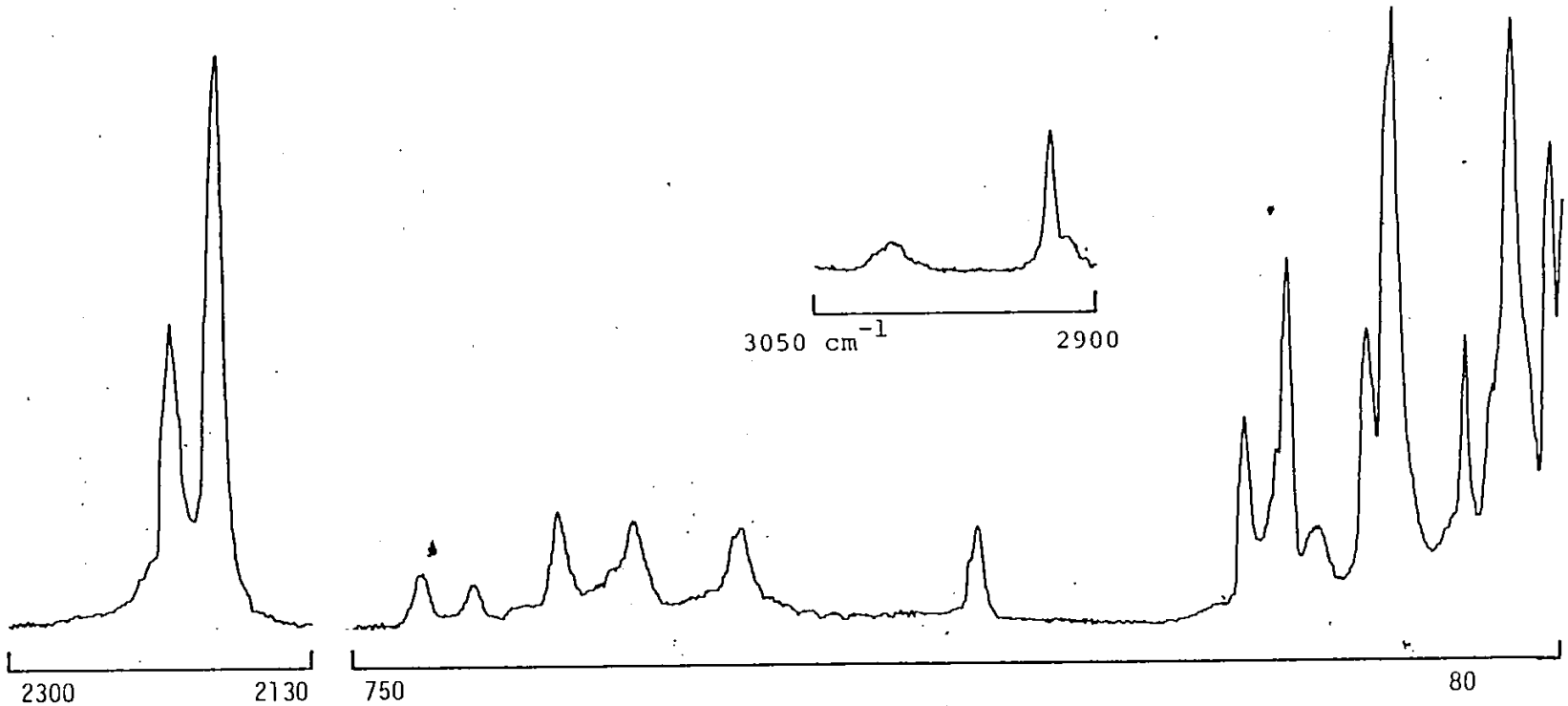

Fig. III.4. Selected regions of the solid Raman spectrum of $MeAsH_2.BI_3$.

Table III.1. The approximate description and symmetry species of the fundamental vibrations of $MeAsH_2.BX_3$ (X = Cl,Br,I).

a'	a"	Description
ν_1	ν_{17}	CH_3 stretch (a)
ν_2		CH_3 stretch (s)
	ν_{18}	AsH_2 stretch (a)
ν_3		AsH_2 stretch (s)
ν_4	ν_{19}	CH_3 def. (a)
ν_5		CH_3 def. (s)
ν_6		AsH_2 scissors
	ν_{20}	CH_3 rock (a)
ν_7		CH_3 rock (s)
	ν_{21}	AsH_2 twist
ν_8		AsH_2 wag
ν_9		As-B stretch
ν_{10}		C-As stretch
	ν_{22}	AsH_2 rock
ν_{11}	ν_{23}	BX_3 stretch (a)
ν_{12}		BX_3 stretch (s)
ν_{13}		C-As-B def.
ν_{14}	ν_{24}	BX_3 def. (a)
ν_{15}		BX_3 def. (s)
ν_{16}	ν_{25}	BX_3 rock
	ν_{26}	CH_3 torsion
	ν_{27}	BX_3 torsion

Table III.2 Observed I.R. and Raman frequencies (cm^{-1}), ± 3 cm^{-1} for $MeAsH_2.BCl_3$ with potential energy distributions

Assignment	I.R.CsI[a]	Raman (solid)	Raman (soln.)[b]	Calc.	P.E.D.[c]
ν_1, ν_{17}	2982 m	3018 w	solvent	3018	100f(CH^2) - 1f(CH/CH)
ν_2	2920 s	2936 m	2935 vw	2936	98f(CH^2) + 2f(CH/CH)
ν_{18}	2257 w	2254 m	2250 m,dp	2254	99f(AsH^2) + 1f(AsH/AsH)
ν_3	2233 w	2235 vs	2228 w,p	2235	100f(AsH^2) - 1f(AsH/AsH)
ν_4, ν_{19}	1415 m	1410 w	solvent	1409	93f(HCH^2) + 6f($HCAs^2$)
ν_5	1240 w	1242 w	-	1246	54f(HCH^2) + 45f($HCAs^2$) - 19f(HCAs/HCAs)
ν_6	1080 s	1086 vw	-	1082	84f($HCAs^2$) + 23f($HAsC^2$) +10f(HCAs/HCAs)
ν_7, ν_{20}	942 vw	950 s	957 vw,dp	952	59f($HCAs^2$) + 23f($HAsC^2$) + 10f(HCAs/HCAs)
ν_{21}	896 vw	907 w	893 vw,dp	882	22f($HCAs^2$) + 50f($HAsC_2^2$) + 20f($HAsB^2$)
ν_8	872 w	885 vw	887 vw,p	871	20f($HCAs^2$) + 55f($HAsC_2^2$) + 17f($HAsB^2$)
ν_{11}, ν_{23}	705 mw	690 w	-	690	75K(BX) + 9H(XBX)
ν_9	653 s	646 s	639 br,p	647	47K(AsB) + 25K(BX) + 10H(XBX) + 8F(XX)
ν_{10}	600 ms	604 s	590 vw,p	604	89f(CAs^2)
ν_{22}	420 m	418 w	418 w,dp	418	74f($HAsB^2$) + 16f($HAsC^2$) + 7K(BX)
ν_{12}	376 w	373 vs	372 s,p	368	27K(BX) + 48F(XX) + 12K(AsB) + 9F(AsX)
ν_{14}, ν_{24}	255 mw	255 m	255 m,dp	253	60F(XX) + 23H(XBX) + 6F(AsX)
ν_{13}	200 br	200 s	195 sh,p	203	20f($CAsB^2$) + 19F(XX) + 28F(AsX) + 12H(XBX)
ν_{15}	172 w	174 m	170 m,p	170	12F(XX) + 36F(AsX) + 20f($CAsB^2$) + 15H(AsBX)
ν_{16}, ν_{25}	130 w	142 w	138 vw,p?	134	66F(AsX) + 28H(AsBX)

[a] Low frequencies taken from far i.r. spectra in nujol; b. spectrum in CH_2Cl_2 and MeI; c. contribution greater than 10% except for significant interactions.

Table III.3 Observed I.R. and Raman frequencies (cm^{-1}), ± 3 cm^{-1} for $MeAsH_2.BBr_3$ with potential energy distributions

Assignment	I.R. CsI[a]	Raman (solid)	Raman (soln.)[b]	Calc.	P.E.D.[c]
ν_1, ν_{17}	3025 w	3020 w	solvent	3020	100f(CH^2) - 1f(CH/CH)
ν_2	2930 w	2930 m	2935 w,p	2930	98f(CH^2) + 1f(CH/CH)
ν_{18}	2240 ms	2240 mw	2240 m,dp	2240	99f(AsH^2) + 1f(AsH/AsH)
ν_3	2218 ms	2217 s	2217 mw,p	2217	100f(AsH^2) - 1f(AsH/AsH)
ν_4, ν_{19}	1400 s	1407 w	solvent	1400	92f(HCH^2) + 6f($HCAs^2$)
ν_5	1245 m	1258 vw	-	1246	53f(HCH^2) + 57f($HCAs^2$) - 18f(HCAs/HCAs)
ν_6	1050 mw	1055 vw	-	1049	84f($HAsH^2$) + 7f($HAsC^2$) + 9f($HAsB^2$)
ν_7, ν_{20}	940 m	945 m	947 w,dp	947	66f($HCAs^2$) + 13f($HAsC^2$)
ν_{21}	880 ms	890 vw	892 vw,dp	86β	13f($HCAs^2$) + 57f($HAsC_2^2$) + 24f($HAsB^2$)
ν_8	850 w	847 vw	844 vw,p	853	12f($HCAs^2$) + 61f($HAsC_2^2$) + 22f($HAsB^2$)
ν_9	649 s	644 w	640 m,p	638	58K(AsB) + 16K(BX) +8H(AsBX) + 6H(XBX)
ν_{11}, ν_{23}	620 s	618 m	620 w,dp	617	63K(BX) + 8H(AsBX) + 7H(XBX)
ν_{10}	595 s	600 mw	600 w,p	594	82f(CAs^2)
ν_{22}	410 w	408 w	410 vw,dp	410	67f($HAsB^2$) + 17f($HAsC^2$) + 13K(BX)
ν_{12}	238 s	235 vs	238 vs,p	244	33K(BX) + 46F(XX) + 10F(AsX)
ν_{13}	190 m	190 w	187 vw,p	188	44f($CAsB^2$) + 16F(XX) + 12K(BX) + 8F(AsX)
ν_{14}, ν_{24}	155 m	150 ms	150 m,dp?	158	69F(XX) + 16H(XBX) + 7k(BX)
ν_{15}	137 w	132 wsh	130 sh,p	134	25F(XX) + 23F(AsX) + 14f($CAsB^2$) + 10H(AsBX) + 11H(XBX)
$\nu_{16}, 25$	102 m	102 w	100 sh,dp	100	44F(AsX) + 42H(AsBX)

[a] Low frequencies taken from far i.r. spectra in nujol; b. spectrum in CH_2Cl_2 and MeI; c. contribution greater than 10% except for significant interactions.

Table III.4 Observed I.R. and Raman frequencies (cm^{-1}), ± 3 cm^{-1} for $MeAsH_2.BI_3$ with potential energy distributions

Assignment	I.R.CsI[a]	Raman (solid)	Raman (soln.)[b]	Calc.	P.E.D.[c]
ν_1, ν_{17}	3018 m	3010 w	solvent	3018	100f(CH^2) - 1f(CH/CH)
ν_2	2923 s	2921 m	2920 w,p	2923	99f(CH^2) + 1f(CH/CH)
ν_{18}	2197 m	2207 m	2213 w,dp	2207	99f(AsH^2) + 1f(AsH/AsH)
ν_3	2182 s	2183 s	2187 vw,p	2183	100f(AsH^2) - 1f(AsH/AsH)
ν_4, ν_{19}	1400 s	1405 w	solvent	1398	93f(HCH^2) + 6f($HCAs^2$)
ν_5	1260 w	1265 w	-	1263	52f(HCH^2) + 54f($HCAs^2$) - 13f(HCAs/HCAs)
ν_6	1100 m	1090 mw	-	1098	85f($HAsH^2$) + 6f($HAsC^2$) + 8f($HAsB^2$)
ν_7, ν_{20}	930 sh	935 vw	-	933	49f($HCAs^2$) + 35f($HAsC^2$) + 7f($HAsB^2$)
ν_{21}	890 s	892 vw	877 br,dp	877	40f($HCAs^2$) + 35f($HAsC^2$) + 15f($HAsB^2$)
ν_8	850 wsh	860 w	870 br,p	866	34f($HCAs^2$) + 14f($HAsC^2$) + 17f($HAsB^2$)
ν_9	640 mw	640 w	637 w,p	645	67K(AsB) + 9K(BX) + 7H(AsBX)
ν_{10}	600 m	595 w	598 w,dp	597	86f(CAs^2)
ν_{14}, ν_{23}	545 m	537 w	545 w,dp	539	57K(BX) + 13H(AsBX) + 7H(XBX)
ν_{22}	405 s	405 mw	400 vw,dp	401	52f($HAsB^2$) + 13f($HAsC^2$) + 25K(BX)
ν_{13}	192 w	189 ms	187 mw,p	193	32f($CAsB^2$) + 25F(XX) + 19K(BX) + 9F(AsX)
ν_{12}	174 w	175 s	170 ms,p	173	27K(BX) + 37F(XX) + 25f($CAsB^2$)
ν_{14}, ν_{24}	124 m	120 sh	125 mw,dp	124	74 F(XX) + 9K(BX) + 11H(XBX)
ν_{15}	110 wsh	109 s	110 wsh, p	115	43 F(XX) + 14F(AsX) + 11H(AsBX) + 12H (XBX)
ν_{16}, ν_{25}	83 w	85 ms	89 wsh, dp	86	33F(AsX) + 49H(AsBX)

[a] Low frequencies taken from far i.r. spectra in nujol; b. spectrum in CH_2Cl_2 and MeI; c. contribution greater than 10% except for significant interactions.

the arsine.[63] The asymmetric BX_3 stretching frequencies (ν_{11}, ν_{23}) display descending wave numbers at 690, 618 and 537 cm^{-1} compared to those assigned at 709, 613 and 540 cm^{-1} in the $MePH_2.BX_3$[57] and those of $Me_3As.BX_3$[38] at 700, 615 and 548 cm^{-1}. In free BX_3, these asymmetric modes were associated with bands at 956, 819 and 704 cm^{-1} for BCl_3, BBr_3 and BI_3 respectively.[61,62] The deformation modes (ν_{14}, ν_{24} and ν_{15}) naturally decrease in wave number along the series with $BCl_3 > BBr_3 > BI_3$ as shown in the far i.r. spectra (Fig. III.4) with 255, 174; 155, 132; 124, 110 cm^{-1} for the asymmetric and symmetric deformation modes of the BCl_3, BBr_3 and BI_3 adducts respectively. The remaining low frequency bands at 130, 102 and 83 cm^{-1} were assigned to the BX_3 rocking modes (ν_{16}, ν_{25}).

III.4 Normal Coordinate Analysis

The force constants for the adducts and for the free arsine are listed in Table III.5. The calculated frequencies and the potential energy distributions are presented in Tables III.2 - III.4). The geometric parameters (listed in Table III.6) were based initially on the parameters of $MeAsH_2$[54] and $MePH_2.BX_3$. By the time this work on the vibrational analysis neared completion, the structures of the $Me_3As.BX_3$ compounds had been solved.[64] The small adjustments were then made to the geometric para-

meters but in fact this resulted in minimal changes in the calculations. Use was made of both the i.r. and Raman spectra to fit the calculated frequencies.

Initially, a modified valence force field was used. This force field consists of the diagonal force constants and a small number of important interaction force constants. A fairly reasonable fit was obtained for frequencies belonging to the arsine donor. However, the results of the BX_3 end of the molecule were less satisfactory. For example, a frequency of 268 cm^{-1} was calculated for the BCl_3 symmetric stretch while it is actually observed at 373 cm^{-1} and is so characteristic there can be no doubt in assignment. It is well established that when non-bonding interactions, such as in CCl_4 and $TiCl_4$, are significant, the Urey-Bradley model is recommended as a better choice of force field (Chapter II). Also, for the sake of comparison with other related molecules such as $PH_3.BX_3$,[58] $MePH_2.BX_3$,[57] $Me_2PH.BX_3$,[24] $Me_3P.BX_3$[25] and $Me_3As.BX_3$,[38] a modified Urey-Bradley force field was adopted. The $MeAsH_2$ end of the molecule was treated entirely as a valence force field which involved the diagonal force constants along with a few important interaction force constants such as f(CH/CH) and f(HCAs/HCAs). The BX_3 part of the molecule and the dative bond were treated as a Urey-Bradley

force field. Two non-bonding repulsion force constants were also included, the F(XX) between halogens and the F(AsX) between arsenic and halogens.

The methyl group modes are well represented by $f(CH^2)$, $f(HCH^2)$, $f(HCAs^2)$, f(CH/CH) and f(HCAs/HCAs) force constants and are very similar to those obtained for $MePH_2.BX_3$. The inclusion of f(HCAs/HCAs) has rendered the values of $f(HCAs^2)$ to be artificially higher than that in free $MeAsH_2$[54] where the interaction force constant f(HCAs/HCAs) was not considered. The increase in $f(AsH^2)$, $f(HAsH^2)$ and $f(CAs^2)$ upon adduct formation is consistent with rehybridization of the donor arsine resulting in strengthening the As-H and C-As bonds. The progressive increase in $f(CAsB^2)$ along the series Cl<Br<I has also been shown to occur for $Me_3As.BX_3$ adducts. The Urey-Bradley K(AsB) exhibits a gradual increase along the sequence $BCl_3<BBr_3<BI_3$ which agrees with the increase in acidity of the BX_3 group along the same sequence. For $MeAsH_2.BX_3$, the average value (mdyne $\AA^{-1}$) of K(AsB) is 1.46, whereas for $Me_3As.BX_3$ it is 1.67,[38] for $MePH_2.BX_3$ it is 1.58[57] and for $Me_3P.BX_3$ it is 2.00.[25] Inherently, the ratio of K(PB) to K(AsB) is 1.14; not very different from the ratio predicted by simply examining the frequency trends. These results are consistent with established orders of base strengths from phosphorus to arsenic

Table III.5 Modified Urey-Bradley force fields of $MeAsH_2.BX_3$.[a,b,c]

Force Constant	X = Cl	X = Br	X = I	$MeAsH_2$
$f(CH^2)$	4.850	4.848	4.836	4.870
$f(HCH^2)$	0.495	0.488	0.488	0.529
$f(HCAs^2)$	0.515	0.519	0.504	0.430
$f(AsH^2)$	2.930	2.880	2.800	2.611
$f(HAsH^2)$	0.674	0.628	0.693	0.646
$f(HAsC^2)$	0.866	0.797	0.850	
$f(HAsB^2)$	0.386	0.403	0.426	
$f(CAsB^2)$	0.549	0.597	0.705	
$f(CAs^2)$	2.878	2.810	2.812	2.466
K(AsB)	1.269(1.78)	1.437(1.79)	1.680(1.92)	
K(BX)	1.460(2.32)	1.179(1.97)	0.800(1.57)	
H(AsBX)	0.189(0.62)	0.338(0.64)	0.405(0.62)	
H(XBX)	0.368(1.07)	0.280(1.13)	0.246(1.33)	
F(XX)	0.529	0.535	0.550	
F(AsX)	0.290	0.190	0.120	
f(CH/CH)	0.038	0.030	0.020	
f(AsH/AsH)	0.028	0.033	0.034	
f(HCAs/HCAs)	-0.085	-0.082	-0.063	

[a] General valence force constants f_{ij}; Urey-Bradley force constants K (stretch), H (bend), F^{ij} (repulsions).

[b] Stretching constants in mdyn $Å^{-1}$ ($10^2 Nm^{-1}$) and bending in mdyn Å rad^{-2} ($10^2 Nm\ rad^{-2}$).

[c] The corresponding F-matrix values are listed in brackets.

Table III.6 Geometric parameters of $MeAsH_2.BX_3$[a]

Parameter	X=Cl	X=Br	X=I
CH	1.09	1.09	1.09
CAs	1.19	1.90	1.93
AsH	1.52	1.52	1.52
AsB	2.065	2.04	2.03
BX	1.83	2.00	2.22
HCH	109.5	109.5	109.5
HCAs	109.5	109.5	109.5
HAsH	100.0	100.0	100.0
HAsC	105.0	105.0	105.0
CAsB	111.0	111.0	111.0
AsBX	109.5	109.5	109.5
XBX	109.5	109.5	109.5

[a]Bond lengths in Å and bond angles in degrees

on one hand and methyl group substitutions on the other hand. The bending force constants H(AsBX) and H(XBX) and the repulsion force constants F(XX) and F(AsX) are close to those reported for related compounds indicating only a slight sensitivity of the BX_3 group with respect to the donor molecule. The value of K(BX) decreases in the order $BCl_3 > BBr_3 > BI_3$ as expected from the relative strengths of these bonds. The F-matrix elements are shown in brackets in Table III.5 for the Urey-Bradley force constants for the sake of comparison with other studies.

CHAPTER IV

VIBRATIONAL AND NORMAL COORDINATE ANALYSIS OF $Me_2AsH.BX_3$ (X=Cl,Br,I)

The fourteen-atom molecules of the $Me_2AsH.BX_3$ adducts were assumed to have C_s point group symmetry. The vibrational representation is $\Gamma_v = 20\ a' + 16a''$ with both modes active in the i.r. and Raman spectra. Similarly, as in the case of $MeAsH_2.BX_3$, the CH_3 and BX_3 vibrations were considered degenerate and symmetric in terms of local group symmetry. The description of normal modes and the numbering of the frequencies are listed in Table IV.1. Spectroscopic information on each adduct along with calculated frequencies and potential energy distributions are shown in Tables IV.2 - IV.4. Figures IV.1 - IV.4 display the i.r. and Raman spectra.

IV.1 The Dimethylarsine Frequencies

The asymmetric (ν_1, ν_2, ν_{21}, ν_{22}) CH_3 stretching vibrations appear in the Raman spectra in the range 3020-3000 cm^{-1} and are almost unshifted relative to those of Me_2AsH[56] and $MeAsH_2.BX_3$ (Chapter III). The polarized band at ca 2930 cm^{-1} in the Raman spectra was associated with the symmetric CH_3 (ν_3, ν_{23}) stretch. The symmetric (ν_7, ν_{26}) and asymmetric (ν_5, ν_6, ν_{24}, ν_{25}) CH_3 deformation modes were assigned to weak bands in the ranges 1190-1265 cm^{-1} and 1400-1420 cm^{-1} respectively as in $MeAsH_2.BX_3$ (Chapter III). The CH_3 rocks (ν_8, ν_9, ν_{27}, ν_{28}) were assigned in the 900-950 cm^{-1} region compared to 912-922 in free Me_2AsH[56] As in $MeAsH_2.BX_3$ series, these

modes in general appear to be shifted slightly to higher frequencies upon adduct formation.

The AsH (ν_4) stretching frequency was assigned with relative ease to the sharp polarized band at ca 2200 cm^{-1} in the Raman effect. This mode lies at considerably higher wave-numbers than in the uncoordinated Me_2AsH[56] where the AsH stretching frequency occurs at 2080 and 2073 cm^{-1} in the i.r. and Raman spectra respectively. The two AsH deformation modes are considered degenerate and were assigned to bands in the 780-810 cm^{-1} region as compared to ca 660 cm^{-1} in Me_2AsH.[56] These vibrations lie in the 800-850 cm^{-1} region in $Me_2PH.BX_3$[24] and ca 720 cm^{-1} in Me_2PH.[65] The AsC_2 stretching modes (ν_{11}, ν_{29}) are considered degenerate occuring at ca 600 cm^{-1} as in $MeAsH_2.BX_3$ (Chapter III). In free Me_2AsH these modes were assigned at ca 580 cm^{-1} and in $Me_3As.BX_3$[38,39] they were assigned in the 575-618 cm^{-1} region. The slight increase towards higher wave-numbers of the CAs stretching mode upon coordination is consistent with strengthening of the CAs bonds by rehybridization as already discussed for the $MeAsH_2.BX_3$ series. The only modes remaining to be assigned are the AsC_2 deformation (ν_{15}) and rocking modes (ν_{16}, ν_{32}). These were assigned to the 220 cm^{-1} and 190 cm^{-1} regions respectively which agreed well with the corresponding motions in $Me_3As.BX_3$.[38,39]

IV.2 The As-B Stretching Frequency

The AsB stretch (ν_{10}) was usually observed as two lines with the lower frequency, more intense line corresponding to that of the ^{11}B isotope and a weak shoulder at higher frequency corresponding to the ^{10}B-As stretch. This vibration appears as a polarized strong bond in the Raman spectra and varies very slightly in the adducts. It has been assigned in the same region in $MeAsH_2.BX_3$ (Chapter III), and in the 650-670 cm^{-1} region in $Me_3As.BX_3$.[38] The analogous PB stretch in $Me_2PH.BX_3$ has been assigned at ca 760 cm^{-1}, and as in Chapter III f_{PB}/f_{AsB} can be calculated to be ca 1.16 thus indicating that the PB bond is stronger than the AsB bond.[31]

IV.3 The BX_3 Frequencies

Other studies [24,25,38,58,60] have provided the basis for the assignments of the vibrations of the BX_3 group. The intense and polarized bonds at 373, 238 and 171 cm^{-1} were assigned to the symmetric BX_3 stretch (ν_{13}) where X = Cl, Br, and I, respectively, hardly different from those in $MeAsH_2.BX_3$ (Chapter III). These modes are shifted to lower wave-numbers in comparison with those for planar uncoordinated BCl_3, BBr_3 and BI_3 at 471, 278 and 190 cm-1, respectively.[61,62] The rehybridization of BX_3 from sp^2 to sp^3 on adduct formation can be considered as the cause of this shift. The asymmetric BX_3 stretching

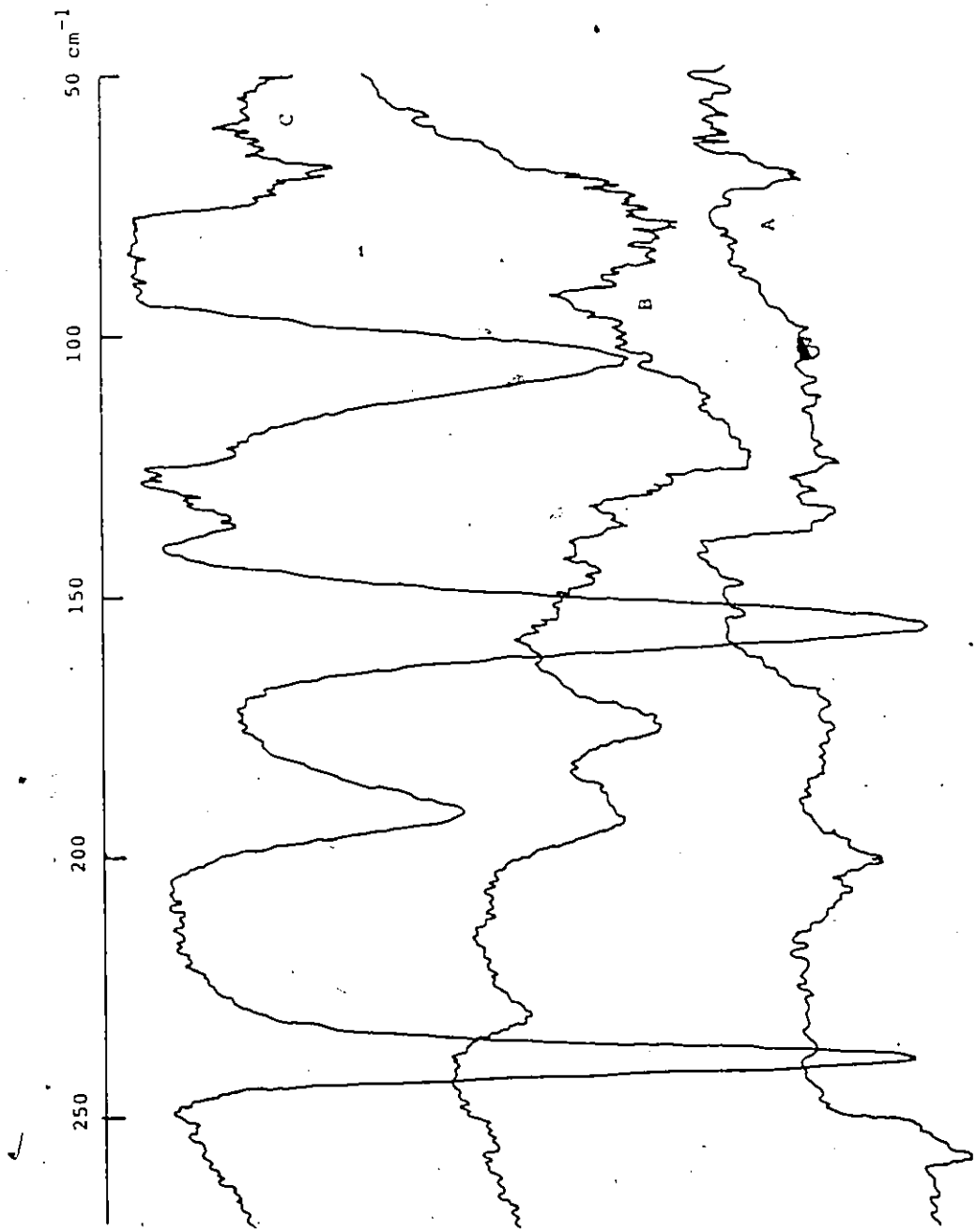

Fig. IV.1. Far i.r. spectra of $Me_2AsH.BCl_3$ (A), $Me_2AsH.BBr_3$ (B), and $Me_2AsH.BI_3$ (C).

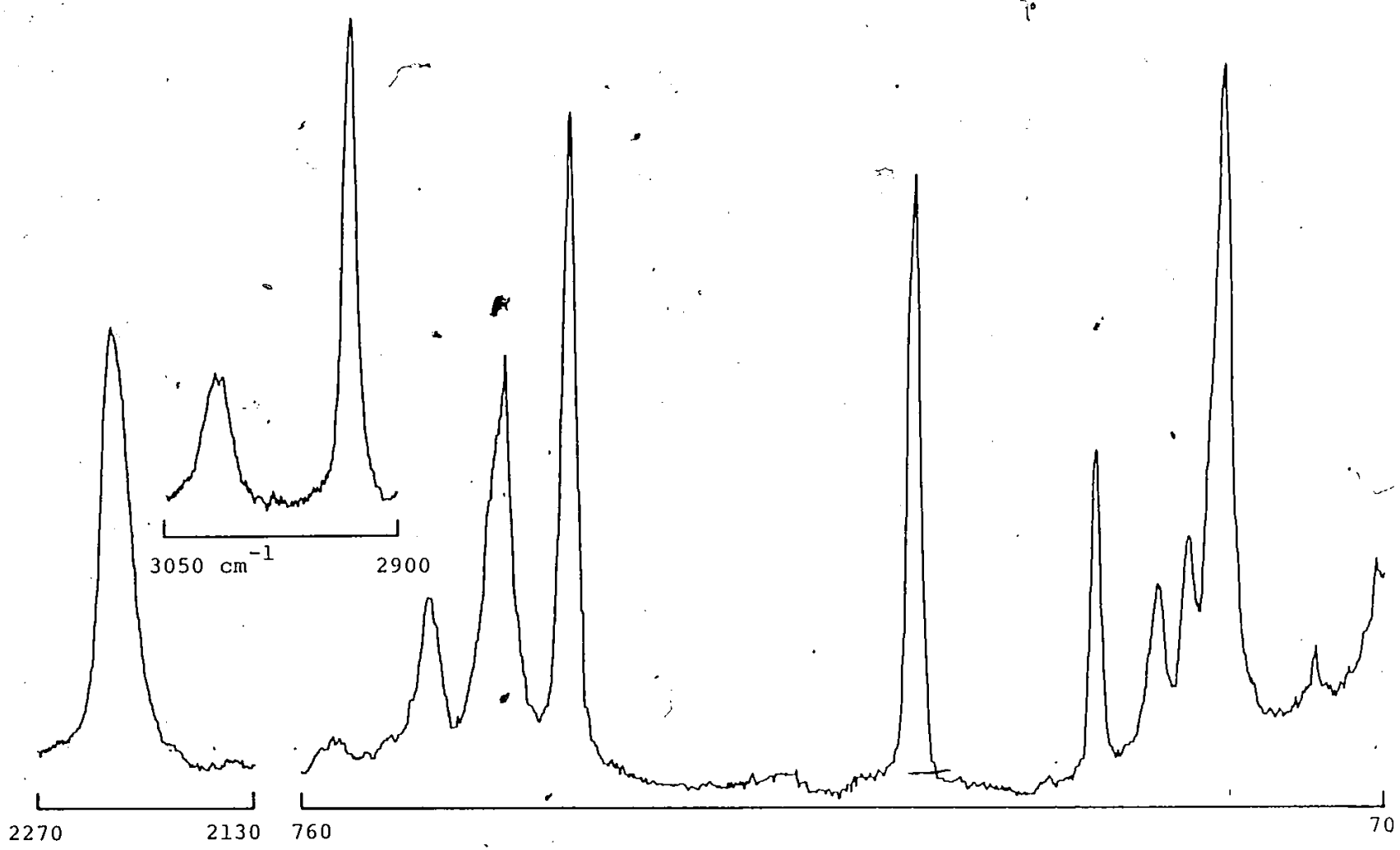

Fig. IV.2. Selected regions of the solid Raman spectrum of $Me_2AsH.BCl_3$.

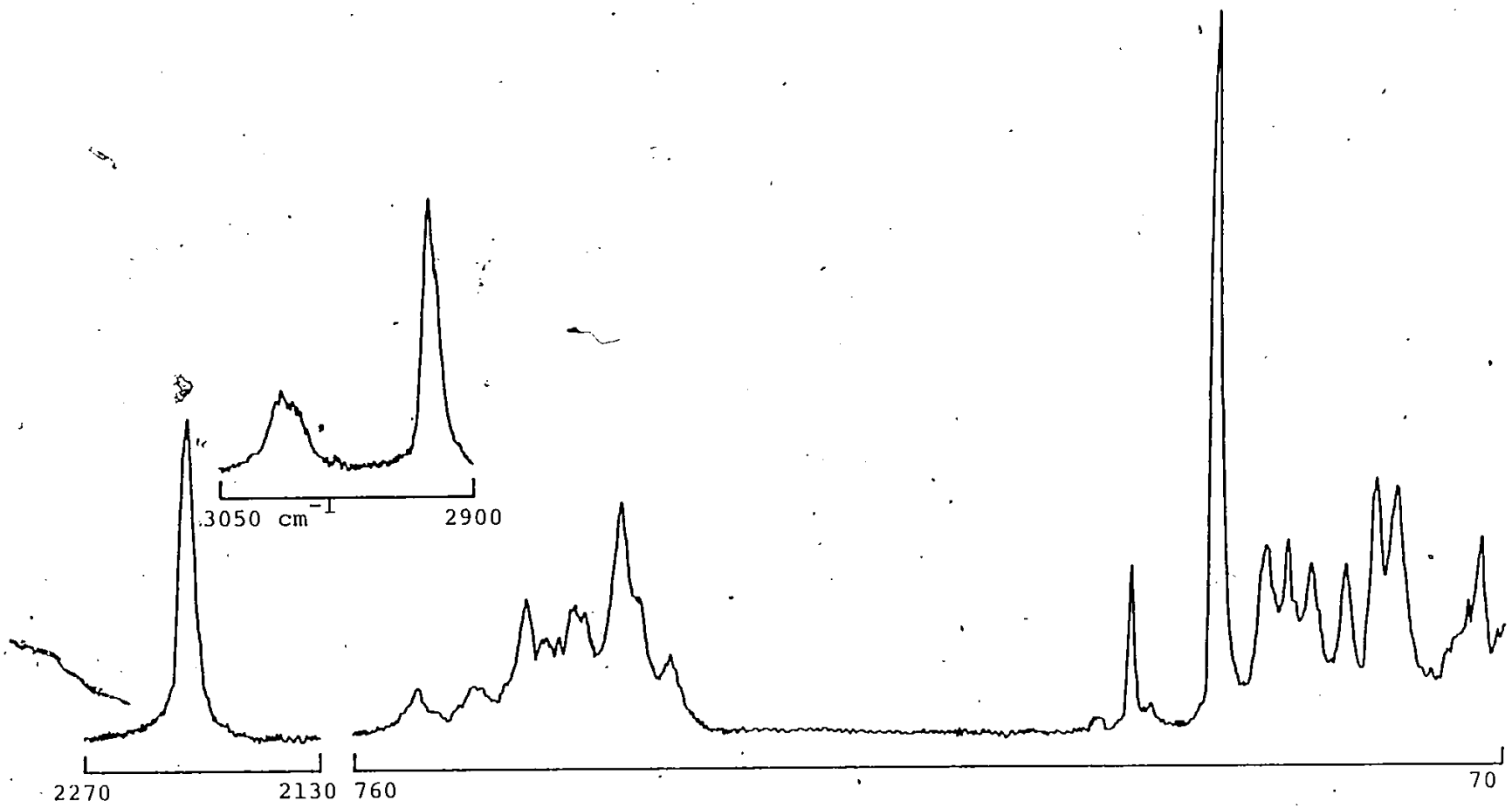

Fig. IV.3. Selected regions of the solid Raman spectrum of $Me_2AsH.BBr_3$.

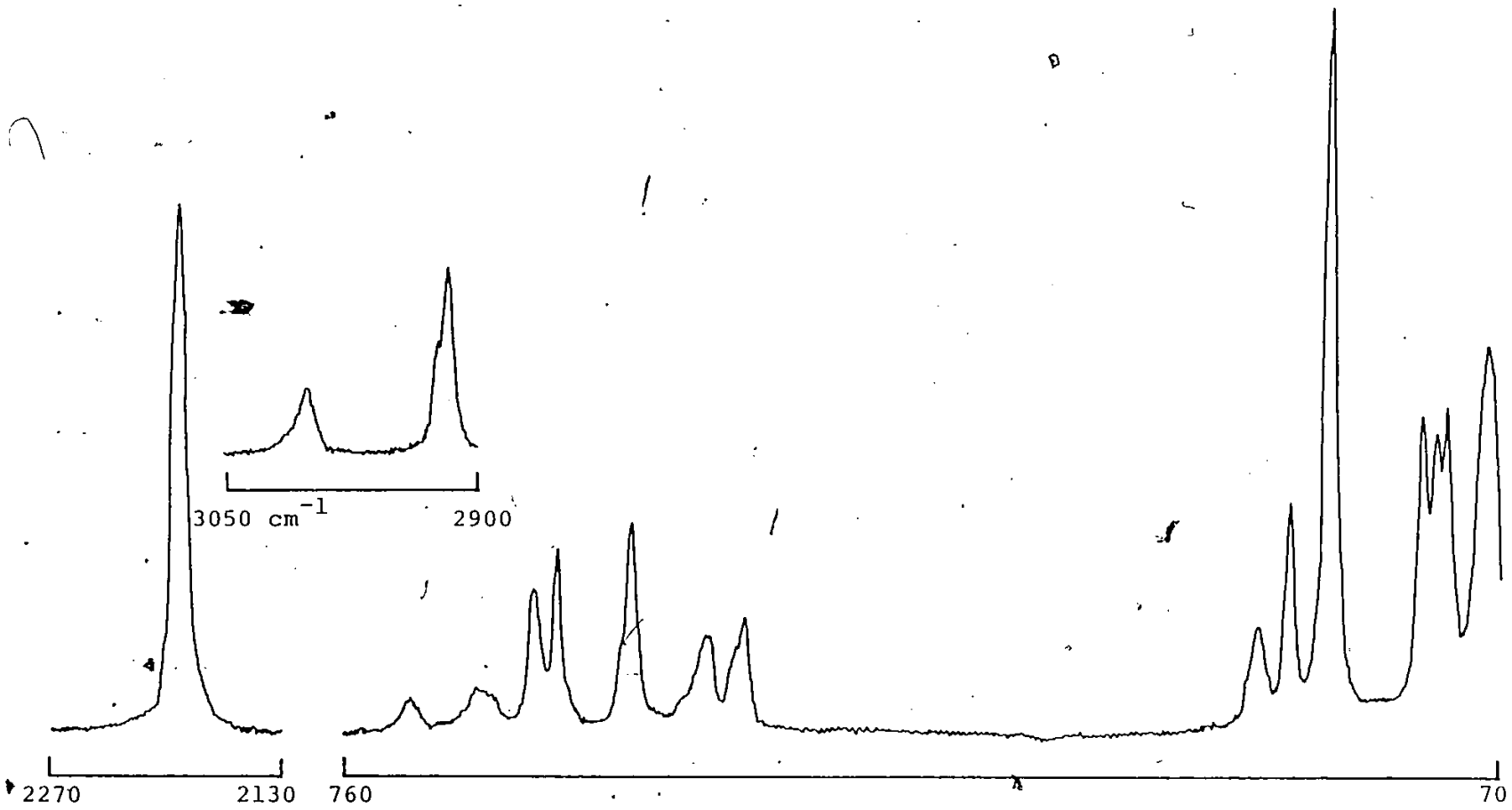

Fig. IV.4. Selected regions of the solid Raman spectrum of $Me_2AsH.BI_3$.

Table IV.1. The approximate description and symmetry species of the fundamental vibrations of $Me_2AsH.BX_3$ (X = Cl,Br,I)

a'	a"	Description
ν_1, ν_2	ν_{21}, ν_{22}	CH_3 stretch (a)
ν_3	ν_{23}	CH_3 stretch (s)
ν_4		AsH stretch
ν_5, ν_6	ν_{24}, ν_{25}	CH_3 def. (a)
ν_7	ν_{26}	CH_3 def. (s)
ν_8, ν_9	ν_{27}, ν_{28}	CH_3 rock
ν_{10}		As-B stretch
ν_{11}	ν_{29}	AsC_2 stretch
ν_{12}	ν_{30}	BX_3 stretch (a)
ν_{13}		BX_3 stretch (s)
ν_{14}	ν_{31}	AsH def.
ν_{15}		AsC_2 def.
ν_{16}	ν_{32}	C-As-B bend
ν_{17}	ν_{33}	BX_3 def. (a)
ν_{18}		BX_3 def. (s)
ν_{19}	ν_{34}	BX_3 rock
ν_{20}	ν_{35}, ν_{36}	torsions

Table IV.2 Observed I.R. and Raman frequencies (cm^{-1}), ± 3 cm^{-1}, for $Me_2AsH.BCl_3$ with potential energy distributions.

Assignment	I.R. KBr[a]	Raman (solid)	Raman (soln)[b]	Calc.	P.E.D.[c]
$\nu_1, \nu_2, \nu_{21}, \nu_{22}$	3020 w	3017 w	solvent	3017	100f(CH^2)-1f(CH/CH)
ν_3, ν_{23}	2933 mw	2931 ms	2932 mw, p	2933	98f(CH^2) + 1f(CH/CH)
ν_4	2220 w	2224 s	2223 s,p	2224	100f(AsH^2)
$\nu_5, \nu_6, \nu_{24}, \nu_{25}$	1400 wbr	1412 w	solvent	1400	92f(HCH^2) + 6(HCAs^2)
ν_7, ν_{26}	1190 s	1192 vw	-	1191	58f(HCH^2) + 59(HCAs^2) − 27 f(HAs/HCAs)
$\nu_8, \nu_9, \nu_{27}, \nu_{28}$	943 w	936 w	-	942	73f(HCAs^2) + 16f(HCAs/HCAs)
ν_{14}, ν_{31}	810 s	817 vw	-	811	34f($CAsH^2$) + 52 f(HAsB^2)
ν_{12}, ν_{30}	705 w	688 m	-	692	70K(BX) + 6H(AsBX) + 8H(XBX)
ν_{10}	650 m	640 s	645 m,p	649	47K(AsB) + 23K(BX) + 8F(XX) + 8H(AsBX) + 8H(XBX)
ν_{11}, ν_{29}	595 w	595 vs	594 ms, p	595	94f(CAs^2)
ν_{13}	373 w	373 vs	362 s,p	371	30K(BX) + 47F(XX) + 10K(AsB) + 10F(AsX)
ν_{17}, ν_{33}	256 mw	254 m	254 m,dp	257	50F(XX) + 10F(AsX) + 12f($CAsB^2$) + 14H(XBX)
ν_{15}	221 w	218 w	223 m,p	226	27f($CAsC^2$) + 20f($CAsB^2$) + 20F(XX) + 14F(AsX)
ν_{16}, ν_{32}	195 w	196 w	194 mw, dp	195	37f($CAsB^2$) + 20F(XX) +19F(AsX) + 11H(XBX)
ν_{18}	173 w	172 vs	177 mw, p	169	12F(XX) + 33F(AsX) + 12K(AsB) + 9H(AsBX)
$\nu_{19}, 34$	136 vw	145 wsh	137 vw, dp	133	40F(AsX) + 23H(AsBX) + 30f($CAsB^2$)

a. Low frequencies taken from far i.r. spectra in nujol; b. spectrum in CH_2Cl_2 and MeI; c. contribution greater than 10% except for significant interactions.

Table IV.3 Observed I.R. and Raman frequencies (cm^{-1}) ± 3 cm^{-1}, for $Me_2AsH.BBr_3$ with potential energy distributions

Assignment	I.R. KBr [a]	Raman (solid)	Raman (soln.) [b]	Calc.	P.E.D. [c]
$\nu_1, \nu_2, \nu_{21}, \nu_{22}$	3018 mw	3014 w	solvent	3014	100f(CH^2) - 1f(CH/CH)
ν_3, ν_{23}	2940 mw	2926 m	2930 mw,p	2940	98f(CH^2) + 2f(CH/CH)
ν_4	2217 w	2208 m	2220 mw,p	2217	100f(AsH^2)
$\nu_5, \nu_6, \nu_{24}, \nu_{25}$	1410 s	1407 w	solvent	1409	93f (HCH^2) + 6f($HCAs^2$)
ν_7, ν_{26}	1265 ms	1272 vw	1280 w,p	1266	53f(HCH^2) + 54f($HCAs^2$) - 15f(HCAs/HCAs)
$\nu_8, \nu_9, \nu_{27}, \nu_{28}$	920 s	928 vw	-	920	79f($HCAs^2$) + 11f(HCAs/HCAs)
ν_{14}, ν_{31}	805 m	799 vw	-	803	37f($CAsH^2$) + 54f($HAsB^2$)
ν_{10}	650 w	655 m	649 vw,p	661	58K(AsB) + 15K(BX) + 6F(XX) + 9H(AsBX)
ν_{12}, ν_{30}	631 s	623 s	628 vwdp?	621	63K(BX) + 10H(AsBX)
ν_{11}, ν_{24}	600 ms	596 ms	595 m,p	595	88f(CAs^2)
ν_{13}	238 m	240 mw	240 vs,p	249	31K(BX) + 36F(XX) + 10F(AsX)
ν_{15}	213 vw	212 w	210 vw,p	212	34f($CAsC^2$) + 32f($CAsB^2$) + 20F(XX)
ν_{16}, ν_{32}	183 mw	185 mw	189 vw,dp	188	48f($CAsB^2$) + 19K(BX) + 19F(XX) + 8F(AsX)
ν_{17}, ν_{33}	146 m	147 w	149 w,dp	151	61F(XX) + 18H(XBX) + 13f($CAsB^2$)
ν_{18}	126 vw	135 m	130 w,p	130	20F(XX) + 25F(AsX) + 15K(AsB) + 10H(XBX) + 10H(AsBX)
ν_{19}, ν_{34}	97 m	92 vw	-	95	36F(AsX) + 46H(AsBX) + 14f($CAsB^2$)

[a] Low frequencies taken from far i.r. spectra in nujol; b. spectrum in CH_2Cl_2 and MeI; c. contribution greater than 10% except for significant interactions.

Table IV.4 Observed I.R. and Raman frequencies (cm^{-1}), ± 3 cm^{-1}, for $Me_2AsH.BF_3$ with potential energy distributions

Assignment	I.R. KBr[a]	Raman (solid)	Raman (soln.)[b]	Calc.	P.E.D.[c]
ν_1 ν_2 ν_{21},ν_{22}	3019 w	3000 w	solvent	3019	100f(CH^2) - 1f(CH/CH)
ν_3,ν_{23}	2925 m	2915 m	2928 w,p	2925	98f(CH^2) + 1f(CH/CH)
ν_4	2195 vw	2194 s	-	2195	100f(AsH^2)
ν_5,ν_6,ν_{24},ν_{25}	1405 w	1402 vw	-	1405	94f(HCH^2) + 5f(HCAs^2)
ν_7,ν_{26}	1255 w	1258 vw	1262 w,p	1256	53f(HCH^2) + 53f(HCAs^2) - 14f(HCAs/HCAs)
ν_8,ν_9,ν_{27},ν_{28}	905 s	916 vw	-	905	80f(HCAs^2) + 11f(HCAs/HCAs)
ν_{14},ν_{31}	780 w	784 vw	-	781	38f(CAsH^2) + 56f(HAsB^2)
ν_{10}	643 m	646 mw	642 w,p	649	64K(AsB) + 8K(BX) +8H(AsBX) + 6F(XX)
ν_{11},ν_{29}	590 ms	589 mw	585 mw,p	590	81f(CAs^2)
ν_{12},ν_{30}	539 s	520 s	532 w,dp	530	54K(BX) + 9f(CASB^2) + 16H(AsBX)
ν_{15}	219 w	213 m	227 m,p	223	30f(CAsC^2) + 44f(CAsB^2) + 10K(BX)
ν_{16},ν_{32}	197 mw	195 mw	-	188	69f(CAsB^2) + 20K(BX)
ν_{13}	171 m	168 vs	173 s,p	176	26K(BX) + 57F(XX)
ν_{17},ν_{33}	123 m	115 m	118 w,dp	119	79 F(XX) + 11H(XBX)
ν_{18}	110 sh	109 m	112 w,sh	114	37F(XX) + 19F(AsX) + 11K(AsB) + 15H(AsBX) + 9H(XBX)
ν_{19},ν_{34}	85 w	78 w	-	81	32F(AsX) + 51H(AsBX)

[a] Low frequencies taken from far i.r. spectra in nujol; b. spectrum in CH_2Cl_2 and MeI; c. contribution greater than 10% except for significant interactions.

vibrations (ν_{12}, ν_{30}) were associated with bands at 705, 625 and 539 cm^{-1} compared to those assigned at 710, 620 and 540 cm^{-1} in $Me_2PH.BX_3$.[24] In free planar BX_3, these modes occur at 956, 819 and 704 cm^{-1} for BCl_3, BBr_3 and BI_3, respectively.[61,62] The deformation modes (ν_{17}, ν_{33} and ν_{18}) were assigned at 256, 173; 146, 128; 123, 110 cm^{-1} for the asymmetric and symmetric vibrations of the BCl_3, BBr_3 and BI_3 adducts, respectively. These are consistent with assignments of the same modes in $MeAsH_2.BX_3$ (Chapter III) indicating the negligible significance of the nature of the arsine with respect to the skeletal BX_3 motions. The low frequency bands at 136, 97 and 85 cm^{-1} were associated with the rocking modes (ν_{19}, ν_{34}) of BX_3.

IV.4 Normal Coordinate Analysis

The calculated frequencies and the potential energy distributions are presented in Tables IV.2 - IV.4. The force constants for the adducts and free arsine are listed in Table IV.4. The structural parameters (presented in Table IV.6) were based initially on the parameters of Me_2AsH[56] and $Me_2PH.BX_3$.[24] The structures of $Me_3As.BX_3$ were determined later[64] and as a result the geometric parameters were slightly adjusted. However, the calculations were not affected in any significant way. The i.r. and Raman spectra were both employed to fit the calculated frequencies. The force constant

calculations were performed in an exactly analogous manner as for the $MeAsH_2.BX_3$ series in Chapter III. Thus as was the case with $Me_2AsH.BX_3$, the Me_2AsH end of the molecule was treated entirely as a valence force field which involved the diagonal force constants along with a few important interaction force constants such as f(CH/CH) and f(HCAs/HCAs). The BX_3 part of the molecule, along with the coordinate AsB bond, was treated by using a Urey-Bradley force field. Two non-bonding Urey-Bradley interactions were also included, the F(XX) between the halogens on boron, and the F(AsX) between arsenic and the halogens on boron.

Judging by the good correspondence between the calculated and observed frequencies, the force-field model can be considered reasonable. The methyl group vibrations are well represented by $f(CH^2)$, $f(HCH^2)$, f(CH/CH) and f(HCAs/HCAs) force constants and these are similar to those calculated for $Me_2PH.BX_3$.[24] The increase in $f(CAs^2)$ and $f(CAsH^2)$ upon adduct formation is consistent with rehybridization of arsenic allowing for more s-character, and hence stronger CAs and AsH bonds. The Urey-Bradley K(AsB) displays a gradual increase along the series $BCl_3<BBr_3<BI_3$ and that agrees with the established order of the BX_3 group Lewis acidity. The average value of K(AsB) is 1.46, 1.495 and 1.67 for $MeAsH_2.BX_3$, $Me_2AsH.BX_3$

Table IV.5 Modified Urey-Bradley force fields of $Me_2AsH.BX_3$[a,b,c]

Force Constant	X = Cl	X = Br	X = I	Me_2AsH
f(CH^2)	4.845	4.846	4.840	4.84
f(HCH^2)	0.487	0.499	0.494	0.45
f(HCAs^2)	0.497	0.509	0.494	0.49
f(CAsH^2)	0.612	0.606	0.569	0.85
f(CAsC^2)	0.523	0.505	0.540	0.84
f(CAsB^2)	0.706	0.697	0.980	
f(HAsB^2)	0.469	0.462	0.447	
f(AsH^2)	2.880	2.857	2.800	2.55
f(CAs^2)	2.811	2.812	2.800	2.59
K(AsB)	1.245(1.80	1.560(1.89)	1.680(1.96)	
K(BX)	1.471(2.35)	1.190(1.98)	0.770(1.53)	
H(AsBX)	0.294(0.77)	0.408(0.70)	0.495(0.74)	
H(XBX)	0.298(1.00)	0.280(1.13)	0.197(1.26)	
F(XX)	0.530	0.535	0.540	
F(AsX)	0.318	0.180	0.140	
f(CH/CH)	0.036	0.047	0.030	0.049
f(CAs/CAs)	0.152	0.143	0.117	
f(HCAs/HCAs)	-0.103	-0.068	-0.064	

[a] General valence force constants f_{ij}; Urey-Bradley force constants K (stretch), H (bend), F (repulsions).

[b] Stretching constants in mdyn Å^{-1} (10^2Nm^{-1}) and bending in mdyn Å rad^{-2} (10^2Nm rad^{-2}).

[c] The corresponding F-matrix values are listed in brackets.

Table IV.6 Geometric parameters of $Me_2AsH.BX_3$[a]

Parameter	X=Cl	X=Br	X=I
CH	1.09	1.09	1.09
CAs	1.90	1.90	1.93
AsH	1.52	1.52	1.52
AsB	2.065	2.04	2.03
BX	1.83	2.00	2.22
HCH	109.5	109.5	109.5
HCAs	109.5	109.5	109.5
HAsC	107.0	107.0	107.0
CAsC	107.0	107.0	107.0
CAsB	111.0	111.0	111.0
AsBX	109.5	109.5	109.5
XBX	109.5	109.5	109.5

[a]Bond lengths in Å and bond angles in degrees.

and $Me_3As.BX_3$,[38] respectively. The average value of K(PB) is 1.58, 1.827 and 2.00 for $MePH_2.BX_3$,[57] $Me_2PH.BX_3$[24] and $Me_3P.BX_3$,[25] respectively. The average ratio of K(PB) to K(AsB) can be calculated to be 1.17; not very different from the ratio calculated in Chapter III. It is notable also that the values of K(AsB) in these $Me_2AsH.BX_3$ molecules fall between those of $MeAsH_2.BX_3$ (Chapter III) and $Me_3As.BX_3$[38] series, and this is consistent with an increase in Lewis basicity along the series $MeAsH_2$<Me_2AsH<Me_3As.

CHAPTER V

A ^{11}B N.M.R. SPECTROSCOPIC INVESTIGATION OF Me_nAsH_{3-n} ADDUCTS OF BORON TRIHALIDES (n = 1,2,3)

V.1 Introduction

The halides of boron, their preparation, structures and chemistry have been extensively studied. They are strong Lewis acids and coordinate with a wide range of donor Lewis bases to form simple 1:1 adducts. Several reviews of their chemistry have appeared.[1,66-69] The adducts of the mixed trihalides of boron have been the subject of a well written review.[70] Many articles have been dedicated to the ^{11}B n.m.r. spectroscopy of the mixed free trihalides of boron.[71-73] It is common practice to consider the ^{11}B chemical shifts as a gauge of the electron density on boron.[74-75] Therefore, when a donor-acceptor bond is formed between a trivalent boron halide and a donor, the fourth bonding electron pair around boron increases the shielding of the boron nucleus. Thus, the chemical shift trend toward high field on complexation is accepted as a measure of the donor-acceptor bond strength. Also, it seems reasonable to expect that the order of ^{11}B chemical shifts for a series of adducts of a fixed boron acid can be indicative of the relative donor strength toward that particular boron acid.

The order of acceptor strength once believed to be $BF_3>BCl_3>BBr_3>BI_3$[76] has been found to be opposite to the order assumed with respect to electronegativity.[16,77] The rationale behind the order of acidity $BI_3>BBr_3>BCl_3>BF_3$

is suggested in terms of (p-p) π bonding between the vacant p_z boron orbital and the occupied non-bonding orbitals on the halogens.[78] On adduct formation, the boron halide must lose its planar sp^2 arrangement and achieve a near-tetrahedral configuration around boron. For that to happen, energy is needed to overcome the bond energy associated with the delocalized π-system. In addition, energy is required for small changes in the BX σ-bonding on rehybridization. The sum of these two quantities is called the reorganization energy which has been determined for all boron trihalides except for BI_3.[78] Based on the determination of ionization potentials, molecular orbital calculations and nuclear quadrupole resonance results,[79,80] it has been suggested that the back-donation order is $BI_3 > BBr_3 \approx BCl_3 > BF_3$, which is opposite to that above. However, other workers[81] have argued that stabilization due to back-bonding is in the opposite order and thus consistent with BI_3 requiring the least deformation energy.

Many methods have been employed to assess the stability of these addition complexes and to evaluate the relative Lewis acidity and basicity.[82] Gas phase dissociation data have shown the order of stability of some BMe_3 adducts to be $H_3N.BMe_3 < MeH_2N.BMe_3 < Me_3N.BMe_3 < Me_2HN.BMe_3$.[83,84] Miller and Onyszchuk[15] have employed gas phase displacement reactions of boron trihalides from their trimethylamine

adducts to show that the order of Lewis acidity is $BBr_3 > BCl_3 > BF_3 > BH_3$. Other similar studies have also been carried out.[48,85,86] On adduct formation significant rehybridization of the donor and acceptor orbitals takes place. The coupling constant values are affected directly by this rehybridization. For example, the coupling constant (J_{PB}) between phosphorus and boron in the PH_3 and $MePH_2$ adducts[28] has been used as an index of relative acceptor strength of boron trihalides. The order was found to be: $BI_3 > BBr_2I > BClI_2 > BCl_2I > BBr_2I > BBr_3 > BCl_3$. Although the order of acidity of the unmixed boron trihalides was in agreement with expectation, the order of the mixed halides between BI_3 and BBr_3 varied from the PH_3 to the $MePH_2$ adducts. The ^1H n.m.r. complexation shifts have been utilized to estimate the order of acid strength. The acceptor power of boron trihalides toward trimethylamine[87] has been correlated to the additivity of the halogen substituents and the order was found to be $BI_3 > BBrI_2 > BBr_2I > BClI_2 > BBr_3 > BClBrI > BClBr_2 > BCl_2I > BCl_2Br > BCl_3$. This order has been explained in terms of π-bonding from halogen to boron in the free acids and the survival of some residual π -bonding in the adducts.[88] Both $\delta^{11}B$ and $\Delta\delta^{11}B$ [$\delta^{11}B(\text{adduct}) - \delta^{11}B(BX_3)$] were used to indicate relative acidities of boron trihalides.[27,46,89] Several authors[90-94] attributed the shielding difference $\Delta\delta^{11}B$ for the same boron compound on complexation with

various Lewis bases to the difference in the donor-acceptor bond strength. The order of base strength has been found to vary from one boron trihalide to the other. In a study[91] of the adducts of pyridine, triethylamine and benzophenone, the order of Lewis basicity was found to be $Py>Et_3N>Ph_2CO$ toward BF_3 and $PH_2CO>Py>Et_3N$ toward BBr_3. These variations were ascribed to the extent of face-to-face steric hindrance[95] encountered between the donor and the acceptor. ^{15}N, ^{19}F and ^{31}P n.m.r. studies have also been carried out in attempts to provide a better understanding of such systems.[27,96,97]

It is clear that the ^{11}B chemical shifts cannot be considered as sensitive indicators of donor strength and therefore, a simple relationship between the ^{11}B chemical shifts and donor strength is not to be expected. Also, the nature of the donor molecules in this study, Me_nAsH_{3-n} (n = 1,2,3) makes it difficult to include other parameters like J_{As-B}, the coupling constant between arsenic and boron.

V.2 Experimental

All adducts were prepared by direct combination as described in the beginning of part two of this manuscript and thus will not be repeated here. Since the $MeAsH_2$ adducts were found to be prone to decomposition, the ^{11}B n.m.r. spectra were recorded at -20°C.

V.3 Results and Discussion

All ^{11}B chemical shifts and the mean complexation shifts $\bar{\Delta}\delta^{11}B$ are listed in Table V.1. Fig. V.1 displays the changes in the ^{11}B chemical shifts across the series BCl_3, BBr_3 and BI_3. Typical ^{11}B n.m.r. spectra for the $MeAsH_2/BCl_3/BBr_3$, $Me_2AsH/BBr_3/BI_3$, $Me_3As/BCl_3/BI_3$, and $Me_3As/BCl_3/BBr_3/BI_3$ systems are shown in Figs. V.2, V.3, V.4 and V.5 respectively.

The only ^{11}B chemical shift data available[37] are those of $Me_3As.BBr_3$ and $Me_3As.BI_3$ at - 16.4 and -38.1 ppm respectively from external $Et_2O.BF_3$. Our results agree with that for $Me_3As.BBr_3$ but not with $Me_3As.BI_3$. It is important to mention that the $Me_3As.BI_3$ compound was found to decompose in chloroform[37] depositing a red brown precipitate believed to be a mixture of $[Me_3AsI^+]I^-$ and $[Me_3AsI]^+ I_3^-$.[98,99] All ^{11}B n.m.r. spectra were recorded in CD_2Cl_2 solutions from which good quality crystals were grown (Chapter VI) thus indicating the reliability of results obtained in this investigation.

As expected, the increased shielding of the boron atom in the adducts is characterized by an upfield trend in the chemical shift. The mean shift difference $\bar{\Delta}\delta^{11}B$ increases in the same accepted order of Lewis acidity: $BI_3 > BBr_3 > BCl_3$. The $\bar{\Delta}\delta^{11}B$ values of 72.11, 56.27 and 43.22 agree with those obtained for methylated phosphine adducts[27] which

Table V.1. ^{11}B chemical shifts of unmixed and mixed boron halides adducts of Me_nAsH_{3-n} (n = 1,2,3)[a]

	$\delta^{11}B$ Chemical Shifts				
		Adducts of			
	Free acid[b]	$MeAsH_2$[c]	Me_2AsH	Me_3As	$\overline{\Delta\delta}^{11}B$[d]
BCl_3	+46.91(+46.96)	+3.92	+3.33	+3.81	43.22
BCl_2Br	+45.66(+45.34)	-2.50	-2.32	-1.79	47.86
$BClBr_2$	+43.04(+42.88)	-9.82	-9.22	-8.16	52.10
BBr_3	+39.29(+39.20)	-18.33	-17.26	-15.36	56.23
BCl_2I	+36.79(+36.30)	-16.19	-16.30	-14.46	52.44
BClBrI	+32.56(+32.10)	-26.01	-24.87	-22.80	57.08
BBr_2I	+27.3(+27.00)	-36.79	-34.52	-32.03	61.74
$BClI_2$	+18.87(+18.30)	-45.48	-43.00	-40.54	61.87
$BBrI_2$	+12.09(+11.80)	-58.52	-55.24	-51.73	67.25
BI_3	-7.44(-6.90)	-84.53	-79.51	-74.53	72.11

[a] Values are relative to external $Et_2O.BF_3$, positive shifts refer to low field.

[b] Literature values from references 71-73, 89 are listed in brackets.

[c] Recorded at -20°C to minimize decomposition.

[d] $\overline{\Delta\delta}^{11}B = \left| \frac{\Sigma\delta^{11}B(\text{adduct}) - \delta^{11}B(\text{free acid})}{3} \right|$

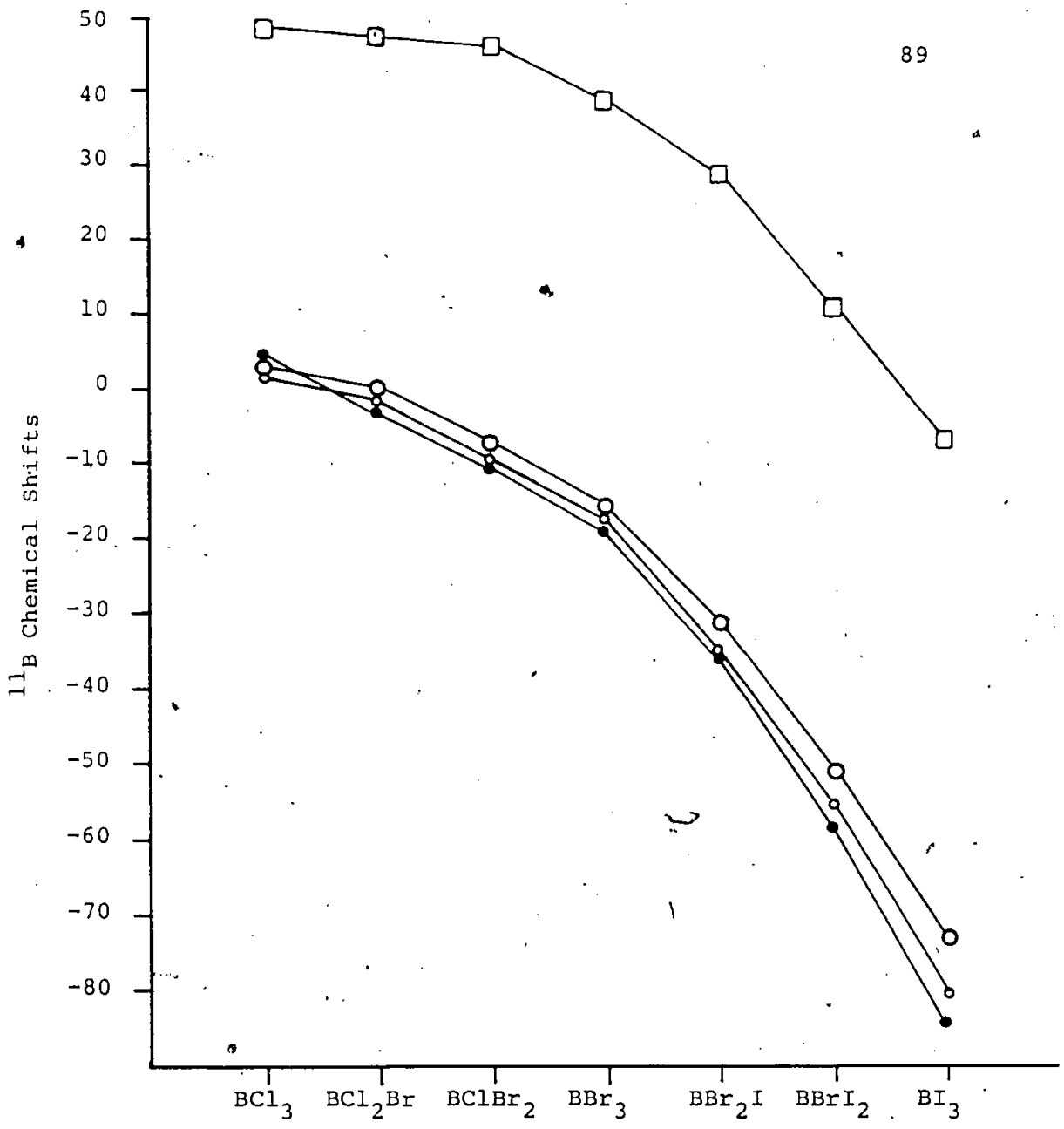

Fig. V.1. Changes in ^{11}B chemical shifts across the series BCl_nBr_{3-n} and BBr_nI_{3-n} (n = 1,2,3) for the $MeAsH_2$ ●, Me_2AsH ◐, and Me_3As ○ adducts and free boron halides □.

are 73.9, 56.9 and 44.3 for the BI_3, BBr_3 and BCl_3 adducts respectively. The order of the mixed and unmixed boron trihalides is almost the same as that of the free boron trihalides which might suggest weak acid-base bonding. The only exception is that BBr_3 was found to cause a greater shift than BCl_2I, implying it is a stronger acid, although the order is opposite in the uncoordinated acids.

In Fig. V.1, the trends are similar to those observed for the Me_2S and Me_3N[100] adducts including the divergence encountered which is parallel to the acceptor ability. $BI_3 > BBr_3 > BCl_3$. A glance at Fig. V.1 leads one to believe that the order of Lewis basicity is $MeAsH_2 > Me_2AsH > Me_3As$, an order which is exactly opposite to the one expected from the inductive effect of the methyl group. However, it is some consolation to note the literature is full of examples where the ^{11}B chemical shifts predict the opposite order of basicity.[3,27,47,101]

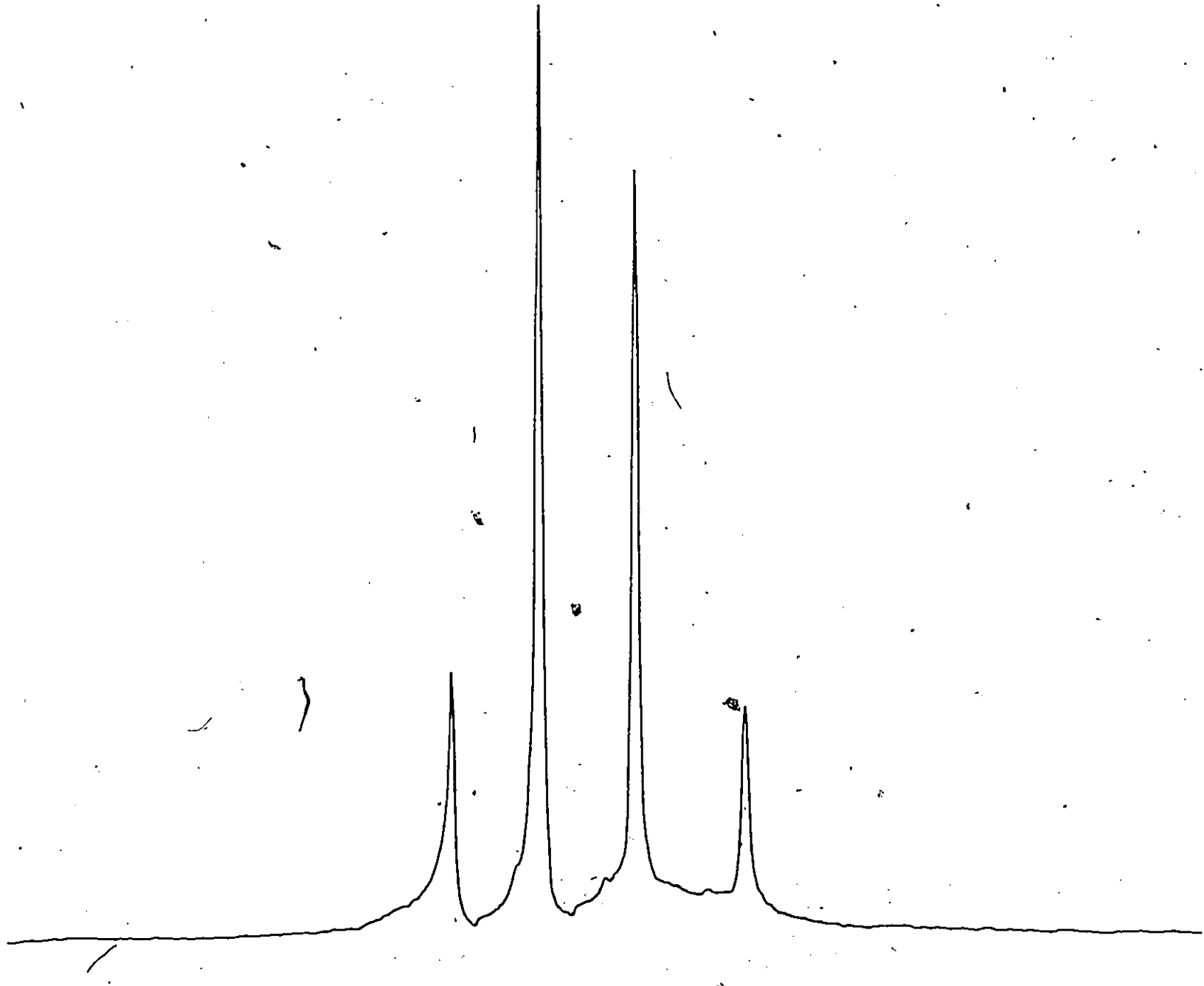

Fig. V.2. The ^{11}B n.m.r. spectrum of $MeAsH_2/BCl_3/BBr_3$ system.

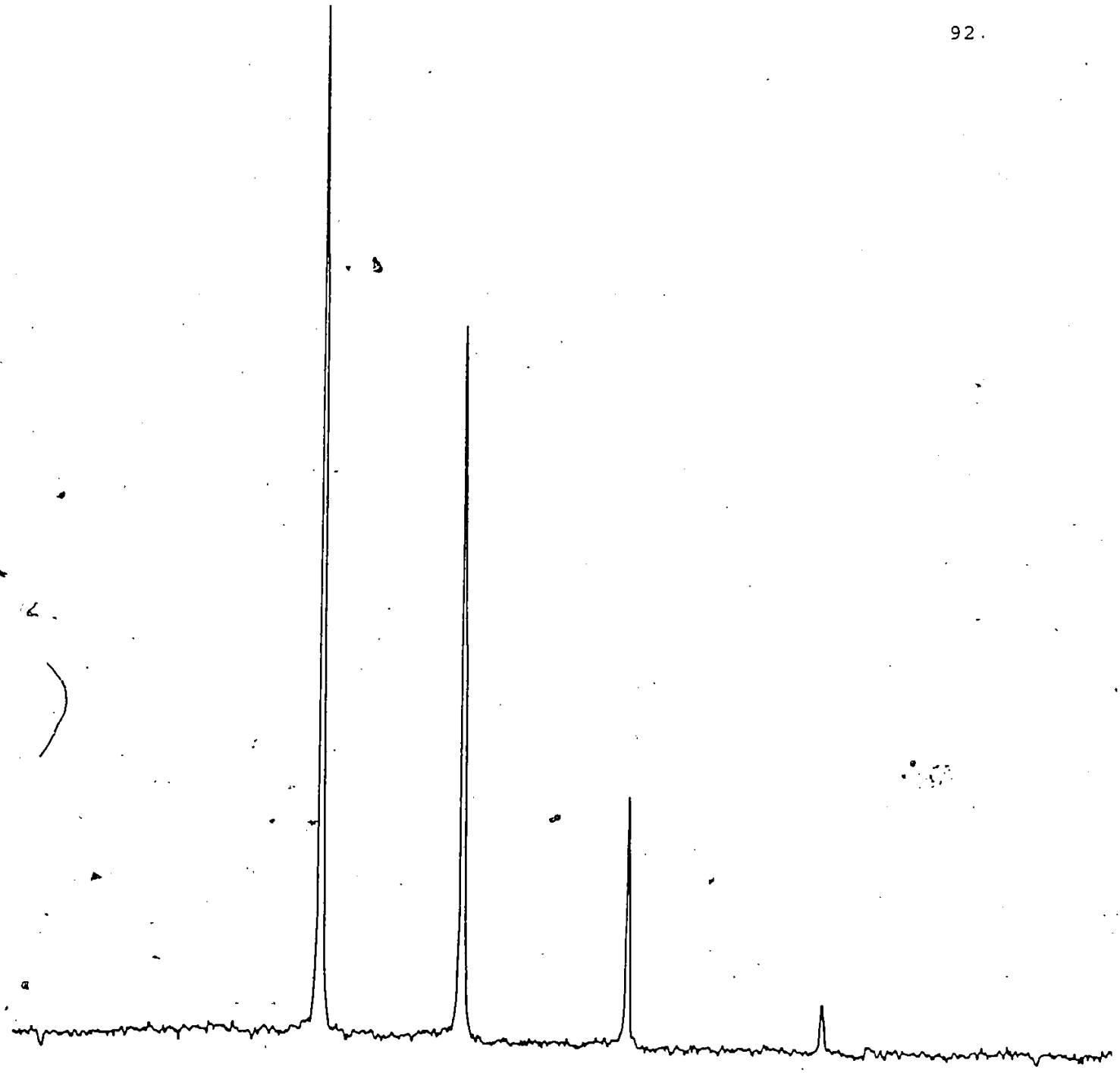

Fig. V.3. The ^{11}B n.m.r. spectrum of $Me_2AsH/BBr_3/BI_3$ system.

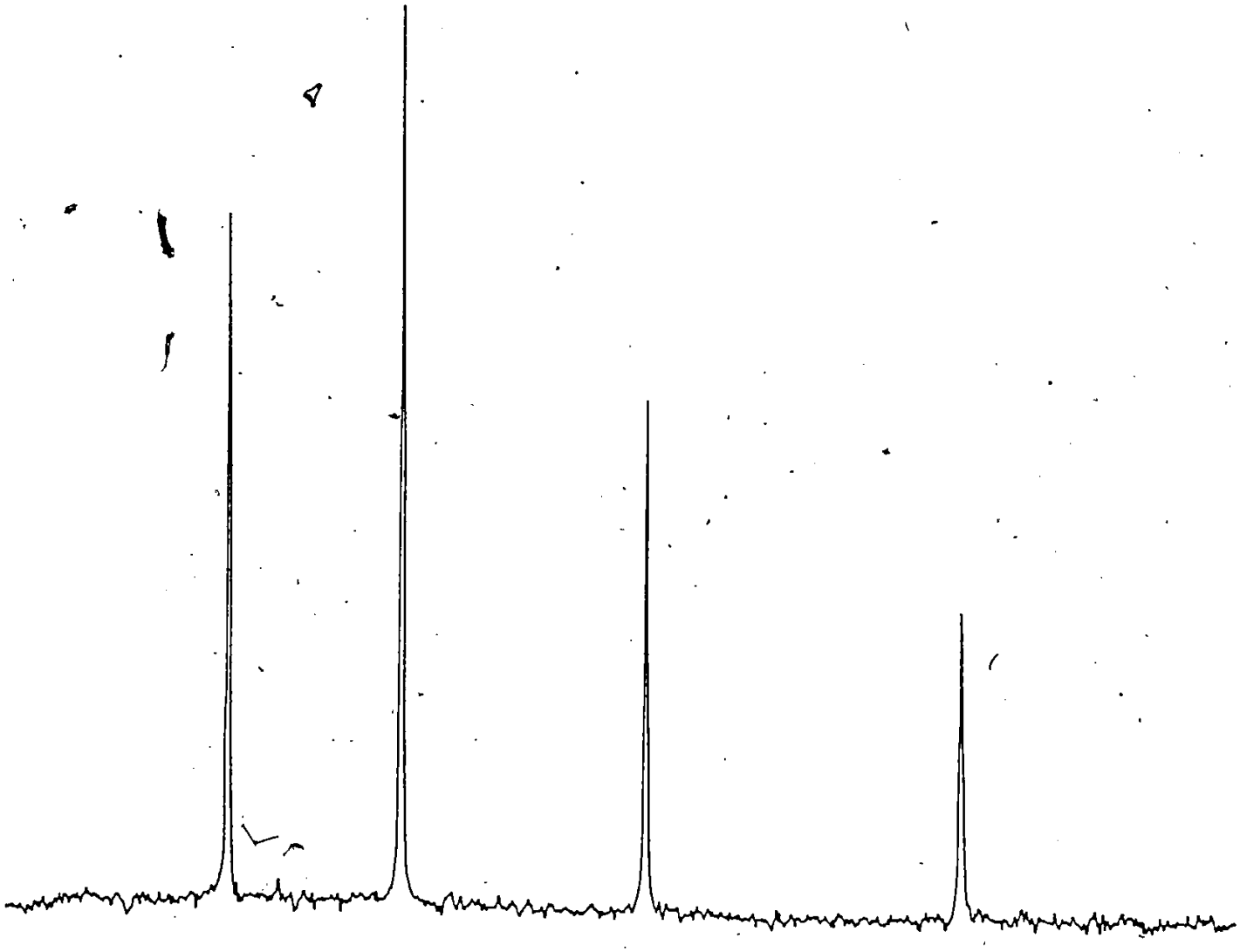

Fig. V.4. The ^{11}B n.m.r. spectrum of $Me_3As/BCl_3/BI_3$ system.

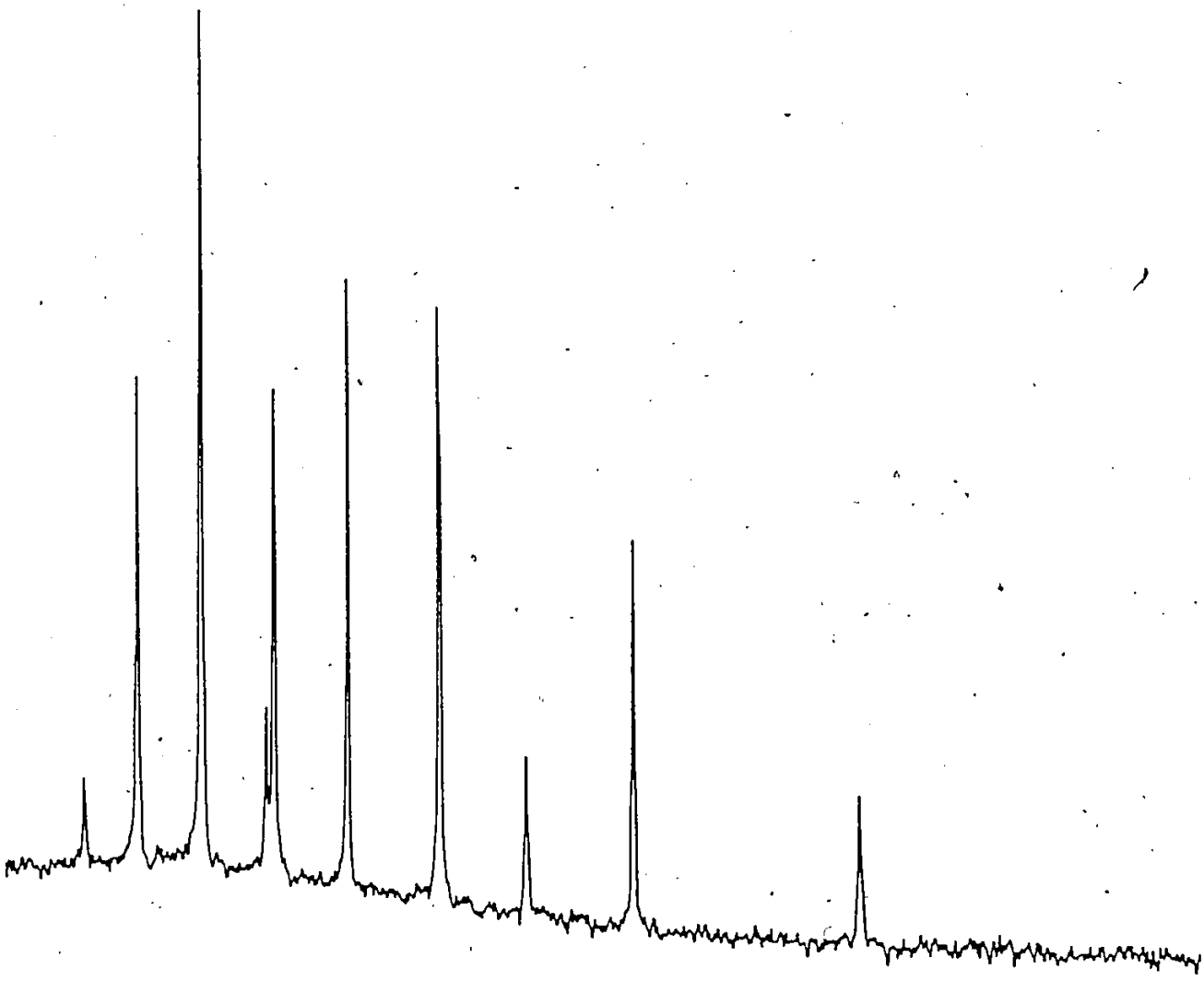

Fig. V.5. The ^{11}B n.m.r. spectrum of $Me_3As/BCl_3/BBr_3/BI_3$ system.

CHAPTER VI

THE CRYSTAL STRUCTURES OF $Me_3As.BX_3$ ADDUCTS (X = Cl,Br,I)

VI.1 Introduction

For some time there has been an interest at Windsor in the adducts of boron trihalides with Lewis bases of the group V elements. The work has been centered on the adducts of phosphine and methylphosphine, with particular emphasis on vibrational spectroscopy supported by normal coordinate analysis[24,25,58] and n.m.r. spectroscopy.[47,58] Recently Drake et al. have studied the vibrational spectroscopy of the trimethylarsine and triphenylarsine adducts of boron trihalides.[38] These spectroscopic studies lead to discussions of relative bond strengths, bond lengths, bond angle changes and relative Lewis acid and Lewis base strengths. Structural studies have been carried out elsewhere on $Me_3N.BX_3$[9] and $Me_3P.BX_3$[26] but no such studies are available for the $Me_3As.BX_3$ compounds.

VI.2 Experimental

All these compounds were prepared by the direct combination of trimethylarsine and boron trihalide using a vacuum line and inert atmosphere techniques as described earlier in this manuscript (Preparations, in Part Two) Crystals were grown over a period of 3-4 weeks in sealed tubes of methylene chloride solutions. The densities were measured by the flotation method in CCl_4/CH_3I for the chloride and CH_3I/CH_2I_2 for the bromide and iodide compounds.

The crystal and refinement data are summarized in Table VI.1. In each determination, a colorless cylindrical crystal sealed in a capillary tube was mounted along the largest dimension, which was subsequently shown to be the c axis, and data were collected with a Syntex $P2_1$ diffractometer using a highly oriented graphite monochromotor. The intensities of three monitor reflections did not change significantly during data collection. Systematic absences of 0k0 were noted for odd k in $(CH_3)_3As.BCl_3$ and $(CH_3)_3As.BBr_3$ indicating the choice of space group $P2_1$ or $P2_1/m$. The systematic absences (0kl, k+l = 2n+1, hk0, h = 2 n+1) in $(CH_3)_3AsBI_3$ indicated Pnma or $Pn2_1a$. The data were corrected for Lorentz and polarization effects, and analytical absorption corrections were applied.

The structure of $(CH_3)_3As.BCl_3$ was solved by using conventional sharpened Patterson synthesis and those of $(CH_3)_3As.BBr_3$ and $(CH_3)_3As.BI_3$ by the direct methods using the program SHELX. Upon refinement of the structure of $(CH_3)_3As.BCl_3$ by the full matrix least squares method, it was observed that a mirror symmetry was present in the molecule. Therefore, the centrosymmetric space groups were subsequently used for all of the three compounds. The choices were confirmed by successful structure refinements. The function $(|Fo|-|Fc|)^2$ was minimized

during least squares refinement, while in the final cycles of calculation a weighting scheme of the form $W=1/[\sigma^2(F) + \rho F^2]$ was employed, with a final ρ value of 0.0004, 0.0002 and 0.0001 in $(CH_3)_3As.BCl_3$, $(CH_3)As.BBr_3$ and $(CH_3)_3As.BI_3$ respectively. Convergence to the final R values was achieved in six to ten cycles. H atoms were not visible in the final difference maps and no attempt was made to include them. For $(CH_3)_3As.BI_3$, a few low angle reflections were found to be affected by secondary extinction. These reflections were omitted from the calculations.

The other pertinent refinement data are summarized in Table VI.1. The final coordinates and standard deviations are given in Table VI.2, and important interatomic distances and angles given in Table VI.3. Figs. VI.1 and VI.2 show the packing. The computer programs used during analysis include CHECK (Check reflections), PROC (data reduction), ABSORB (analytical absorption correction),[101] SHELX77 (full matrix least square refinement and Fourier Synthesis),[102] XANADU (librational analysis and medium plane calculations)[103] and ORTEP (thermal ellipsoid plotting program).[104] The anomalous scattering factors for the atoms were taken from reference 105.

Table VI.1. Crystallographic and refinement data.[a]

	$Me_3As.BCl_3$	$Me_3As.BBr_3$	$Me_3As.BI_3$
a (A°)	6.497(3)	6.672(4)	13.113(7)
b (A°)	10.753(3)	11.135(7)	11.733(5)
c (A°)	7.070(2)	7.199(4)	7.387(3)
β (°)	111.8(3)	111.5(1)	-
V ($A°^3$)	458.4(3)	497.7(5)	1136.5(1)
crystal system	monoclinic	monoclinic	orthorhombic
space group	$P2_1/m$	$P2_1/m$	Pnma
cell dimensions (mm)	0.31x0.31x0.38	0.19x0.27x0.33	0.27x0.29x0.38
mol. wt.	237.1	370.4	511.4
Z	2	2	4
$\rho c(g\ cm^{-3})$	1.70	2.47	2.99
$\rho o(g\ cm^{-3})$	1.70	2.45	2.96
radiation		Mo kα, λ = 0.71069 Å	
temp (°C)		21	
abs coeff, $\mu(cm^{-1})$	43.41	150.67	104.84
min. abs. corr.	2.826	6.214	7.94
max. abs. corr.	3.519	13.126	11.53
2θ angle (°)		4-50	
Scan type		coupled + (crystal)/ 2θ(counter)	
Scan width		$k\alpha_1$-1° to $k\alpha_2$+1°	
Scan speed ($°min^{-1}$)		variable, 2.02-4.88	
bkgd time/scan time		0.5	
total reflections measured	989	1023	1272
unique data used	722	620	873
no. of parameters (NP)		43	-
R	0.0343	0.434	0.0329
R_{WF}	0.0358	0.0469	0.0372

[a]standard deviations in parentheses.

Table VI.2. Final fractional coordinates and thermal parameters of non-hydrogen atoms of $Me_3As.BX_3$ (X=Cl,Br,I).[a]

	Atom	x	y	z	U_{11}	U_{22}	U_{33}	U_{12}	U_{13}	U_{23}
X=Cl	As	0.2837(1)	0.25	0.1376(1)	0.0419(4)	0.0378(4)	0.0358(4)	0.0	0.0111(3)	0.0
	Cl(1)	0.4609(3)	0.25	-0.2191(3)	0.0581(10)	0.05856(13)	0.0563(9)	0.0	0.0297	0.0
	Cl(2)	0.0393(2)	0.3910(1)	-0.2732(2)	0.0818(9)	0.0615(8)	0.0858(7)	0.0252(7)	0.0149(6)	0.0170(6)
	C(1)	0.0272(13)	0.25	0.2048(11)	0.058(4)	0.082(5)	0.063(4)	0.0	0.026(4)	0.0
	C(2)	0.4527(9)	0.3933(5)	0.2633(8)	0.074(4)	0.063(4)	0.070(3)	-0.017(3)	0.020(3)	-0.014(3)
	B	0.2016(12)	0.25	-0.1740(10)	0.55(4)	0.044(4)	0.034(3)	0.0	0.015(3)	0.0
X=Br	As	0.2977(2)	0.25	0.6483(2)	0.0396(8)	0.0344(7)	0.0353(8)	0.0	0.0128(6)	0.0
	Br(1)	0.4915(2)	0.25	0.2935(2)	0.0494(9)	0.083(12)	0.0575(10)	0.0	0.0296(8)	0.0
	Br(2)	0.0440(2)	0.3980(1)	0.2377(2)	0.0682(8)	0.0514(7)	0.0632(8)	0.0173(5)	0.0183(6)	0.0150(5)
	C(1)	0.0599(23)	0.25	0.7251(22)	0.065(10)	0.048(9)	0.066(10)	0.0	0.030(8)	0.0
	C(2)	0.4659(19)	0.3898(11)	0.7638(15)	0.074(8)	0.065(8)	0.058(7)	-0.020(6)	0.020(6)	-0.0136(6)
	B	0.2144(2)	0.25	0.3458(21)	0.033(8)	0.036(8)	0.043(9)	0.0	0.015(6)	0.0
X=I	As	-0.924(1)	0.25	0.7505(1)	0.0432(6)	0.0339(6)	0.0302(5)	0.0	-0.0016(5)	0.0
	I(1)	-0.2109(1)	0.4061(1)	0.4184(1)	0.0693(5)	0.0431(4)	0.0724(5)	0.0149(3)	-0.0134(3)	0.0100(3)
	I(2)	0.0286(1)	0.25	0.3411(1)	0.0433(5)	0.0996(8)	0.0445(5)	0.0	0.0099(4)	0.0
	C(1)	0.0155(9)	0.3819(9)	0.8196(13)	0.093(7)	0.061(6)	0.060(6)	-0.030(6)	-0.008(6)	-0.017(5)
	C(2)	-0.2174(9)	0.25	0.890(2)	0.071(9)	0.078(10)	0.039(7)	0.0	0.022(7)	0.0
	B	-0.1211(9)	0.25	0.4806(15)	0.037(6)	0.034(6)	0.024(5)	0.0	0.005(5)	0.0

[a]Standard deviation in parenthesis ().

Table VI.3. Bond lengths (Å) and angles (°) [a,b]

Bond	$Me_3As.BCl_3$	$Me_3As.BBr_3$	$Me_3As.BI_3$
As-C(1)	1.895(7)	1.89(1)	1.93(1)
As-C(2)	1.908(5)	1.92(1)	1.92(1)
B-X(1)	1.828(7)	2.02(1)	2.22(1)
B-X(2)	1.830(4)	1.99(1)	2.23(1)
B-As	2.065(6)	2.04(1)	2.03(1)
C(1)-As-C(2)	106.9(2)	107.5(4)	107.8(4)
C(2)-As-C(2)'	107.7(3)	108.2(8)	107.7(7)
C(1)-As-B	111.4(3)	112.6(6)	111.3(5)
C(2)-As-B	111.9(2)	111.5(4)	111.1(3)
X(1)-B-X(2)	111.7(2)	111.0(5)	111.9(3)
X(2)-B-X(2)'	111.8(4)	111.7(6)	110.8(5)
X(1)-B-As	107.3(3)	106.8(6)	107.0(5)
X(2)-B-As	107.0(2)	108.1(5)	107.5(3)

[a] Standard deviations in parentheses.

[b] Symmetry equivalent positions': x, 0.5-y,z.

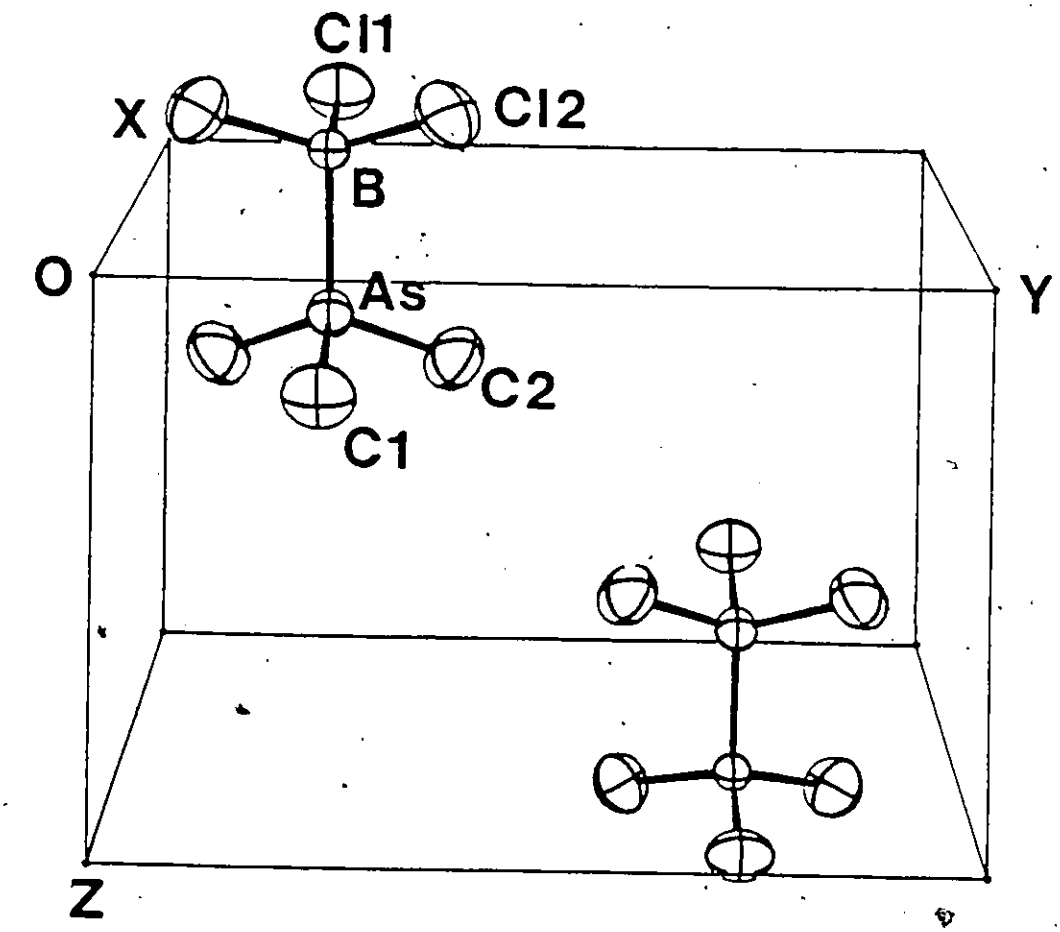

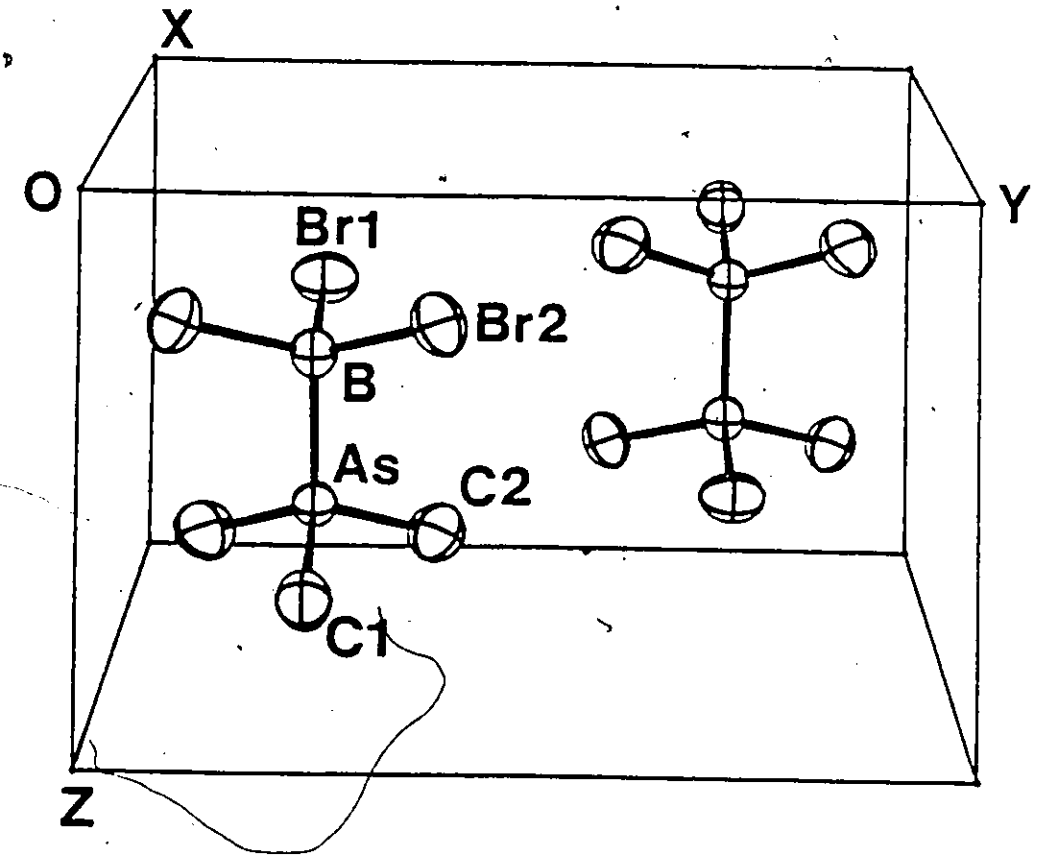

Fig. VI.1. Unit cell packing of $Me_3As.BCl_3$ and $Me_3As.BBr_3$.

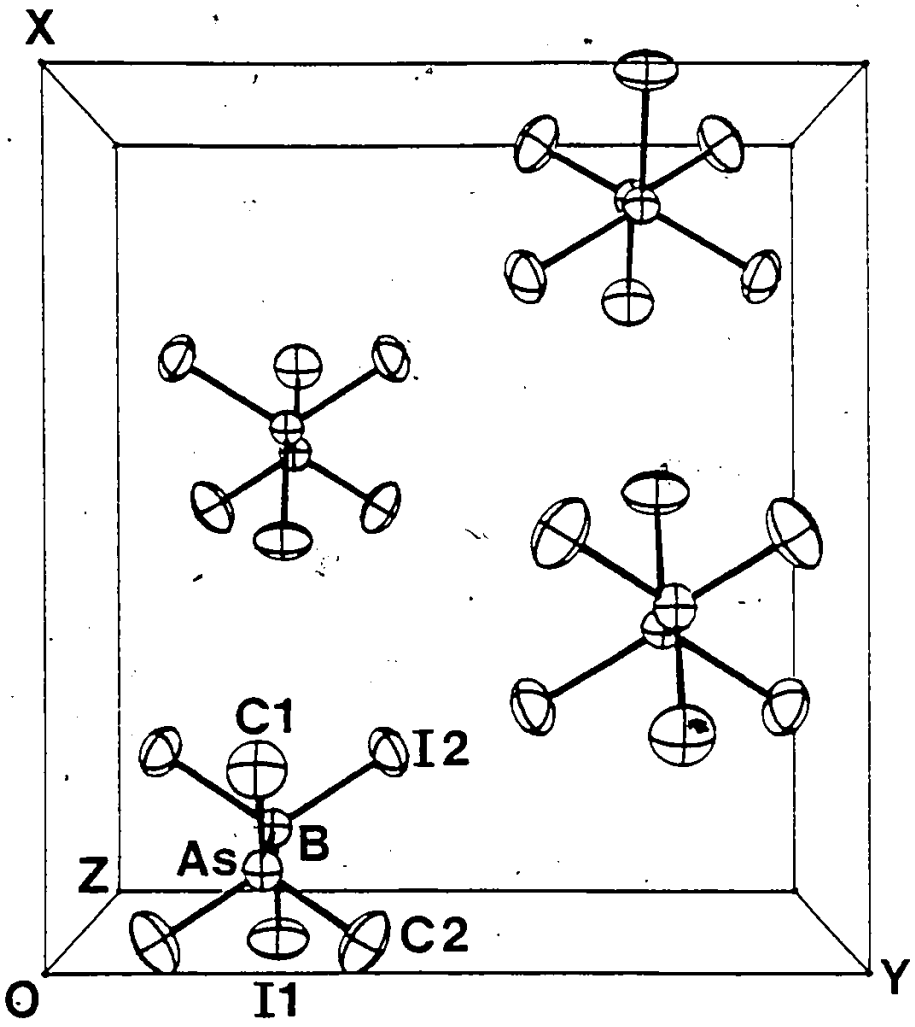

Fig. VI.2. Unit cell packing of $Me_3As.BI_3$.

VI.3 Discussion

$(CH_3)_3As.BCl_3$, $(CH_3)_3As.BBr_3$ and $(CH_3)_3As.BI_3$ all exist as discrete molecules with an effective C_{3v} symmetry and staggered conformations. The average As-B bond length of 2.045(10)Å is only slightly longer than that reported by Hencher and Mustoe[106] for the Ge-C bond [1.945(3)Å] in $(CH_3)_3Ge-CH_3$ with which it may be considered to be "isoelectronic". The apparent decrease in the As-B bond length along the series $(CH_3)As.BCl_3$ - $(CH_3)_3As.BBr_3$ - $(CH_3)_3As.BI_3$ = [2.065(6), 2.04(1), 2.03(1)Å respectively] is consistent with the gradual increase in bond strength predicted from force constant calculations (1.532, 1.652 and 1.855 mdyne $Å^{-1}$ respectively) and is also consistent with the established order of increasing Lewis acidity for the boron trihalides from chloride through to iodide. The only structural data reported for the As-B bond length is that of $(CH_3)_3As.BH_3$. In a microwave study by Durig[34] this is given as 2.035Å which would suggest that BH_3 falls between BBr_3 and BI_3, in its Lewis acidity towards trimethylarsine. However, the BH_3 adduct structure was determined in the gas phase.

In examining the structures of the analogous trimethylphosphine series, it was noted that the similar decrease in the length of the P-B bond (1.957(5)Å) in $(CH_3)_3P.BCl_3$ to (1.918(15)Å) in $(CH_3)_3P,BI_3$ although slight, is more marked than for the trimethylamine series. The %

change from chloride to iodide is 29% for $(CH_3)_3P.BX_3$ and only 17% for $(CH_3)_3As.BX_3$ and 15% for $(CH_3)_3N.BX_3$. Clearly steric crowding is least around arsenic and greatest around nitrogen, so that it cannot be the rationale for the difference. The P-B bond length in $(CH_3)_3P.BH_3$ has been reported in a microwave study by Bryan and Kuczkowski[107] to be 1.901Å, once again close to that of the BI_3 adduct.

The average As-C bond length is increasing (weakening) slightly along the series $(CH_3)_3As\text{-}BCl_3$, $-BBr_3$, $-BI_3$. In this it parallels the weighted average of the As-C vibrations at 626, 620 and 615 cms^{-1} respectively. All bonds are shorter than that reported for free $(CH_3)_3As$[108] (1.959(10)Å). It has been suggested that this is to be expected as the rearrangement of bonds around arsenic approaches the all-tetrahedral structure. Indeed the CAsC bond angles are only slightly less than the tetrahedral angle. Conversely, the BX_3 moieties have become rearranged from the 120° angle of a trigonal plane toward tetrahedral and the accompanying decrease in B-X bond strength is reflected by the increase in the bond lengths of B-Cl, B-Br and B-I relative to the free BX_3 species [1.74, 1.87 and 2.10 Å respectively for X = Cl, Br and I]. This was also suggested by their vibrational spectra. The BX bonds do not increase in length to quite the same degree as in the $(CH_3)_3N$ or $(CH_3)_3P$ adducts

consistent with the arsine being the weakest Lewis base and hence causing least change in the BX_3 system. This is also shown in bond angle changes where, for example, the average IBI angles are 111.5° for $(CH_3)_3As.BI_3$, 110.8° for $(CH_3)_3P.BI_3$ and further reduced to 108.2° for $(CH_3)_3N.BI_3$.

Thus the subtle changes are all reflecting predictions based on chemical and spectroscopic evidence. These comparisons are presumably valid because all $(CH_3)_3M.BCl_3$ and $(CH_3)_3M.BBr_3$, M = N, P, As compounds are in the space group $P2_1/m$ and in a staggered configuration leading to essentially C_{3v} symmetry. The $(CH_3)_3M.BI_3$ species have the same local symmetry but for M = P or As the space group is Pnma while for M = N it is again $P2_1/m$.

REFERENCES

PART TWO

1. T. D. Coyle and F.G.A. Stone, in Progress in Boron Chemistry, Vol. I, H. Steinberg and A. L. McCluskey, ed., pp. 83-160, MacMillan, New York, N.Y. (1964).

2. K. Niedenzu and J. W. Dawson, in The Chemistry of Boron and its Compounds, E. L. Muetterties, ed., p. 378 ff, 617 ff. John Wiley, New York (1967).

3. B. Rapp. Ph.D. Thesis, University of Windsor (1973).

4. M. Manchurek. M.Sc. Thesis, University of Windsor (1974).

5. L. Khasrou. Ph.D. Thesis, University of Windsor (1980).

6. J. L. Hoard, S. Geller, and W. M. Cashin. Acta Cryst. 4, 396 (1951).

7. S. Geller and J. L. Hoard. Acta Cryst. 4, 399 (1951).

8. J. L. Hoard, S. Geller and T. B. Owen. Acta Cryst. 4, 405 (1951).

9. P. H. Clippard, J. C. Hanson and R. C. Taylor. J. Cryst., Mol. Structure, 1, 363 (1971).

10. J. R. Durig, Y. S. Li and J. D. Odom. J. Mol. Structure 16, 443 (1973).

11. J. D. Odom, J. A. Barnes, B. A. Hudgens and J. R. Durig. J. Phys. Chem. 78, 1503 (1974).

12. B. Benton-Jones and J. M. Miller. Inorg. Nucl. Chem. Lett. 8, 485 (1972).

13. J. M. Miller and T. R. B. Jones. Inorg. Chem. 15, 284 (1976).

14. G. F. Lanthier and J. M. Miller. J. Chem. Soc. (A), 346 (1971).

15. J. M. Miller and M. Onyszchuk, Can. J. Chem. 41, 2898 (1963).

16. J. M. Miller, and M. Onyszchuk, Can. J. Chem. 42, 1518 (1964).

17. E. L. McGandy, Diss. Abst., 22, 754 (1961).

18. J. R. Durig, Y. S. Li, L. A. Carreira and J. D. Odom, J. Amer. Chem. Soc., 95, 2491 (1973).

19. R. W. Rudolph, R. W. Parry and C. F. Farran, Inorg. Chem., 5, 723 (1966).

20. J. Davis and J. E. Drake, J. Chem. Soc. (A), 2959 (1970).

21. W. Sawodny and J. Groubeau, Z. Anorg. Allgem. Chem. 356, 289 (1967).

22. J. E. Drake and J. Simpson, J. Chem. Soc., (A), 974 (1968).

23. J. R. Durig, B. A. Hudgens, Y. S. Li, and J. D. Odom, J. Chem. Phys., 61, 4890 (1974).

24. J. E. Drake, J. L. Hencher and L. N. Khasrou Can. J. Chem. 59, 2898 (1981).

25. J. E. Drake, J. L. Hencher and B. Rapp Inorg. Chem. 16, 2289 (1977).

26. D. L. Black and R. C. Taylor, Acta Cryst. B31, 1116 (1975).

27. B. Rapp and J. E. Drake, Inorg. Chem., 12, 2868 (1973).

28. J. E. Drake and B. Rapp, J. Inorg. Nucl. Chem. 36, 2613 (1974).

29. E. L. Muetterties, J. Inorg. Nucl. Chem. 15, 182 (1960).

30. W. Gee, R. A. Shaw and B. C. Smith, J. Chem. Soc. 4180 (1964).

31. F.G.A. Stone and A. B. Burg, J. Amer. Chem. Soc. 76, 386 (1954).

32. A. P. Lane and A. B. Burg, J. Amer. Chem. Soc. 89, 1040 (1967).

33. A. B. Burg and R. I. Wagner, J. Amer. Chem. Soc. 75, 3872 (1953).

34. J. R. Durig, B. A. Hudgens, and J. D. Odom, Inorg. Chem. 13, 2306 (1974).

35. F. Hewitt and A. K. Holliday, J. Chem. Soc. 530 (1953).

36. G. M. Phillips, J. S. Hunter and L. E. Sutton, J. Chem. Soc., 146 (1945).

37. M. L. Denniston and D. R. Martin, J. Inorg. Nucl. Chem. 36, 2179 (1974).

38. J. E. Drake, L. N. Khasrou and Abdul Majid, Can. J. Chem. 59, 2417 (1981).

39. Y. Gushikem and F. Watari. J. Chem. Soc. Dalton, 10, 2016 (1980).

40. M. L. Denniston and D. R. Martin, J. Inorg. Nucl. Chem. 36, 1461 (1974).

41. A. G. Murray and A. J. Park, J. Organomet. Chem. 5, 218 (1966).

42. A. Derek, H. Clague and A. Danti. Spectrochim. Acta 23 (A), 2359 (1967).

43. J. R. Blackborow. J. Chem. Soc. Dalton, 2139 (1973).

44. G. E. Ryschkewitsch and W. J. Rademaker. J. Magn. Reson. 1, 584 (1969).

45. G. E. Ryschkewitsch and A. H. Cowley, J. Amer. Chem. Soc. 92, 745 (1970).

46. P. H. Clippard and R. C. Taylor, Inorg. Chem. 8, 2802 (1969).

47. J. E. Drake and B. Rapp, J. Chem. Soc. Dalton, 2341 (1972).

48. A. H. Cowley and M. C. Damasco, J. Amer. Chem. Soc. 93, 6815 (1971).

49. C. W. Heitsch, Inorg. Chem. 4, 1019 (1965).

50. R. W. Rudolph and C. W. Shultz, J. Amer. Chem. Soc. 93, 6821 (1971).

51. A. H. Cowley and J. L. Mills, J. Amer. Chem. Soc. 91, 2911 (1969).

52. J. M. VanPaasschen and R. A. Geanangel, Inorg. Chem. 17, 3302 (1978).

53. D. C. Mente and J. L. Mills, Inorg. Chem. 14, 1862 (1975).

54. A. H. Harvey and M. K. Wilson, J. Chem. Phys. 44 3535 (1966).

55. P.J.D. Park and P. J. Hendra, Spectrochim. Acta 24 (A) 311 (1978).

56. A.J.F. Clark, J. E. Drake and Q. Shen, Spectrochim. Acta 34 (A), 311 (1978).

57. J. M. Chehayber, J. E. Drake, and B. Rapp. To be published.

58. J. E. Drake, J. L. Hencher, and B. Rapp, J. Chem. Soc. Dalton, 595 (1974).

59. F. Watari, Bull. Chem. Soc. Jap. 50, 1287 (1977).

60. D. F. Shriver and B. Swanson, Inorg. Chem. 10, 1354 (1971).

61. R. E. Sruby, J. R. Lacher and J. D. Park, J. Chem. Phys. 19, 386 (1951).

62. T. Wentink, Jr., and V. H. Tiensuu, J. Chem. Phys. 28, 826 (1958).

63. J. R. Durig, V. F. Kalasinsky, Y. S. Li and J. D. Odom, J. Phys. Chem. 79, 468 (1975).

64. R. K. Chadha, J. M. Chehayber and J. E. Drake, J. Cryst. Spect. Res. (1984).

65. A.J.F. Clark and J. E. Drake, Spectrochim. Acta 34(A) 307 (1978).

66. A. G. Massey, Advances in Inorganic Chemistry and Radiochemistry, 10, 1-152 (1967)

67. W. Gerrard and M. F. Lappert, Chem. Rev. 58, 1081 (1958).

68. N. N. Greenwood and R. L. Martin, Quart. Rev. Chem. Soc. 8, 1 (1954).

69. G. Urry, in The Chemistry of Boron and Its Compounds (E. L. Muetterties, ed.) Chapter 6, Wiley, New York (1967).

70. J. S. Hartman and J. M. Miller, Advances in Inorganic Chemistry and Radiochemistry 21, 147-177 (1978).

71. P. N. Gates, E. F. Mooney and D. C. Smith, J. Chem. Soc., 3511 (1964).

72. M. F. Lappert, M. R. Litzow, J. B. Pedley, T. R. Spalding and H. Nöth, J. Chem. Soc. (A), 383 (1971).

73. M. F. Lappert, M. R. Litzow, J. B. Pedley and A. Tweedale, J. Chem. Soc. (A). 383 (1971).

74. T. P. Onak, H. Landesman, R. E. Williams and I. Shapiro, J. Phys. Chem. 63, 1533 (1959).

75. W. D. Phillips, H. C. Miller, and E. L. Muetterties, J. Amer. Chem. Soc., 81, 4496 (1959).

76. D. R. Martin, Chem. Revs. 45, 461 (1944).

77. H. C. Brown and R. R. Holmes, J. Amer. Chem. Soc. 78, 2173 (1956).

78. F. A. Cotton, and J. R. Leto, J. Chem. Phys. 30, 993 (1959).

79. M. F. Lappert, M. R. Litzow, J. B. Pedley, P.N.K. Riley and A. Tweedale, J. Chem. Soc. (A), 3105 (1968).

80. J.A.S. Smith and D. A. Tong. J. Chem. Soc. (A), 173 (1971).

81. P. J. Bassett and D. R. Lloyd, J. Chem. Soc. (A), 1551 (1971).

82. F.G.A. Stone, Chem. Revs. 58, 101 (1958).

83. H. C. Brown, M. D. Taylor and M. Gerstein, J. Amer. Chem. Soc. 66, 431 (1944).

84. H. C. Brown and M. Gerstein, ibid., 72, 2923 (1950).

85. D. E. Young, G. E. McAchran and S. G. Shore, J. Amer. Chem. Soc. 88, 4390 (1966).

86. R. Rorster and K. Cohn, Inorg. Chem. 11, 2590 (1972).

87. B. Benton-Jones, M.E.A. Davidson, J. S. Hartman, J. J. Klassen and J. M. Miller, J. Chem. Soc. Dalton, 2603 (1972).

88. D. G. Brown, R. S. Drago and T. F. Bolles, J. Amer. Chem. Soc. 90, 2182 (1968).

89. E. Muylle, G. P., Van Der Kelen and E. G. Claeys, Spectrochim. Acta. 32 (A), 1149 (1976).

90. E. F. Mooney, M. A. Qaseem and P. H. Winson, J. Chem. Soc. (B), 224 (1968).

91. P. N. Gates, E. J. McLauchlan and E. F. Mooney, Spectrochim. Acta 21, 1445 (1965).

92. P. G. Davies and E. F. Mooney, Spectrochim. Acta. 23 (A), 953 (1966).

93. E. F. Mooney and M. A. Qaseem, J. Inorg. Nucl. Chem. 30, 1439 (1968).

94. E. F. Mooney and M. A. Qaseem, Spectrochim. Acta 24 (A), 969 (1968).

95. H. C. Brown, J. Chem. Soc., 1248 (1956).

96. J. M. Miller, Inorg. Chem. 22, 2384 (1984).

97. J. S. Hartman and J. M. Miller, Inorg. Chem. 13, 1467 (1974).

98. G. S. Harris, Proc. Chem. Soc., 65 (1961).

99. R. A. Zingaro and E. A. Myers, Inorg. Chem. 1, 771 (1962).

100. M. J. Bula and J. S. Hartman, J. Chem. Soc. Dalton, 1047 (1973).

101. D. Templeton and L. Templeton (1973) ABSORB. An analytical absorption correction program. Univ. of California, Berkely.

102. G. M. Sheldrick (1977), SHELX. Program for crystal structure determination. Univ. of Cambridge, England.

103. P. Roberts and G. M. Sheldrick (1975), XANADU. Program for crystallographic calculation. Univ. of Cambridge, England.

104. C. K. Johnson (1965), ORTEP. Report ORNL-3794. Oak Ridge National Laboratory, Tennessee.

105. J. A. Ibers and W. C. Hamilton (1974). In International Tables for X-ray Crystallography. Vol. IV. Birmingham: Kynoch Press.

106. J. L. Hencher and F. J. Mustoé, Can. J. Chem. 53, 3542 (1975).

107. P. S. Bryan and R. L. Kuczkowski, Inorg. Chem. 11, 553 (1972).

108. D. R. Lide, Spectrochim. Acta 15, 473 (1959).

PART THREE

SYNTHESIS, CHARACTERIZATION AND SELECTED REACTIONS OF SELENIUM-GROUP IV LIGANDS

CHAPTER VII

SYNTHESIS, CHARACTERIZATION AND SELECTED REACTIONS OF SELENIUM-GROUP IV LIGANDS

VII.1 Introduction

Sulphur compounds of silicon, germanium and tin have been studied considerably.[1-3] These compounds have been used as reagents in organic synthesis[4-7] and as ligands for transition metal complexes.[8,9] Abel and his coworkers have synthesized many of these compounds to study the inversion at pyramidal sulphur in transition metal complexes by dynamic nuclear magnetic resonance.[10-13] Several references provide a general background of the synthetic routes to these sulphur ligands.[14-22] Analogous selenium compounds have received much less attention but nevertheless have already been used in organic synthesis.[23] For example, the lithium salt of Me_3SiCH_2SePh has been used to convert halides into their homologous aldehydes.[24] These selenium compounds have also been used as ligands in the preparation of transition metal complexes.[10,12,13,25-28] The chemistry of organo-selenium compounds, and of palladium and platinium has been the subject of two books.[29,30] At Windsor, the chalcogen compounds of group IV have been extensively studied. These investigations included synthesis, characterization by n.m.r., i.r., Raman spectroscopy and mass spectrometry and reactivity of such species.[31-36] Methyl and phenylseleno, and methyl and phenyltelluro derivatives of group IV compounds have been prepared by selenium or tellurium insertion reactions into methyl or phenyllithium followed by the

reaction with the corresponding group IV halide.[37-41] It is interesting to note that the scarcity of such work has lead some authors to assume that the synthesis of lithium methyl selenide, a common intermediate, was original in 1983.[42]

The neopentyl groups, Me_3MCH_2 (M = Si,Ge,Sn) have been recently seen as ligands in transition metal complexes. Their reactivities towards the iodide and ethoxide ions,[46] their electronic effects in organometallic sulphides[47] and their group VA compounds have been investigated.[48] This study was initiated because of an interest in selenium compounds of the neopentyl group Me_3MCH_2. It is hoped that the selective reactions of these ligands with Na_2PdCl_4 and K_2PtCl_4 can shed some light as to the potential diversity of such work. The tellurium analogues of these compounds should be available using the same synthetic route but the yield might be lower due to the fact that tellurium insertion reactions proceed with lower yields than their selenium counterparts. Finally, it is worth mentioning that besides the usage of similar ligands as reagents in organic synthesis,[4,23,24] a wide variety of palladium and platinum complexes have been employed as catalysts in hydrosilylation, hydrogenation, hydroformylation and other reactions.[49-50] Whether the palladium and

platinum complexes of these selenium ligands could be used as catalysts for such reactions remains to be seen.

VII.2 Preparation

Elemental selenium (0.5 g, 6.3 mmole) was placed in the reaction flask C (Fig. I.2) and the flask evacuated. THF (ca. 10 mL) was then distilled into the vessel and this was followed by the introduction of LiR ($R=CH_3, C_6H_5$; ca 8 mmole) by a syringe. The reaction mixture was then stirred at room temperature for 1.5 h. After ca 20 minutes of reaction time, the mixture turned milky then colourless when $R = CH_3$, and to red-brown or mustard when $R = C_6H_5$. The solvents were distilled off and for effective removal of THF, the reaction vessel was left open to the pump for 24 h. The difficulty in removing THF has been attributed to a possible coordination between THF and LiSeR in the solid state. Then diethyl ether (ca 10mL) was distilled into the reaction vessel and finally Me_3MCH_2X(M = Si,Ge,Sn) was distilled from the graduated storage flask F (Fig. I.2) in a slight excess. The reaction mixture was stirred for 3 h at room temperature after which the contents were passed through traps held at -45°C and -196°C. The -196°C trap contained ether and the -45°C trap contained a small amount of Me_3MCH_2SeR,THF and ether. The contents of the -196°C

trap were discarded and the process repeated through traps held at -23°C and -196°C traps. The desired product Me_3MCH_2SeR is a heavy liquid and was transferred with the help of a hot air gun. The difficulty of transferring the product was found to increase with the increase in molecular weight. Purification was effected by successive passages through traps held at -23°C and -196°C. The yields ranged between 70 and 90% based on selenium. All ligands were heavy liquids with a pungent and persistent smell.

VII.3 Characterization

A. Vibrational spectra

(i) Me_3MCH_2SeMe (M = Si,Ge,Sn)

The i.r. and Raman spectra of this series are displayed in Figs. VII.1-6. The frequencies and their tentative assignments are listed in Table VII.1. The assignments were made with some confidence based on comparisons with spectra of Me_2Se,[51] MeSeH,[52] Me_2Se_2,[53] Me_3MSeMe,[38] Me_3MCH_2X[54] and Me_nMX_{4-n}[55-60] (M = Si,Ge,Sn; n = 0-3).

As expected, the positions of the characteristic vibrations of CH_3M and CH_3Se species were relatively unshifted upon changing M. In this region, two distinct envelopes appear in the Raman spectra and can be assigned to the symmetric (polarized) and asymmetric (depolarized)

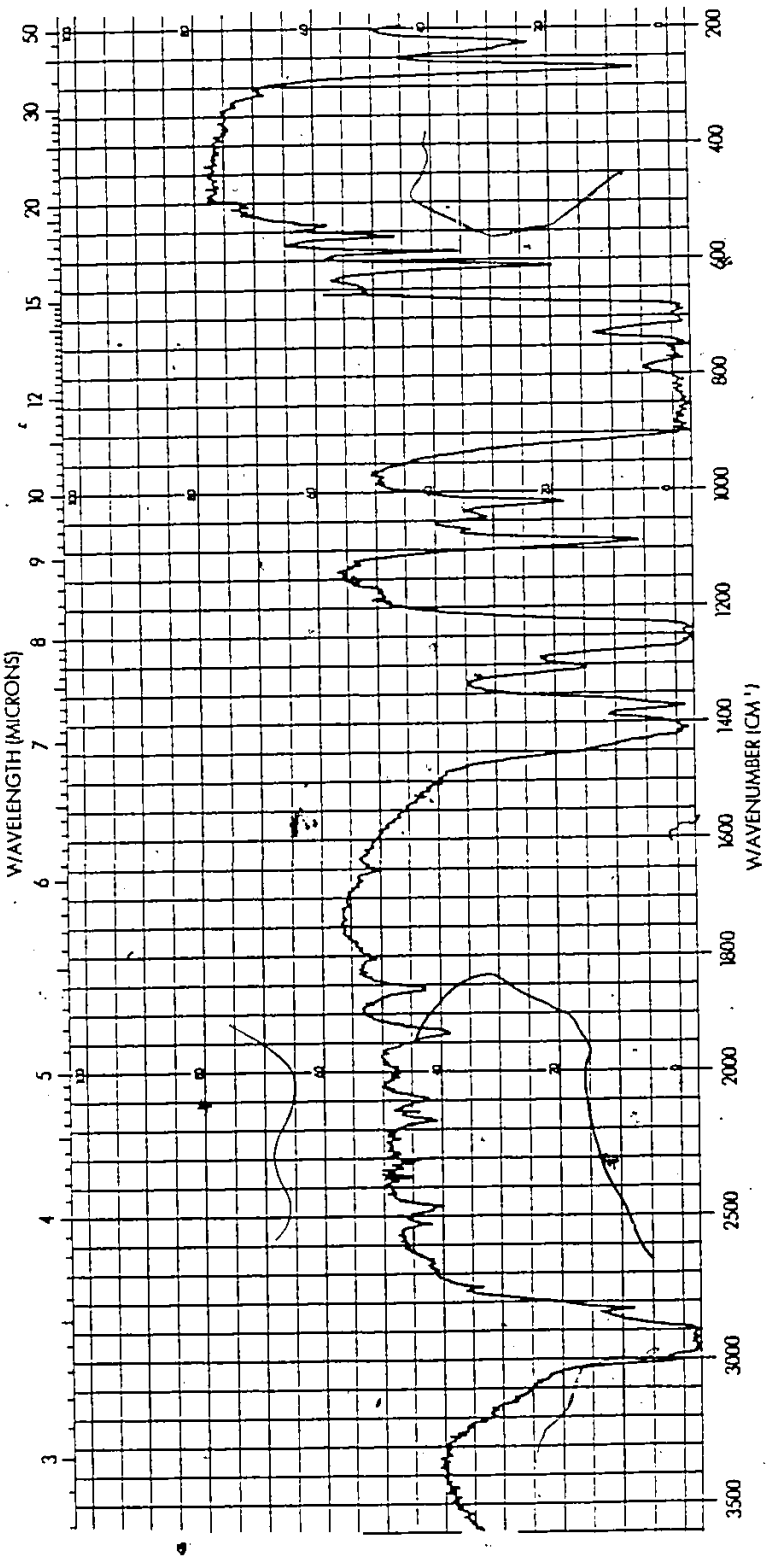

Fig. VII.1. The i.r. spectrum of Me_3SiCH_2SeMe.

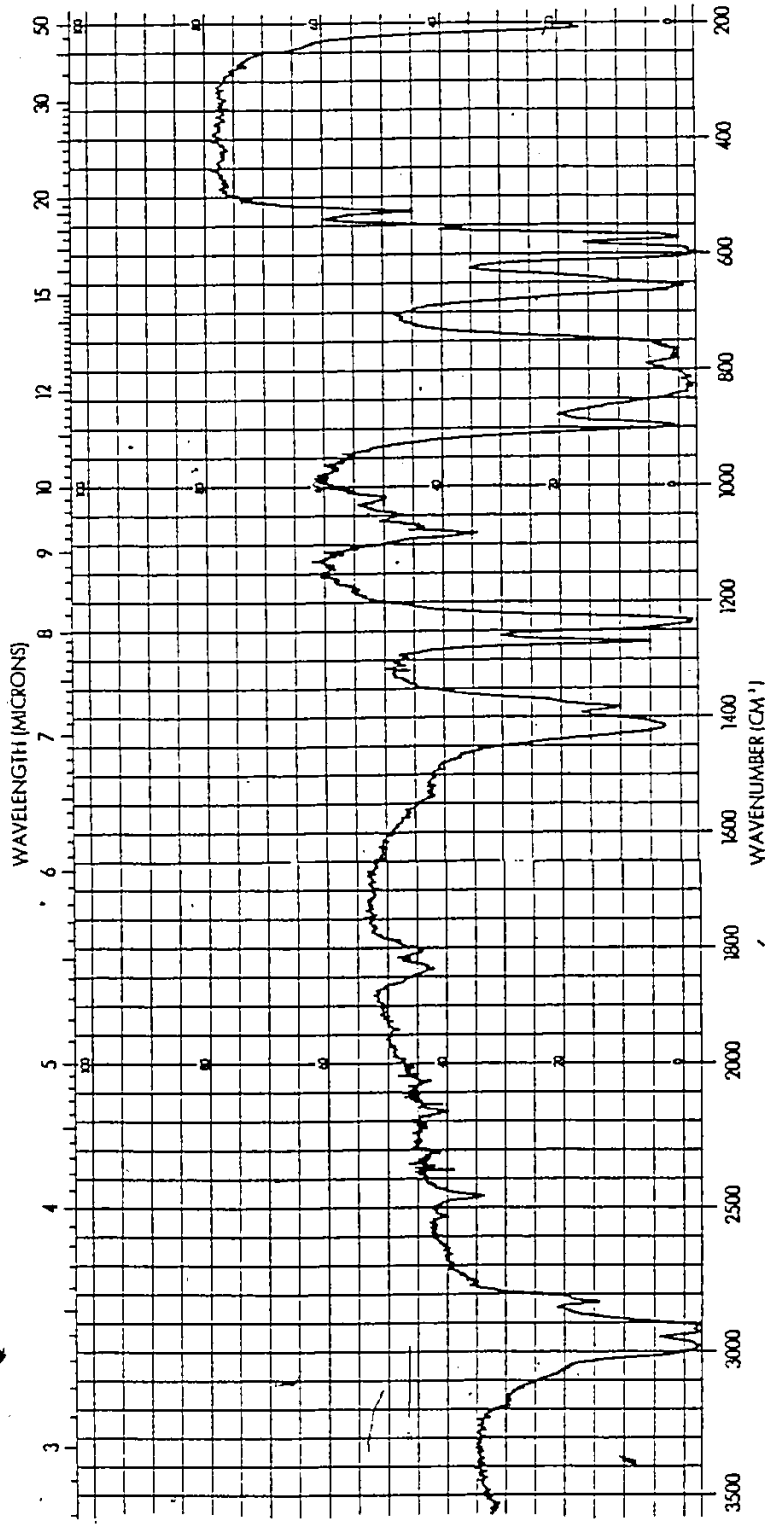

Fig. VII.2. The i.r. spectrum of Me_3GeCH_2SeMe.

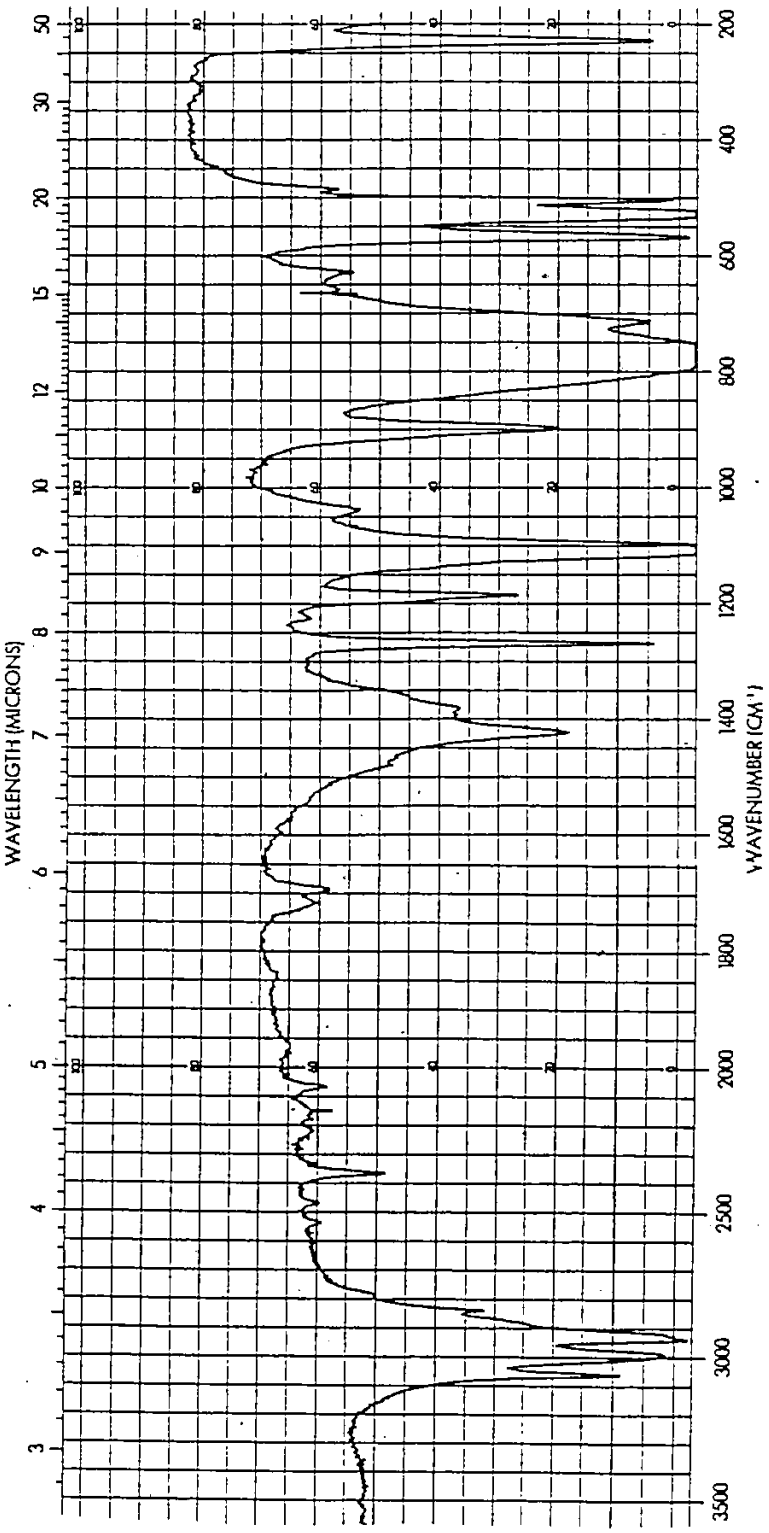

Fig. VII.3. The i.r. spectrum of Me_3SnCH_2SeMe.

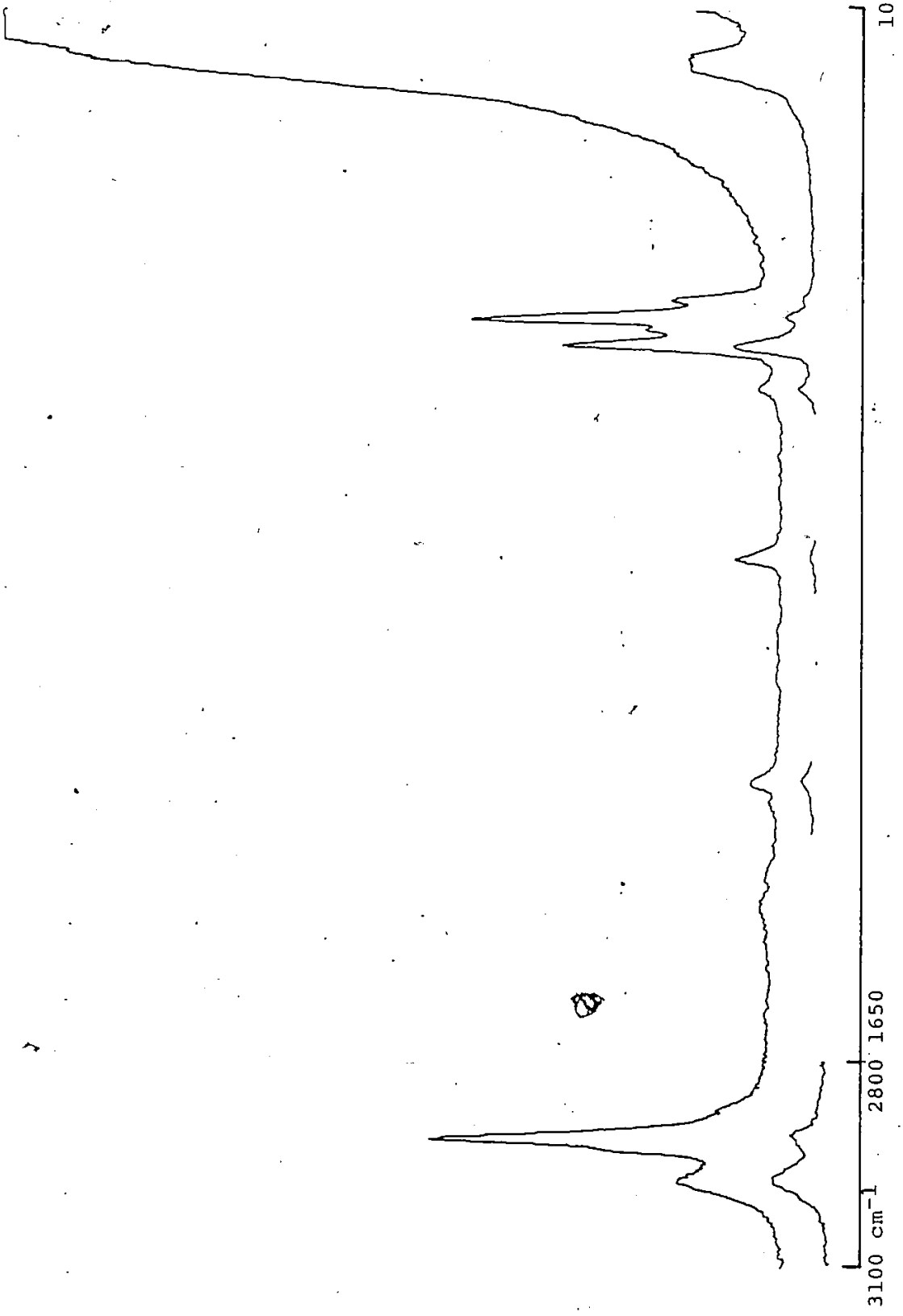

Fig. VII.4. The Raman spectrum of Me_3SiCH_2SeMe.

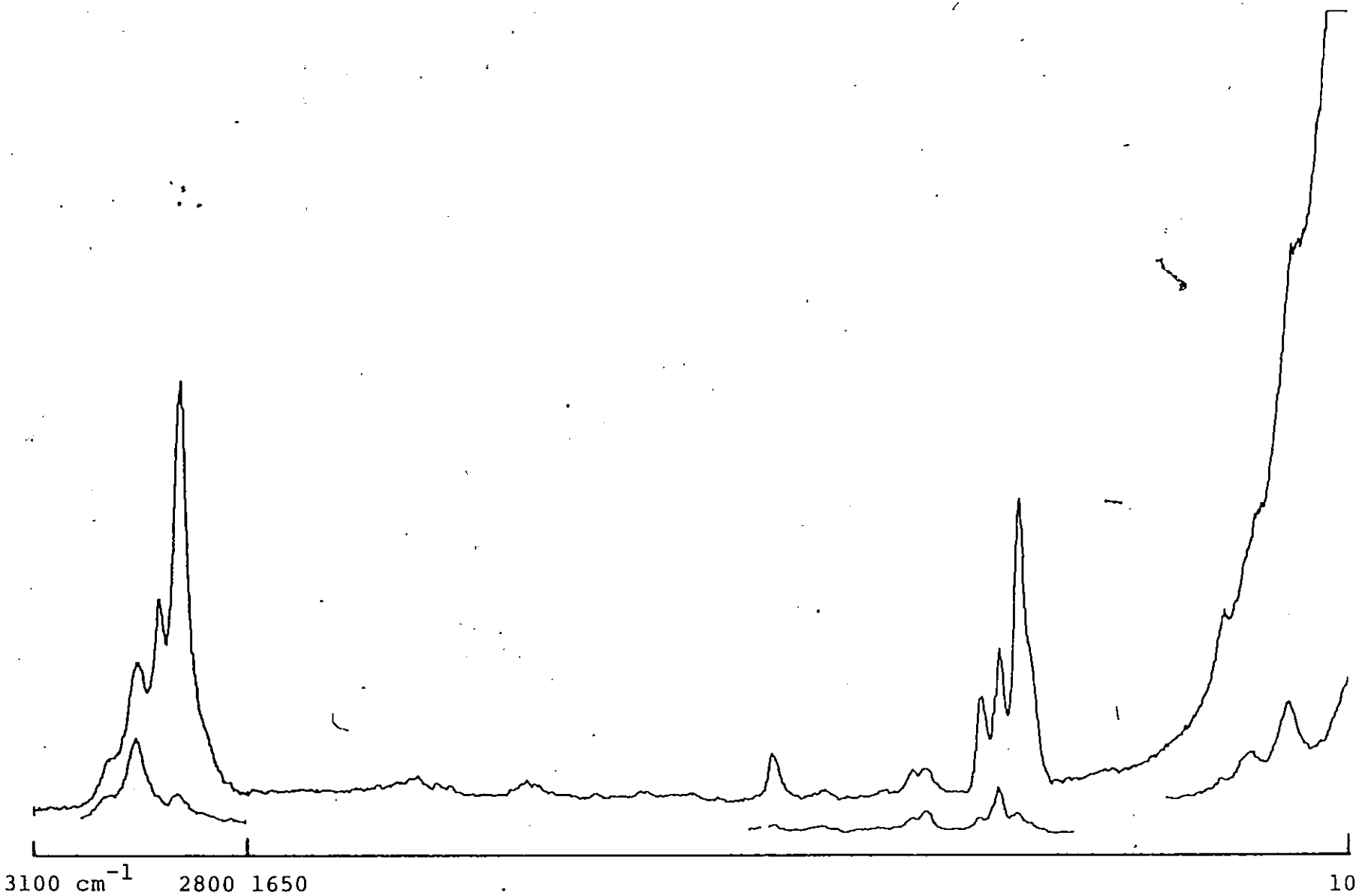

Fig. VII.5. The Raman spectrum of Me_3GeCH_2SeMe.

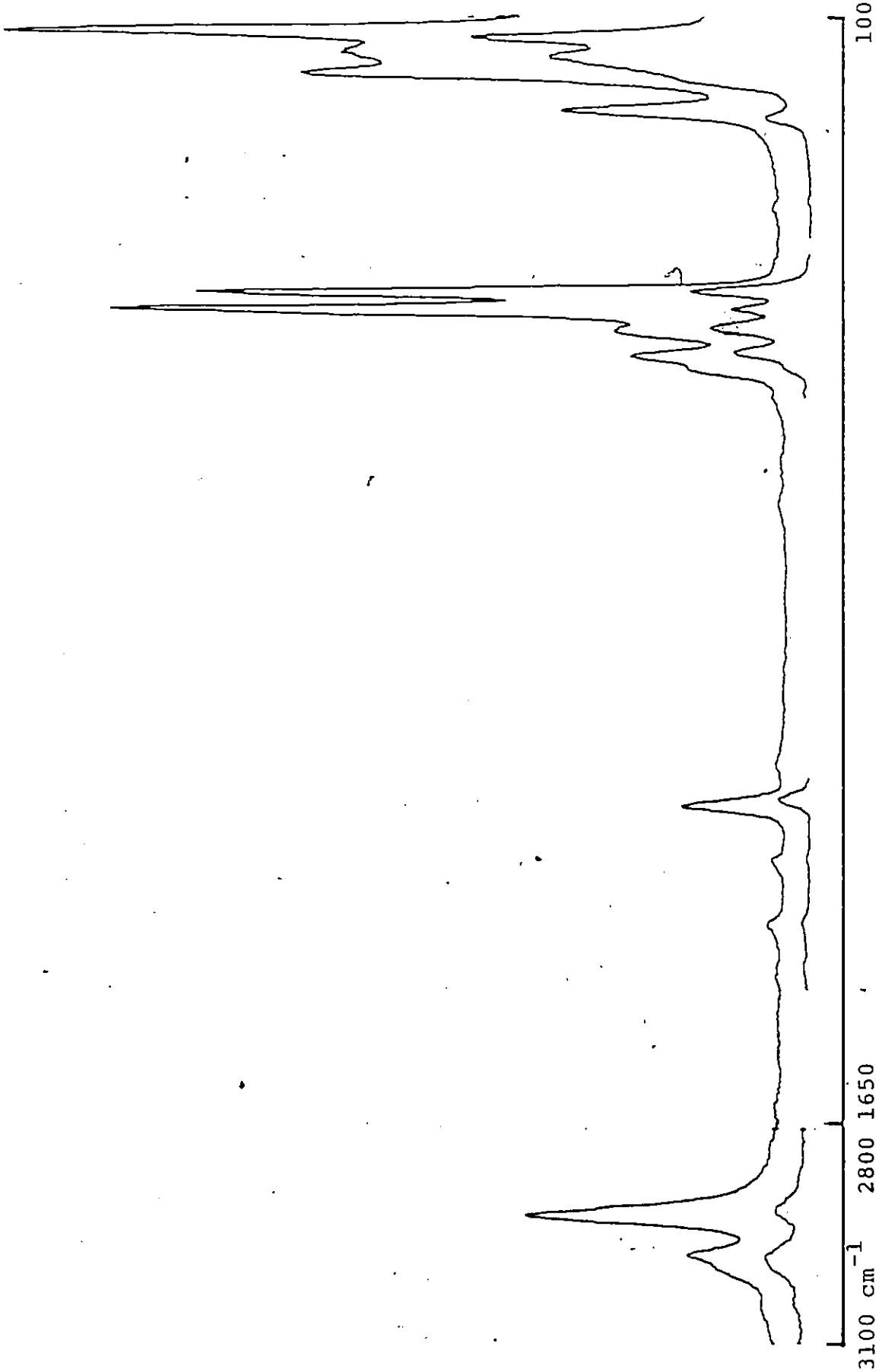

Fig. VII.6. The Raman spectrum of Me_3SnCH_2SeMe.

Table VII.1. The vibrational spectra and the tentative assignments of the series Me_3MCH_2SeMe. (M = Si,Ge,Sn)

Si		Ge		Sn		
I.R. (liq.)	Raman (liq.)	I.R. (liq.)	Raman (liq.)	I.R. (liq.)	Raman (liq.)	Tentative Assignments
2960 s	2956 mw,dp	2992 m	2996 ms,dp	2993 m	2978 mw	(a) $CH_3(M)$, $CH_3(Se)$, CH_2 str
2900 sh	2893 s,p	2926 mw	2930 s,p	2920 ms	2924 s	(s) $CH_3(M)$, $CH_3(Se)$, CH_2 str
1410 s	1410 w,dp	1417 w	1419 w,dp	1428 vw	1436 w,dp	(a) $CH_3(M)$, $CH_3(Se)$, CH_2 def.
1269 mw	1262 w	1267 w	1272 w	1274 w	1283 w	(s) CH_2 def.
1250 s	1256 w,p	1238 w	1234 w	1190 w	1197 w	(s) $CH_3(M)$, $CH_3(Se)$ def.
1090 vs	1085 vw	1085 s	1082 vw	1090 w	1098 vw	CH_2 rock
908 mw	915 mw	900 w	909 w	900 m	890 w	$CH_3(Se)$ rock
850 mw	843 vw	810 s	810 mn	775 s	776 w	$CH_3(M)$ rock
707 ms	715 mw,dp	600 s	593 m,dp	568 m	563 w,dp	(a) M-C str
615 s	617 mw,p	570 m	572 p	505 m	510 s,p	(s) M-C str.
587 m	590 ms,dp	560 sh	560 m,dp	585 ms	595 m,dp	(a) Se-C str
560 w	563 s,p	550 w	553 ms,p	575 m	575 m,p	(s) Se-C str
270 ms	270 mw	200 s	192 sh	230	233 w,dp	(a) MC_3 def.
225 mw	228 m,p		180 w,p		177 w,p	(s) MC_3 def.
	180 sh				153 w	MC_3 rock

CH stretches for CH_3M,CH_3Se and CH_2. When M = Si, these two envelopes show some splittings but no attempt was made to separate these modes since the spectra were used for characterization rather than as a basis for accurate calculations (such as normal coordinate analysis). The asymmetric CH_3 and CH_2 stretches occur in the 2990 cm^{-1} region while the corresponding symmetric stretches occur in the 2920 cm^{-1} region. The CH_3 and CH_2 deformation modes were assigned in the 1190-1250 cm^{-1} and 1400 cm^{-1} regions for the symmetric and asymmetric vibration respectively. The rocking modes appear as weak bands in the Raman spectra in the 770-1100 cm^{-1} region. The C-Se and M-C stretching vibrations are easily assigned and virtually unchanged compared to those reported for the Me_3MSeMe series (M = Si,Ge,Sn).[38] The same is noted for the MC_3 deformation and rocking modes.

(ii) Me_3MCH_2SePh (M = Si,Ge,Sn)

The i.r. and Raman spectra of this series are displayed in Figs. VII 7-12. The frequencies and their tentative assignments are listed in Table VII.2. The vibrations associated with the Me_3MCH_2 moieties were assigned similarly to those above for Me_3MCH_2SeMe. The assignments were made assuming free rotation about the Se-Ph bond. The effective symmetry of the ring is C_{2V}

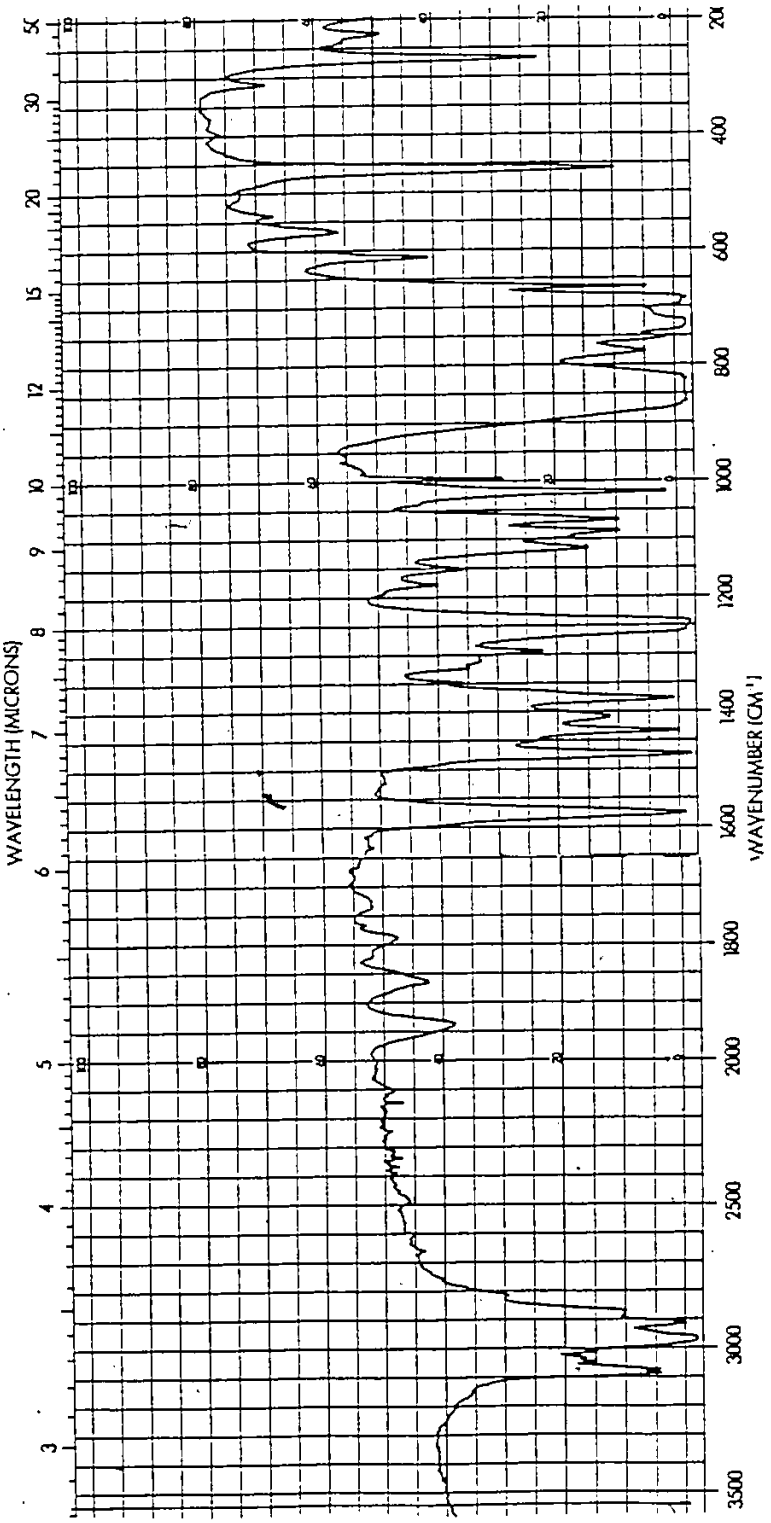

Fig. VII.7. The i.r. spectrum of Me_3SiCH_2SePh.

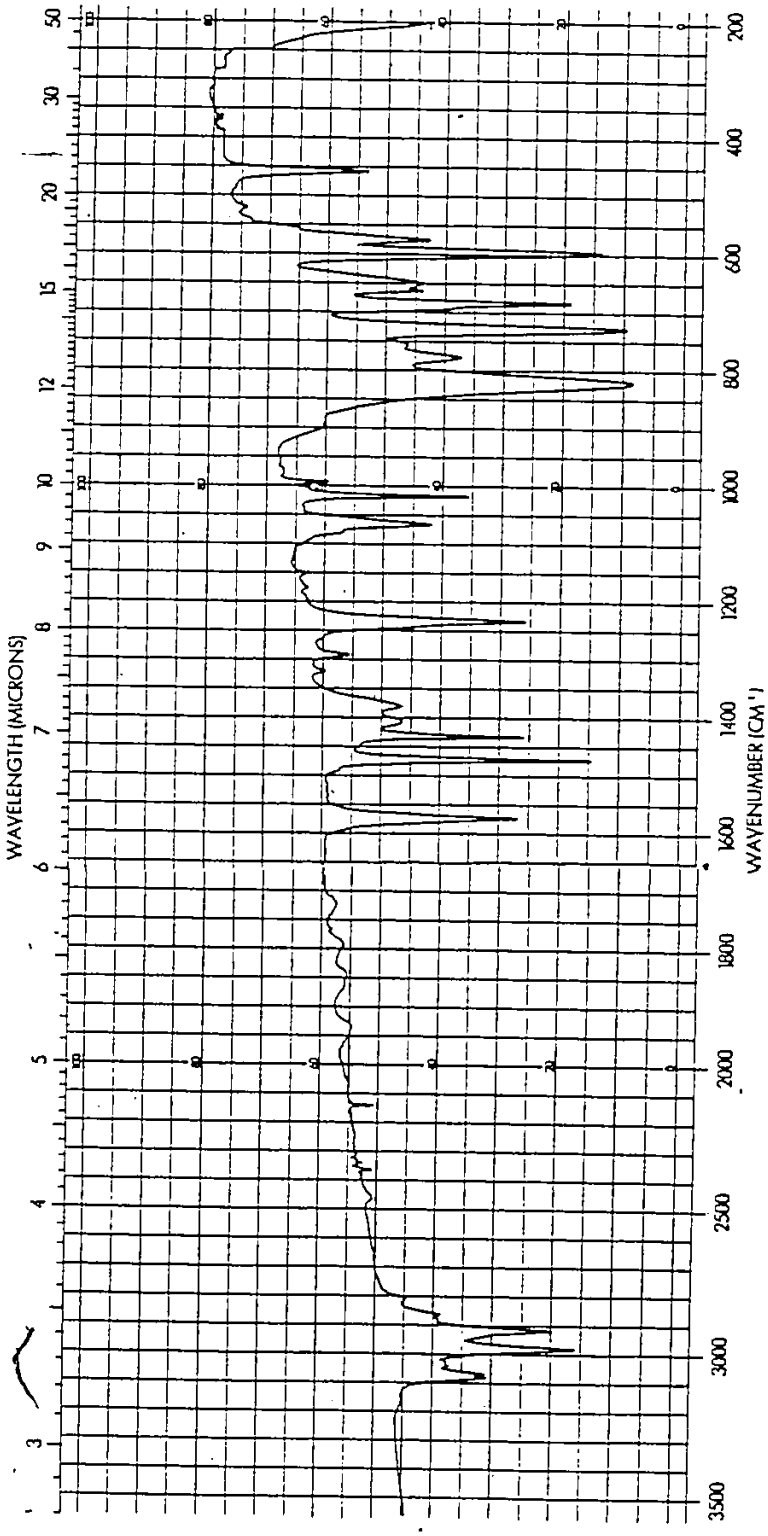

Fig. VII.8. The i.r. spectrum of Me_3GeCH_2SePh.

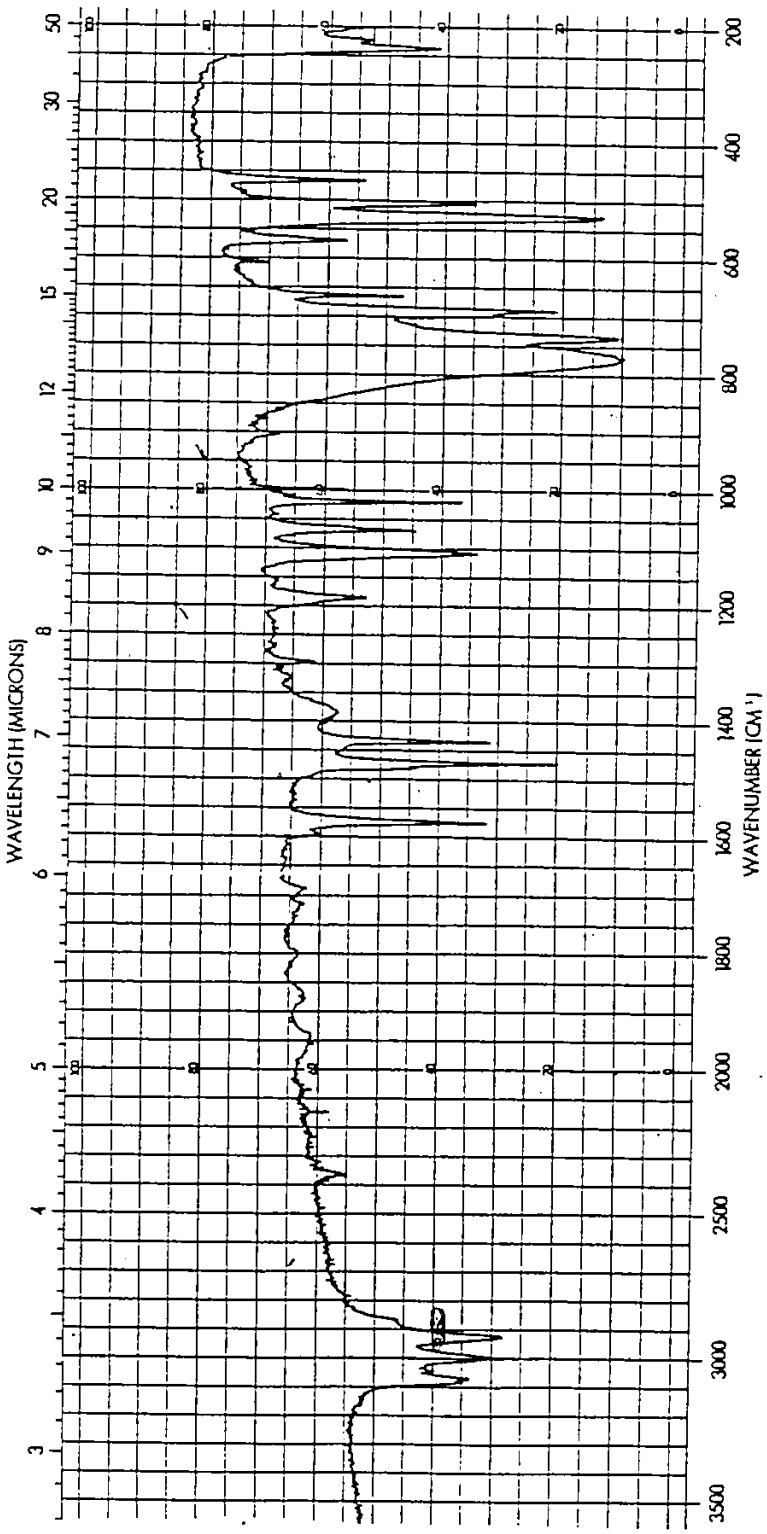

Fig. VII.9. The i.r. spectrum of Me_3SnCH_2SePh.

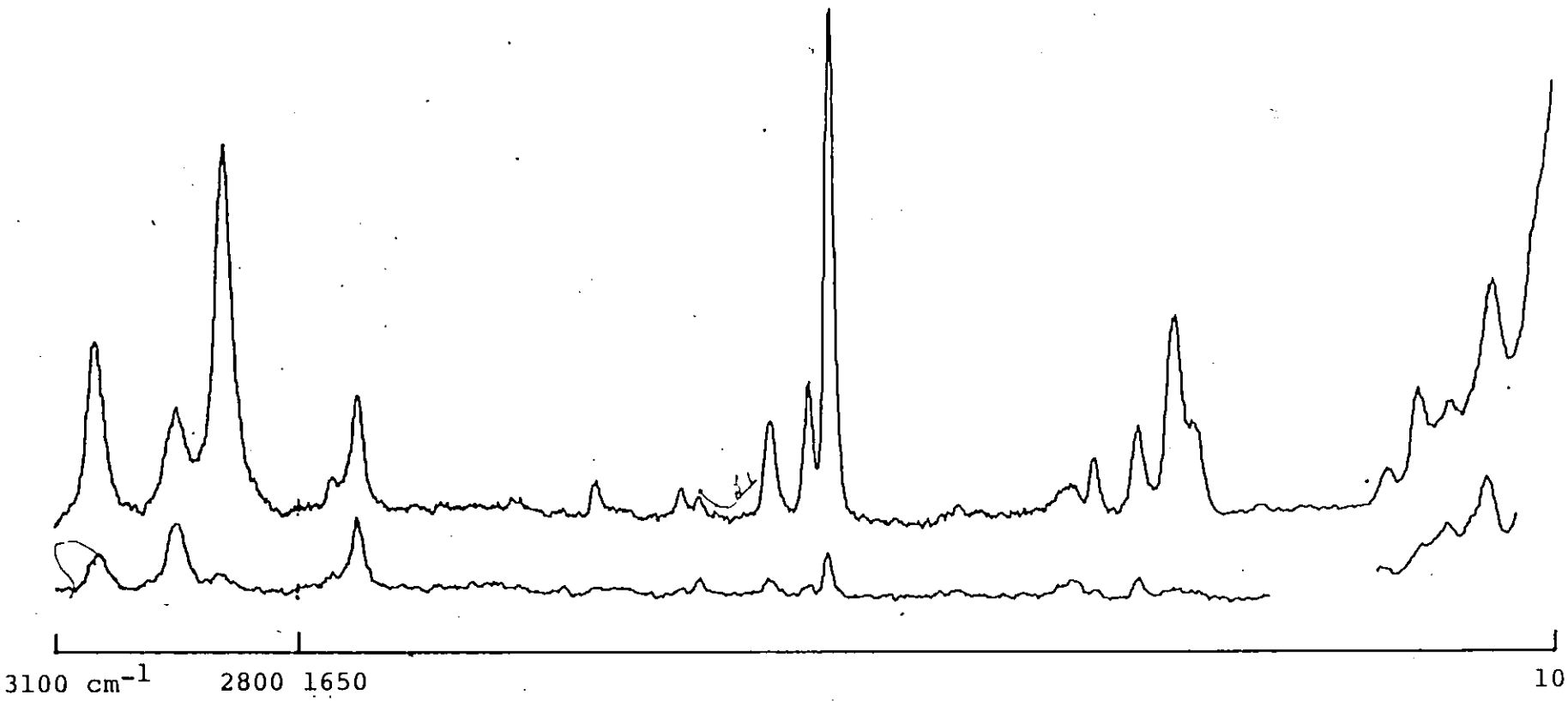

Fig. VII.10. The Raman Spectrum of Me_3SiCH_2SePh.

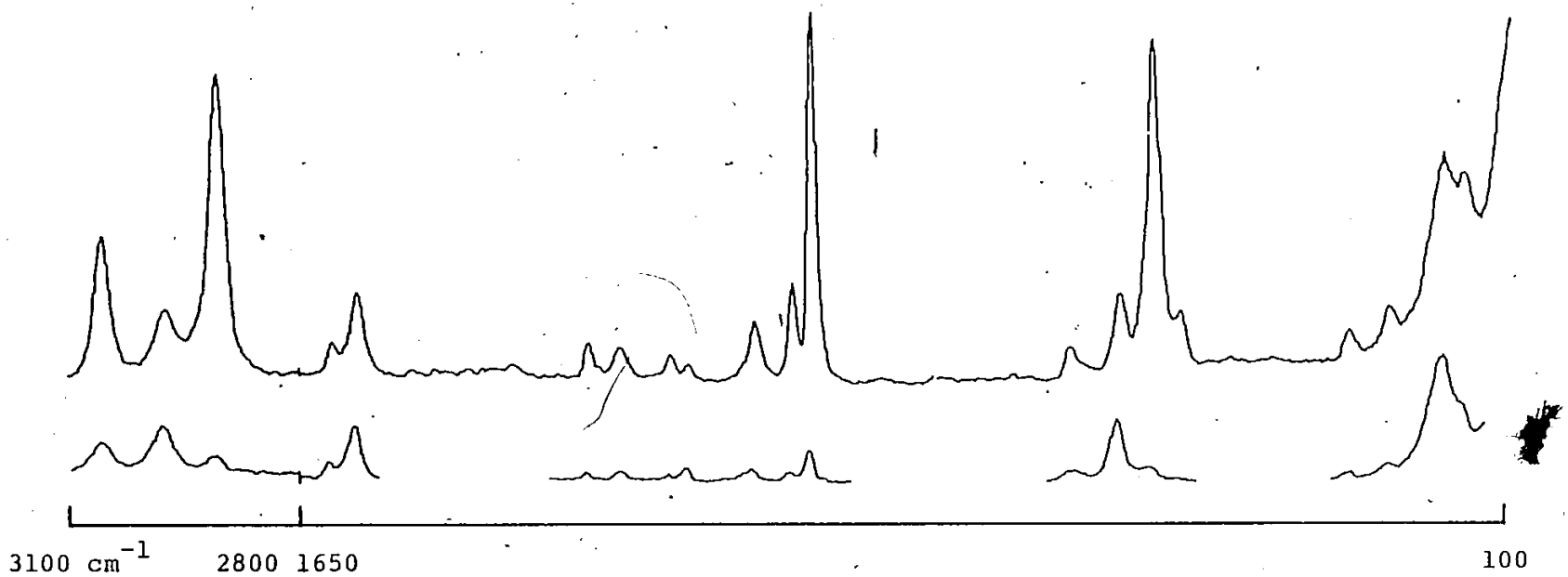

Fig. VII.11. The Raman Spectrum of Me_3GeCH_2SePh.

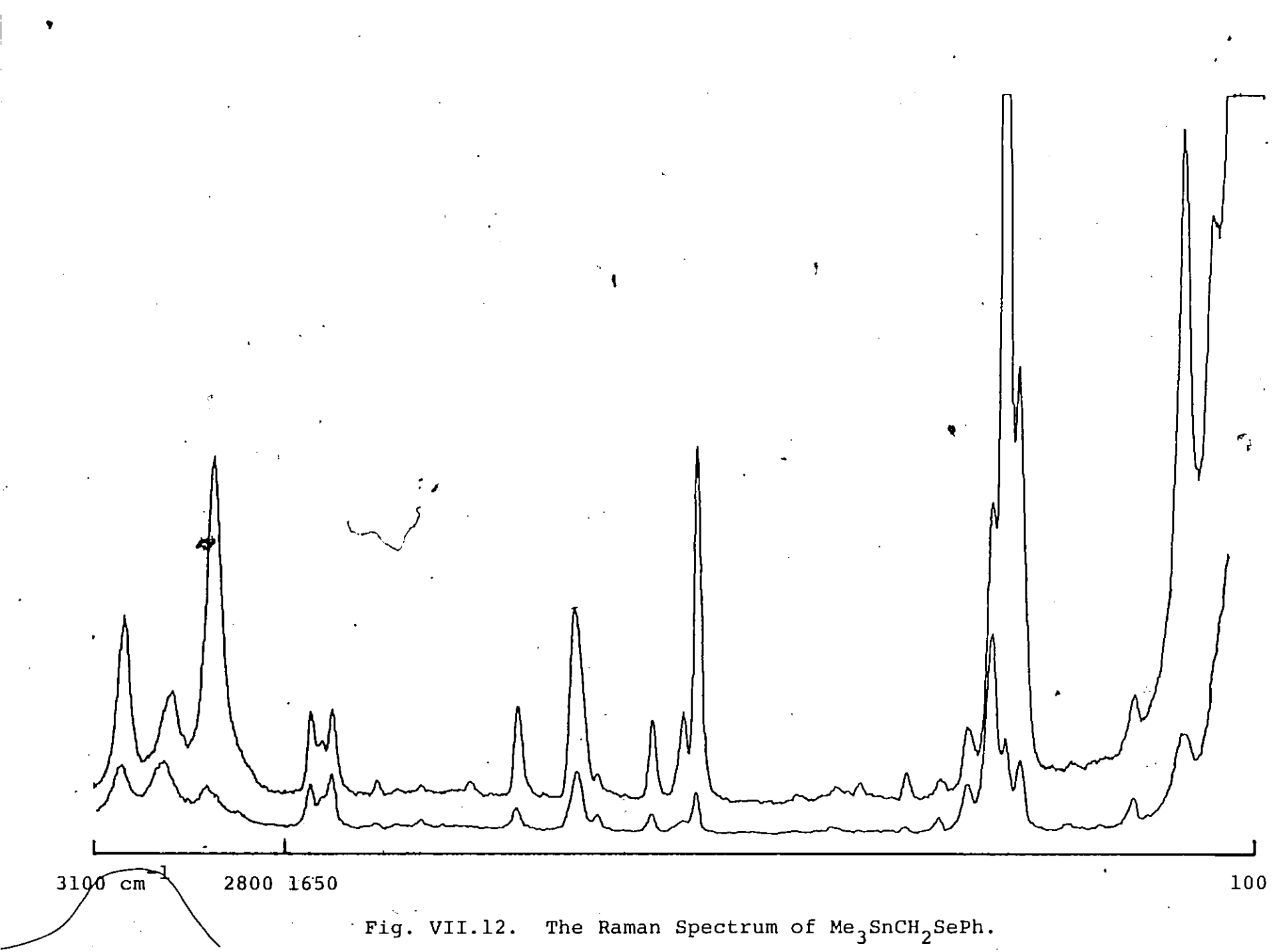

Fig. VII.12. The Raman Spectrum of Me_3SnCH_2SePh.

Table VII.2. The vibrational spectra and the tentative assignments of the series Me_3MCH_2SePh (M = Si,Ge,Sn).

Si		Ge		Sn		
I.R. (liq.)	Raman (liq.)	I.R. (liq.)	Raman (liq.)	I.R. (liq.)	Raman (liq.)	Tentative Assignments
2860 ms	2950 m,dp	2980 m	2972 m,dp	3000 mw	2977 m,dp	(a) CH_3(M),CH_2 str
2910 m	2892 s,p	2917 m	2905 s,p	2917 m	2908 s,p	(s) CH_3(M),CH_2 str
1410 m	1406 w,dp	1405 w	1396 w,dp	1435 mw	1430 vw,dp	(a) CH_3 def.
1260 ms	1264 m	1233 ms	1236 vw,p	1185 mw	1186 m,p	(s) CH_3 def.
1290 w	1284 w	1290 vw	1288 w	1295 vw	1291 mw	CH_2 def.
1075 w	1069 m,p	1065 w	1063 m,p	1070 m	1060 s,p	X-sen.(q),CH_2 rock
838 s	842 w	825 s	833 vw	778 ms	783 vw	(a) CH_3 rock
750 m	753 br	730 w	734 vw	738 ms	745 vw	(s) CH_3 rock
666 ms	672 w,p	662 w	670 mw,p	667 w	670 w,p	x-sen (r)
690 mw	697 w,dp	600 vs	603 m,dp	530 s	537 m,dp	(a) M-C str
570 w	573 m,p	570 mw	562 vs,p	507 ms	510 vs,p	(s) M-C str
460 s	462 vw	460 m	462 vw	465 w	468 vw	X-sen (y)
310 w	307 mw,p	305 vw	307 mw,p		307 mw,p	X-sen (t)
270 s	270 mw,dp		185 ms,dp	222 w	225 mw	(a) MC_3 def.
225 w	228 mw,p		162 ms, p		180 w	(s) MC_3 def.
	180 ms, dp					MC_3 rock

Vibrations associated to the substituent insensitive phenyl modes were observed at:
ν(CH) 3062, p (z), ν(CC) 1612 m,dp (k), 1428 vw (m), 1435 vw (n), 1328 vw (O), β(CH) 1178 w,p (a), 1150 w,dp (C), 1020 m,p (b), ring 995 vs,p, ν(CH) 900 vw (i), 836 vw (g), 738 vw (f), α(CCC) 613 w, dp(s); ϕ(CC) 400 vvw (W).

which has 30 vibrations which may be labeled according to Herzberg's notation.[31] There are six substituent sensitive modes (X-Sen in Table VII.2) which were assigned by comparison with monosubstituted benzenes[62,63] and related molecules[40,41,64-66] such as Me_3MSePh and Me_3MTePh. The remaining 24 substituent-insensitive vibrations may be associated with some confidence to those corresponding modes in benzene[67-69] and are listed as a footnote to Table VII.2.

B. N.m.r. Spectra

The relationship between the ^1H n.m.r. chemical shifts of Me_4Si, Me_4Ge, and Me_4Sn and the relative electronegativities of the group IV elements has been the subject of considerable controversy.[70-72] The net results of that argument is apparently the tacit agreement that the order of electronegativities is probably Ge>Si≥Sn despite the fact that the chemical shifts move in an almost stepwise fashion downfield of TMS. In other words it is recognized that factors effecting the shifts are complex. Thus, it seems appropriate to examine the "internal shifts" given in parentheses (Table VII.3) which reflect the changes in the ^1H n.m.r. chemical shifts relative to the parent compound as a proton on a CH_3 group is replaced by Cl or I, SeMe or SePh. In this manner the shifts may

Table VII.3. ^1H n.m.r. chemical shifts[a] of Me_3MCH_2X (X = H,Cl,I, SeMe, Se,Ph; M = Si,Ge,Sn)

Compound	δMe_3M	δCH_2	$\delta SeMe$	$\delta SePh$[b]
Me_4Si	0.0			
Me_3SiCH_2Cl	0.4	2.98		
Me_3SiCH_2SeMe	0.41	2.00	2.03	
Me_3SiCH_2SePh	0.26	2.15		7.26,7.55
Me_4Ge	0.33			
Me_3GeCH_2Cl	0.66(0.33)	3.30(2.97)		
Me_3GeCH_2SeMe	0.66(0.33)	2.30(1.97)	2.40(2.07)	
Me_3GeCH_2SePh	0.50(0.17)	2.41(2.08)		7.39,7.69(7.06,7.36)
Me_4Sn	0.52			
Me_3SnCH_2I	1.59(1.07)	4.84(4.32)		
Me_3SnCH_2SeMe	1.85(1.33)	4.82(4.30)	3.0(2.48)	
Me_3SnCH_2SePh	1.04(0.52)	4.22(3.70)		7.74,8.12(7.22,7.60)

[a] All shifts are in ppm to low field of external TMS. Values in parentheses indicate shifts relative to Me_4M

[b] Aromatic resonances are resolved into two envelopes for ortho and para (high field) and meta (low field) protons.

be more indicative of electronegativity changes.

The substitution of chlorine into Me_4Si and Me_4Ge has essentially the same effect on the CH_2 group substituted and a slightly larger effect on the other methyl protons in Me_4Si than on Me_4Ge. This could be interpreted as the ability of Cl to pull electron density away through the less electronegative silicon. However, the factors influencing chemical shifts are clearly more subtle than this because although the effect of substituting a SeMe group is similar to that of a Cl atom on the chemical shift of CH_3 protons it is less on the CH_2 protons. Also, the substitution of a SePh group has less effect on the CH_3 protons than SeMe substitution although the effect on the CH_2 protons is similar. Nevertheless, the overall effect is to suggest that Cl is slightly more electronegative than a SeR group, and Ge is slightly more electronegative than Si. The overall effects of substitution in the methyl group of Me_4Sn are much larger than for silicon or germanium analogues which suggests that Sn is much less electronegative than either Si or Ge. The I atom apparently has a similar electronegativity to a SeMe group.

The examination of internal shifts within each phenyl ring might give a further indication of factors influencing these shifts. The ^{13}C chemical shifts for the halides

Table VII.4. The ^{13}C chemical shifts of Me_3MCH_2X and Me_3MCH_2SePh X = Cl,I; M = Si,Ge,Sn.

Compound[a]	δMe_3M	δCH_2	δC_x	δC_m	δC_o	δC_p	σ_R^o
Me_3SiCH_2Cl	-3.56	30.41					
Me_3GeCH_2Cl	-3.43	30.74					
Me_3SnCH_2I	1.82	25.02					
Me_3SiCH_2SePh	-1.16	15.98	133.31	128.76	130.39	125.71	-0.138
Me_3GeCH_2SePh	-1.55	10.92	133.63	128.76	130.38	125.77	-0.135
Me_3SnCH_2SePh	-1.69	5.76	136.94	127.79	127.79	126.88	-0.041

[a]Shifts are to low field of external TMS

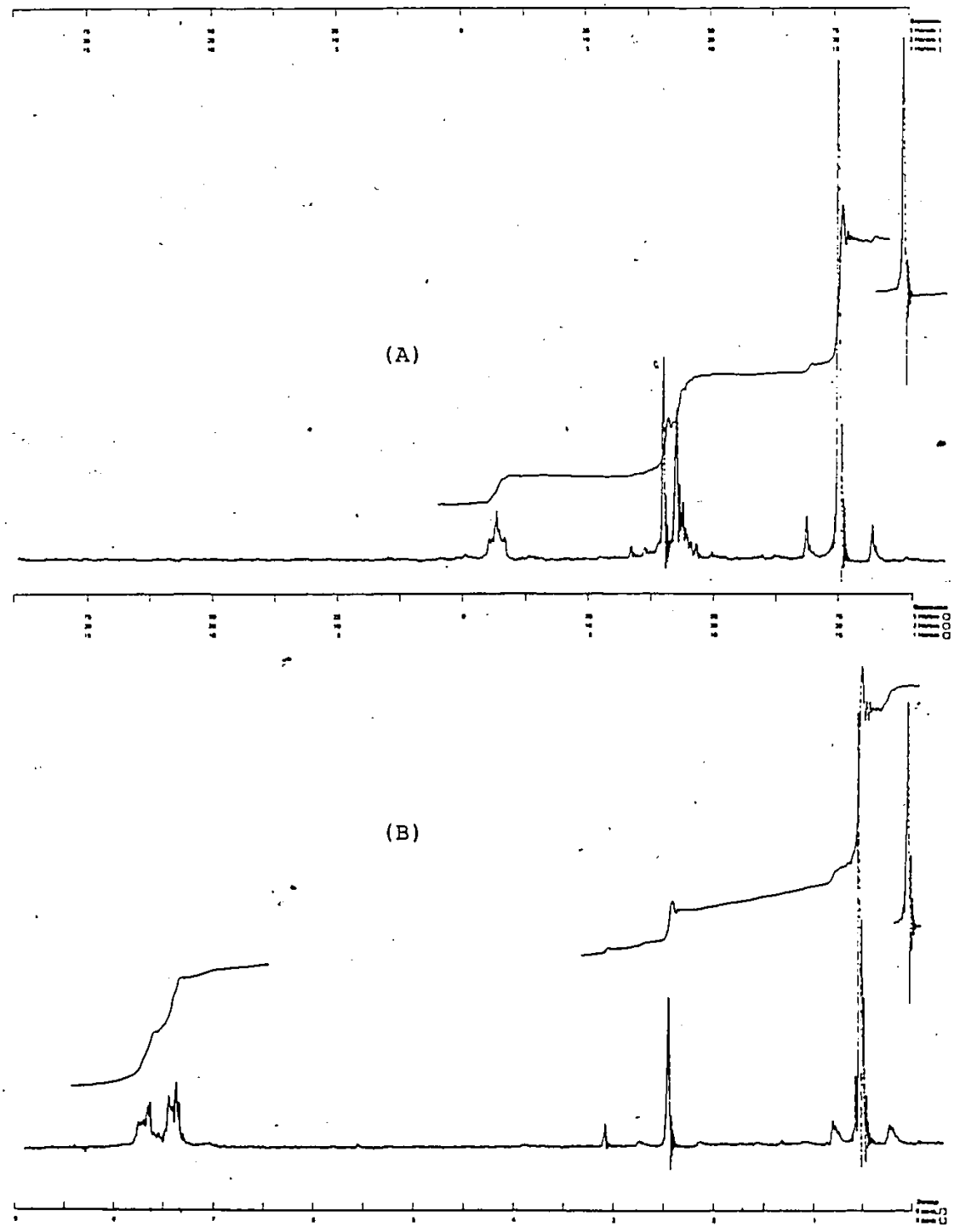

Fig. VII.13. The ^{1}H n.m.r. spectrum of Me_3GeCH_2SeMe (A), and Me_3GeCH_2SePh (B).

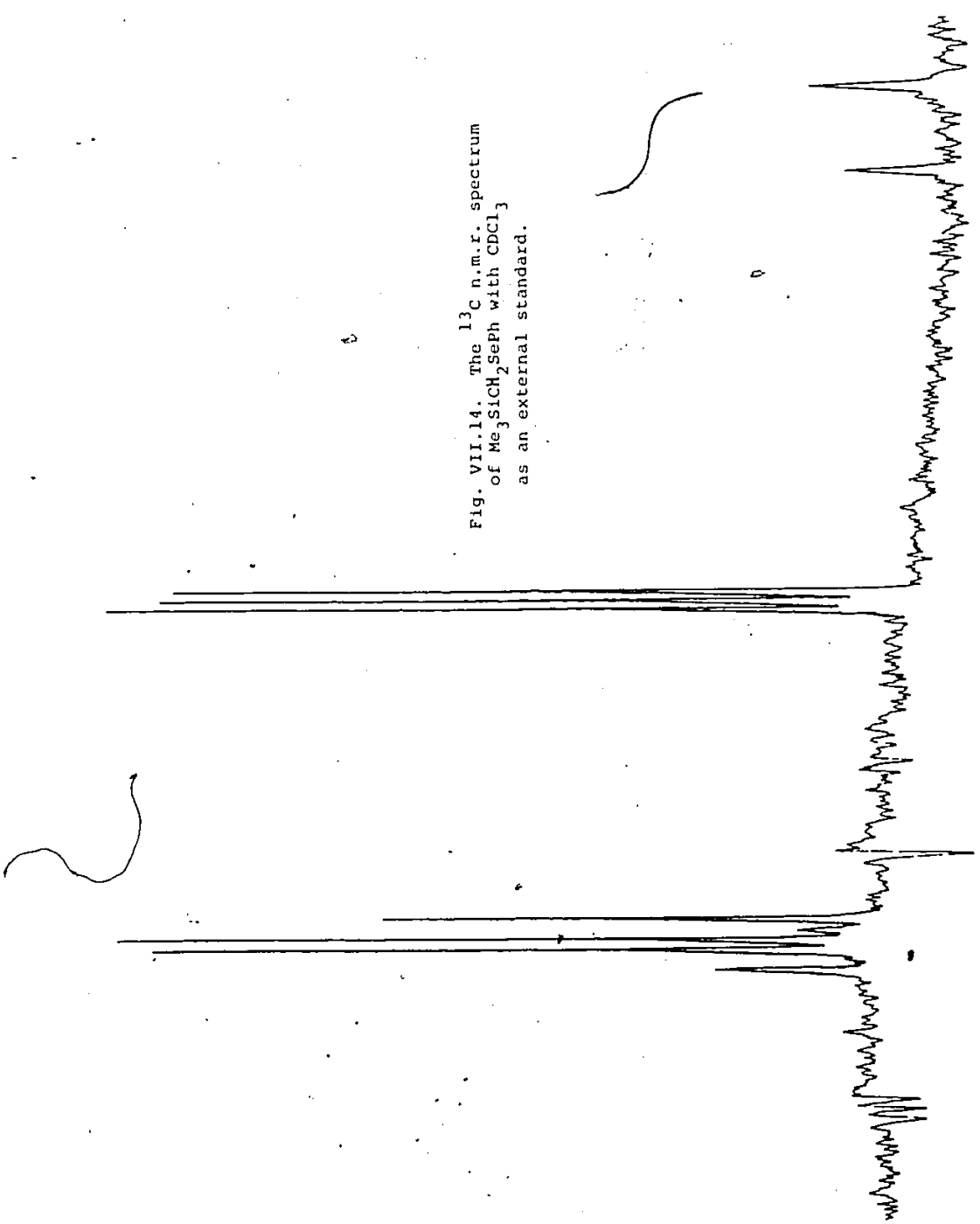

Fig. VII.14. The ^{13}C n.m.r. spectrum of Me_3SiCH_2SePh with $CDCl_3$ as an external standard.

and the SePh compounds are listed in Table VII.4. The Hammett-Taft constants σ_R° [73] were calculated from $\delta_p - \delta_m = 22.06\sigma_R^\circ$ and found to be negative, indicating an electron release from the selenium towards the phenyl ring in the order Si≥Ge>Sn. It is worth mentioning that the results obtained from the ^{13}C n.m.r. spectra are not totally consistent with those obtained from the ^1H spectra. A glance at the CH_2 chemical shifts clearly indicates that Cl is more electronegative than SePh. However, although the electron release towards the phenyl ring is similar for Si and Ge, the CH_2 carbons attached to Si are more deshielded than those attached to Ge indicating Si to be slightly more electronegative then Ge in contrast to the conclusions based on ^1H n.m.r. spectra. This points to the difficulty of arriving at firm conclusions when electronegativity differences are small so that they are presumably not the overriding effect on chemical shifts. The ^1H n.m.r. spectra of Me_3GeCH_2SeMe and Me_3GeCH_2SePh are displayed in Fig. VII. 13 and the ^{13}C n.m.r. spectrum of Me_3SiCH_2SePh is shown in Fig. VII. 14.

VII.4 Preparation of some Pd (II) and Pt (II) Complexes

Compounds of the general formula $(Me_3MCH_2SeR)_2PdCl_2$ and $(Me_3MCH_2SeR)_2PtCl_2$ (M = Si,Ge,Sn; R = Me,Ph) were prepared in a similar manner. Typically, the ligand (ca 4 mmole) and Na_2PdCl_4 or K_2PtCl_4 (ca 2 mmole) were

placed in a 50 mL round bottom flask along with a 1:1 solution of ethanol and water (ca 20 mL) and then stirred under mild reflux for 2 hrs. The solvent was removed in vacuo and the residue was washed with water and filtered. The product was then dissolved in CH_2Cl_2 and filtered. Crystals were formed by the slow evaporation of ethanol. These complexes were soluble in nonpolar solvents such as hexane, ether and methylene chloride but slightly soluble in polar solvents such as ethanol. Table VII.5 shows the complexes prepared, their yield and some of their physical properties.

Table VII.5. Pd(II) and Pt(II) complexes of Me_3MCH_2SeR

Complex	Colour	m.p(°C)	yield %
$(Me_3SiCH_2SeMe)_2PdCl_2$	orange-brown	97	55
$(Me_3SiCH_2SePh)_2PdCl_2$[a]	red-brown	92	74
$(Me_3GeCH_2SePh)_2PdCl_2$	brown	84	66
$(Me_3SiCH_2SeMe)_2PtCl_2$	yellow	93	63
$(Me_3SiCH_2SePh)_2PtCl_2$	yellow	143	96
$(Me_3GeCH_2SeMe)_2PtCl_2$	yellow	91	90

[a]Ref. 13.

When M = Sn, the above reactions proceed with transition metal deposition even when the reaction mixture was stirred at 0°C. The Pt metal that was deposited was characterized by the formation of a ketoxime complex L_2Pt (red) where L = 2-pyridyl-2-thienyl-2-ketoxime.[73a] To make a reasonable assumption of what is happening in this reaction, it should proceed in a closed system preferably on the vacuum line and all products should be analyzed to decide the fate of the Me_3SnCH_2 group. Nevertheless, it is reasonable to assume that the Sn-C bond is cleaved because similar cleavage occurs in the reactions of Me_3SnCH_2I with the sodium salts of transition metal carbonyls.[74]

VII.5 Crystal Structure of $(Me_3SiCH_2SeMe)_2PdCl_2$

A. Experimental

The crystal and refinement data are summarized in Table VII.6. The compound was found to sink in CCl_4 (d = 1.594) but was very soluble in MeI. Thus, the density was measured by the flotation method in an aqueous solution of $ZnCl_2$ and found to be 1.773. A very well shaped crystal was mounted along the largest dimension and data were collected on a Syntex $P2_1$ diffractometer. The intensities of three monitor reflections did not vary significantly during the entire data

collection. The systematic absences (0kl, k≠2n; h0l, l≠2n; hk0, h≠2n) indicated the space group to be Pbca. The data were corrected for Lorentz and polarization effects, and an absorption correction was also applied.

The unit cell dimensions required that the palladium atom be placed at the center of inversion. Using this, the position of the selenium atom was obtained from a sharpened Patterson synthesis. The remaining atoms were revealed by refinement and subsequent difference map. Complete anisotropic refinement minimizing $\Sigma w(|Fo|-|Fc|)^2$ converged at R = 0.0249 and Rw = $[\Sigma w\Delta^2/\Sigma w|Fo|^2]^{1/2}$ = 0.0301 based on 79 variables and 1220 unique reflections for which $I>3\sigma(I)$. The hydrogen atoms were included at the idealized positions (CH = 0.95Å, HCH = 109.5°) with isotropic thermal parameters (U) set at 0.1Å^2 greater than that of the carbon atom to which it is bonded. A weighting scheme of the form $w = 1/[\sigma^2(F) + \rho F^2]$ was utilized with a final ρ value of 0.002. In the last cycle no parameter changed by more than 0.1σ.

Computer programs and sources of scattering factors were the same as used in the structure determination of $Me_3As.BX_3$. The final atomic coordinates and isotropic thermal parameters for non-hydrogen atoms are listed in Table VII.7 while the coordinates of hydrogen atoms and their thermal parameters are displayed in Table VII.8.

Table VII.6 Crystallographic Data

a (Å)	6.492 (4)
b (Å)	11.438 (7)
c (Å)	27.274 (15)
V (Å^3)	2025 (2)
crystal system	Orthorhombic
space group	Pbca
mol. wt.	539.4
Z	4
ρ_c (g cm^{-3})	1.769
ρ_o (g cm^{-3})	1.773
crystal dimensions (mm)	0.18 x 0.18 x 0.3
radiation	MoKα, λ = 0.71069Å
monochromator	highly oriented graphite
temp (°C)	21
abs coeff, μ(cm^{-1})	43
min abs corr	1.961
max bas corr	2.138
2θ angle (°)	4-50
scan type	coupled θ (crystal)/2θ (counter)
scan width	$k\alpha_1$-1° to $K\alpha_2$ + 1°
scan speed (°min^{-1})	variable, 2.02 - 4.88
bkgd time/scan time	0.5
total reflcns measd	2112
unique data used	1220 [I>3σ(I)]
no. of parameters (NP)	79
R	0.0249
R_{WF}	0.0301

Table VII.7. Final fractional coordinates and isotropic thermal parameters for non-hydrogen atoms of $(Me_3SiCH_2SeMe)_2PdCl_2$ with standard deviations in parentheses.

Atom	x		y		z		$U_{eq}^{\dagger}(A^2 x10^3)$	
Pd	0.0	(0)	0.0	(0)	0.0	(0)	36.0	(3)
Se	-0.21950	(8)	0.07759	(4)	0.064351	(2)	41.2	(3)
Cl	0.2142	(2)	-0.0528	(1)	0.0632	(1)	56	(1)
Si	-0.1224	(2)	0.2241	(1)	0.16131	(1)	46	(1)
C (1)	-0.4246	(9)	0.1785	(5)	0.0338	(2)	62	(4)
C (2)	-0.0536	(8)	0.1998	(4)	0.0950	(2)	48	(3)
C (3)	-0.4043	(9)	0.2424	(6)	0.1679	(2)	68	(3)
C (4)	0,0124	(10)	0.3598	(5)	0.1811	(2)	50	(4)
C (5)	-0.0303	(10)	0.0938	(5)	0.1966	(3)	52	(4)

$^{\dagger}U_{eq}$ for non hydrogen atoms is calculated from the refined anisotropic thermal parameters.

$(U_{eq} = 1/3\ \Sigma_i \Sigma_j . U_{ij} a_i^* . a_j^* . a_i a_j)$

Table VII.8. Final fractional coordinates and thermal parameters for hydrogen atoms of $(Me_3SiCH_2SeMe)_2PdCl_2$

Atom	x	y	z	U
H (11)	-0.5218	0.1321	0.0166	70
H (12)	-0.3583	0.2303	0.0116	70
H (13)	-0.4934	0.2224	0.0584	70
H (21)	-0.0748	0.2708	0.0776	60
H (22)	0.0874	0.1782	0.0930	60
H (31)	-0.4720	0.1731	0.1574	70
H (32)	-0.4485	0.3063	0.1483	70
H (33)	-0.4371	0.2573	0.2012	70
H (41)	-0.0191	0.3744	0.2153	80
H (42)	-0.0323	0.4239	0.1624	80
H (43)	0.1570	0.3502	0.1782	80
H (51)	-0.0630	0.1037	0.2303	80
H (52)	0.1146	0.0863	0.1929	80
H (53)	-0.0960	0.0254	0.1845	80

Table VII. 9. Bond lengths (Å) and angles (°) for $(Me_3SiCH_2SeMe)_2PdCl_2$ with standard deviation in parentheses.

Bond lengths		Bond angles[a]	
		Cl-Pd-Cl'	180.0 (1)
Pd-Se	2.429 (1)	Se-Pd-Se	179.9 (1)
Pd-Cl	2.295 (1)	Se-Pd-Cl	84.8 (1)
Se-C (1)	1.949 (5)	C(1)-Se-Pd	108.0 (2)
Se-C (2)	1.952 (4)	C(2)-Se-Pd	104.3 (1)
Si-C (2)	1.884 (5)	C(1)-Se-C(2)	97.8 (2)
Si-C (3)	1.851 (5)	Se-C(2)-Si	112.7 (2)
Si-C (4)	1.868 (5)	C(2)-Si-C(3)	110.1 (2)
Si-C (5)	1.872 (6)	C(2)-Si-C(4)	107.5 (2)
		C(2)-Si-C(5)	107.5 (3)
		C(3)-Si-C(4)	109.5 (3)
		C(3)-Si-C(5)	110.8 (3)
		C(4)-Si-C(5)	111.0 (3)

[a]Symmetry equivalent positions': -x,-y,-z.

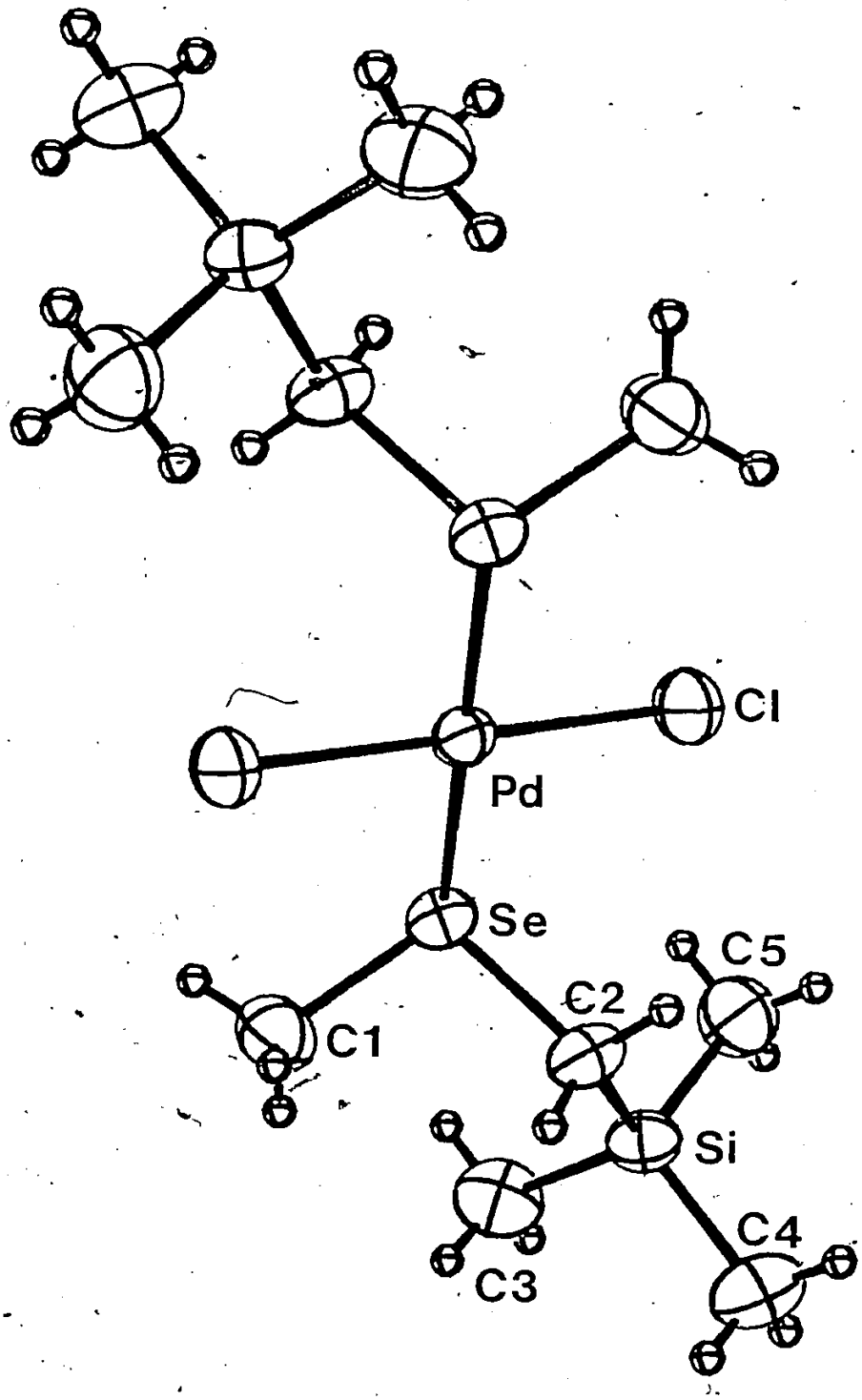

Fig. VII.15 View of $(Me_3SiCH_2SeMe)_2PdCl_2$. Unlabeled atoms are related to labeled ones by the Pd center of inversion.

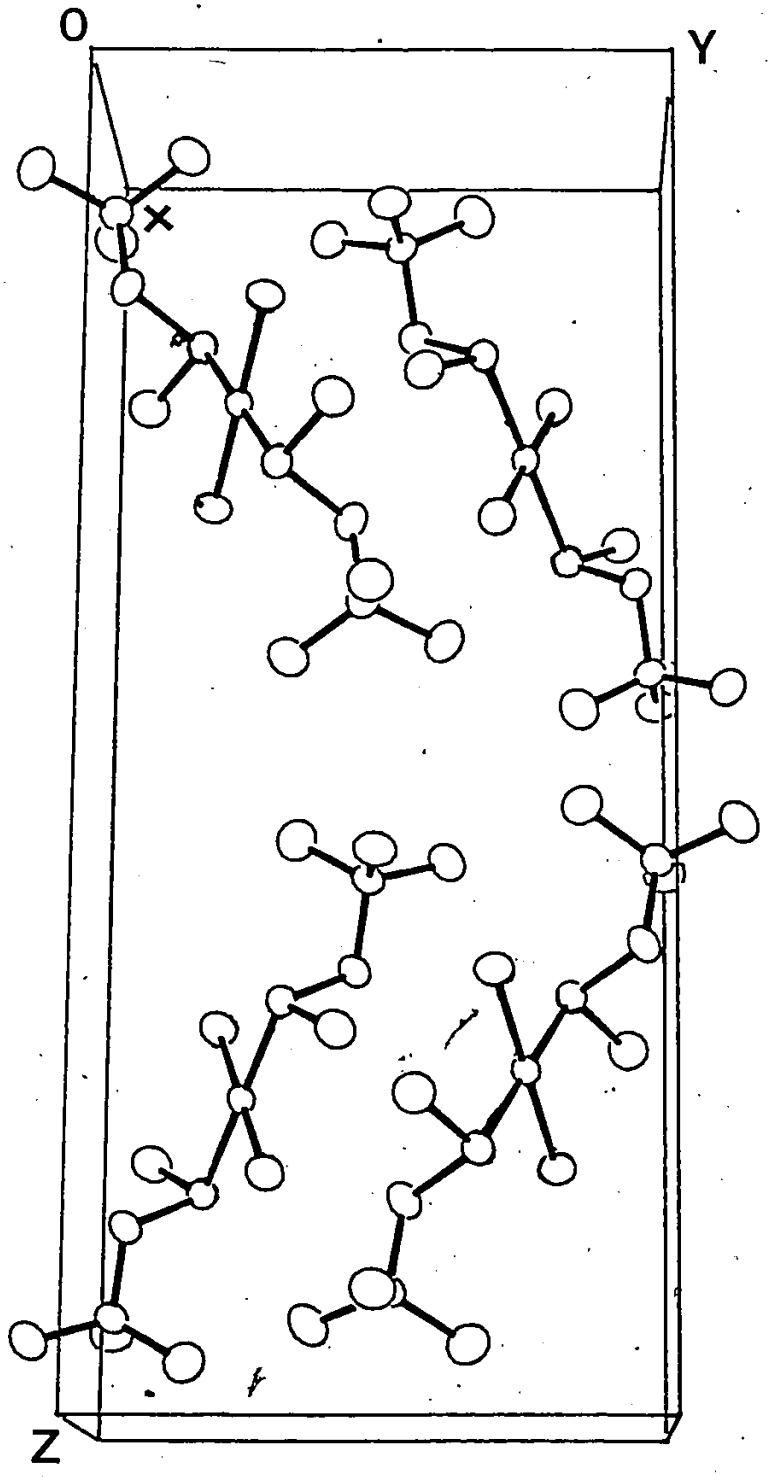

Fig. VII.16 Contents of one unit cell of $(Me_3SiCH_2SeMe)_2PdCl_2$. The cell shown extends along a, b and c from -1/4 to 3/4. H atoms are not included for clarity.

Table VII.9 contains the important bond lengths and angles. Fig. VII.15 shows a view of the molecule with atomic numbering and Fig. VII.16 shows the unit cell packing.

B. Discussion

The single crystal X-ray structure determination confirms the trans structure of $(Me_3SiCH_2SeMe)_2PdCl_2$. This complex exists as discrete and centrosymmetric molecules as shown in Fig. VII.15. The bonding at Pd is approximately square planar[75] (dsp^2) with a Se-Pd-Cl(1) angle of 84.8(1)° rather than 90° and with the $PdSe_2Cl_2$ group lying in one plane. The asymmetry in the groups attached to Se in the ligand may have contributed to the rather chain-like character of the molecule (Fig. VII.13, 14) which is reflected in the fact that one of the cell dimensions c = 27.274(15)Å, is much larger than a or b.

The pyramidal coordination around Se indicates a pseudotetrahedral arrangement about Se with a stereochemically active lone pair occupying the fourth position. The angles C(1)-Se-Pd = 108.0 (2)°, C(2)-Se-Pd = 104.3 (1)° and C(1)-Se-C (2) = 97.8 (2)° being less than the tetrahedral angle of 109.5°, may be indications that the repulsive forces between the lone pair and bonding pairs of electrons result in the observed reduction of these angles which would be in agreement with the VSEPR

(valence shell electron pair repulsion) theory.[76]

The Pd-Se bond length of 2.429 (1) Å is slightly less than the sum (2.45 Å) of the covalent radii, 1.31 Å for square planar [77] Pd(II) and 1.14 Å for tetrahedral Se and therefore π-bonding does not seem to be important. Other Pd-Se bond lengths have been determined to be 2.429 (7) Å in trans-dicholorobis (diethylselenide) palladium (II),[78] and 2.40 (1) Å in cis-dichloro,1,2-bis (isopropylseleno)ethane palladium (II).[79] This Pd-Se bond length falls between reported bond lengths of Pd-S = 2.310 (3) Å and Pd-Te = 2.606 (1) Å.[80] The determined Pd-Cl bond length of 2.295 (1) Å is almost equal to the sum of Pauling covalent radii,[77] 1.32 Å for square planar palladium (II) and 0.99 Å for chlorine and agrees well with 2.266 (9) Å in $(Et_2Se)_2PdCl_2$[78] and 2.29 Å in $(Me_2SO)_2PdCl_2$.[81] The Se-C bond lengths[78] and the Si-C distances are in good agreement with determined values.[80,82-84]

It is interesting to note that there is a "tilt" in the C(1)-Se-C(2) moiety with the C(1) atom close to the plane of the $PdSe_2Cl_2$ group. It would be convenient to relate this to a packing effect resulting from the asymmetric substitution on Se. However, there is essentially the same "tilt" in the $(Et_2Se)_2PdCl_2$ crystal where the substitution is symmetric as well as the related tellurium

compound trans $[(Me_3SiCH_2CH_2CH_2)_2Te]_2Pd(SCN)_2$. In this latter compound[80] it was suggested that the degree of tilt was in some way associated with a repulsive interaction between Te and C atom of the SCN group. This obviously cannot be the case in $(Me_3SiCH_2SeMe)_2PdCl_2$.

A common factor in all these structures is the clear evidence of a stereochemically active lone-pair on selenium (or tellurium). If it is assumed that the Pd-Se bond is along the x-axis, then maximum separation between the Se lone-pair and the chlorine lone-pairs is achieved by a configuration in which the selenium lone pair is in the xz plane below the xy plane with the two carbon atoms attached to it above the xy plane. This is approximately the chosen configuration with the exception of the slight tilt. The position of the selenium lone-pair in the xz plane places it in closest proximity to any electron density about Pd associated with the d_{z^2} orbital. Any shift out of the plane will increase this distance and a simple model suggests that a tilt of 20-30° would lead to a reasonable compromise which would minimize all lone-pair repulsions. The tilt brings the CH_3 group (or one of the CH_2 groups in the case of the other two structures) into closer proximity with one of the Cl atoms which as a result is bent away from 90°. The observed Cl'-Pd-Se (Cl' is generated from Cl by inversion) is 95.22°. In

$(Me_3SiCH_2SeMe)_2PdCl_2$, the tilt is such as to bring the less bulky group towards a Cl atom. The C(1)-Cl' non-bonding distance is 3.307 Å and the C(2)-Cl distance is 3.48 Å. So, even though the Cl' atom is moving away from the CH_3 group and Cl is forced towards the CH_2 group of CH_2SiMe_3, the C-Cl distance is still longer to the bulky group.

REFERENCE

PART THREE

1. E. W. Abel and D. A. Armitage, Adv. Organomet. Chem. 5, 1 (1967).

2. H. Schumann and M. Schmidt, Angew. Chem. Int. Ed. 4, 1007 (1965).

3. M. Lesbre, P. Mazerolles and J. Satgé, The Organic Compounds of Germanium, Wiley (1971).

4. D. J. Ager and R. C. Cookson. Tet. Lett. 21, 1967 (1980).

5. D. J. Peterson, J. Org. Chem. 33, 780 (1968).

6. F. A. Carey and O. Hernandez, J. Org. Chem. 38, 2670 (1973).

7. F. A. Carey and A. S. Court, J. Org. Chem. 37, 939 (1972).

8. H. Schumann, O. Stelzer and W. Crick, Angew. Chem. Int. Ed. 8, 271 (1969).

9. W. Ehrl and H. Vahrenkamp, Chem. Ber. 105, 1471 (1972).

10. E. W. Abel, S. K. Bhargava, K. Kite, K. G. Orrell, V. Šik and B. L. Williams, Polyhedron 1, 289 (1982).

11. E. W. Abel, S. K. Bhargava, K. G. Orrell and V. Šik, Inorg. Chim. Acta 49, 25 (1981).

12. E. W. Abel, G. W. Farrow, K. G. Orrell and V. Šik, J. Chem. Soc. Dalton, 42 (1977).

13. E. W. Abel, A. K. Shamsuddin Ahmed, G. W. Farrow, K. G. Orrell and V. Šik, J. Chem. Soc. Dalton, 47 (1977).

14. K. A. Hooton and A. L. Allred, Inorg. Chem. 4, 671 (1965).

15. W. E. Davidson, K. Hills and M. C. Henry. J. Organomet. Chem. 3, 285 (1965).

16. C. Glidewell, J. Chem. Soc. (A), 823 (1971).

17. J. E. Drake and C. Riddle, J. Chem. Soc. (A). 3134 (1970).

18. E. W. Abel, J. Chem. Soc., 4406 (1960).

19. E.A.V. Ebsworth, R. Taylor and L. A. Woodward, Trans. Far. Soc. 55, 211 (1959).

20. J. T. Wang and C. H. Van Dyke, Inorg. Chem. 7, 1319 (1968).

21. J. E. Drake and C. Riddle, Quart. Revs. 24, 263 (1970).

22. E. Wiberg and E. Amberger, Hydrides of the Elements of Main Group I-IV, Elsevier (1971).

23. H. J. Reich and S. K. Shah, J. Amer. Chem. Soc. 97, 3250 (1975).

24. K. Savhdev and H. S. Sachdev, Tet. Lett. 47, 4223 (1976).

25. E. W. Abel, A. M. Atkins, B. C. Crosse and G. V. Hutson, J. Chem. Soc. (A), 687 (1968).

26. E. W. Abel, B. C. Crosse and G. V. Hutson, J. Chem. Soc. (A), 2014 (1967).

27. E. W. Abel, B. C. Crosse and G. V. Hutson, Chem. and Ind., 238 (1966).

28. H. Shumann and R. Weis, Angew. Chem. Int. Ed. 9, 246 (1970).

29. D. L. Klayman and W.H.D. Gunther, Organic Selenium Compounds: Their Chemistry and Biology. J. Wiley, New York (1973).

30. F. R. Hartley, The Chemistry of Platinum and Palladium, J. Wiley, New York (1973).

31. J. W. Anderson and J. E. Drake, Inorg. Nucl. Chem. Lett. 7, 1007 (1971).

32. J. E. Drake, B. M. Glavinčevski and R. T. Hemmings, J. Inorg. Nucl. Chem. 41, 457 (1979).

33. J. E. Drake and C. Riddle, J. Chem. Soc. (A), 1573 (1969).

34. J. E. Drake, B. M. Glavinčevski and H. E. Henderson, Can. J. Chem. 45, 465 (1928).

35. J. E. Drake, B. M. Glavinčevski, R. Humphries and A. Majid, Can. J. Chem. 57, 3253 (1979).

36. J. E. Drake, B. M. Glavinčevski and R. T. Hemmings, Can. J. Chem. 58, 2161 (1980).

37. G. K. Barker, Ph.D. Thesis, University of Windsor (1972).

38. J. W. Anderson, G. K. Barker and M. Rodger, J. Chem. Soc. Dalton, 1716 (1973).

39. G. K. Barker, J. E. Drake and R. T. Hemmings, J. Chem. Soc. Dalton, 450 (1974).

40. J. E. Drake and R. T. Hemmings, J. Chem. Soc. Dalton, 1730 (1976).

41. J. E. Drake and R. T. Hemmings, Inorg. Chem. 19, 1879 (1980).

42. M. Tiecco, L. Testaferri, M. Tingoli, D. Chianelli and M. Montanucci, Synth. Commun. 13, 617 (1983).

43. C. S. Cundy, B. M. Kingston and M. F. Lappert, Adv. Organomet. Chem. 11, 253 (1973).

44. J. Jeffery, M. F. Lappert, N. T. Luong-Thi, M. Webb, J. L. Atwood and W. E. Hunter, J. Chem. Soc. Dalton, 1593 (1981).

45. E. W. Abel and G. W. Farrow, J. Inorg. Nucl. Chem. 42, 541 (1980).

46. R. W. Bott, C. Eaborn and T. W. Swaddle, J. Organomet. Chem. 5, 233 (1966).

47. F. P. Colonna, R. Danieli, G. Distefano and A. Ricci, J. Chem. Soc. Perkin II, 306 (1976).

48. D. Seyferth. J. Amer. Chem. Soc. 80, 1336 (1968).

49. F. R. Hartley and P. N. Vezey. Adv. Organomet. Chem. 15, 189 (1977).

50. P. M. Henry. Adv. Organomet. Chem. 13, 363 (1975).

51. J. R. Alkins and P. J. Hendra, Spectrochim. Acta 22, 2075 (1965); 23, 1671 (1967).

52. A. B. Harvey and M. K. Wilson, J. Chem. Phys. 45, 678 (1966).

53. W. H. Green and A. B. Harvey, J. Chem. Phys. 49, 3586 (1968).

54. M. Jakoubkova, Z. Papouskova and V. Chvalovsky, Collect. Czech. Chem. Commun. 45, 854 (1980).

55. B. Burger, Spectrochim. Acta 24, 2015 (1968).

56. A. L. Smith, Spectrochim. Acta 19, 849 (1963).

57. J. E. Griffiths, Spectrochim. Acta 20, 1335 (1964).

58. J. R. Durig, C. F. Jumper and J. N. Willis, J. Mol. Spectr. 37, 260 (1971).

59. F. Edgell and C. H. Ward, J. Mol. Spectr. 8, 343 (1962).

60. E. R. Lippincott, P. Mercer and M. C. Tobia, J. Phys. Chem. 57, 939 (1953).

61. G. Herzberg, Infrared and Raman Spectra of Polyatomic Molecules, D. Gan Nostrand, Princeton, New Jersey (1945), p. 118.

62. C. V. Stephensen, W. C. Coburn, and W. S. Wilcox, Spectrochim Acta 17, 933 (1961).

63. D. H. Whiffen, J. Chem. Soc. 1350 (1956).

64. E.A.V. Ebsworth and J. J. Turner, J. Phys. Chem. 67, 805 (1963).

65. D. M. Revitt and D. B. Sowerby, Spectrochim. Acta 26 (A), 1581 (1970).

66. J.H.S. Green and W. Kynaston, Spectrochim. Acta 25 (A), 1677 (1969)..

67. F. A. Miller, J. Chem. Phys. 24, 996 (1956).

68. R. D. Mair and D. F. Hornig, J. Chem. Phys. 17, 1236 (1949).

69. N. Herzfeld, C. K. Ingold and H. G. Poole, J. Chem. Soc. 222, 235, 239, 316 (1946).

70. A. L. Allred and E. G. Rochow, J. Inorg. Nucl. Chem. 5, 269 (1958).

71. R. S. Drago, J. Inorg. Nucl. Chem. 15, 237 (1960).

72. A. L. Allred and E. G. Rochow, J. Inorg. Nucl. Chem. 20, 167 (1961).

73. R. W. Taft, Jr., S. Ehrenson, I. C. Lewis, and R. E. Glick, J. Amer. Chem. Soc. 81, 5352 (1959).

73a. P. W. Beaupre and W. J. Holland, Microchim. Acta 1, 203, 273 (1983).

74. R. B. King and K. C. Hodges, J. Organomet. Chem. 65, 77 (1974).

75. F. A. Cotton and G. Wilkinson, Advanced Inorganic Chemistry, 2nd ed. Interscience; New York (1966).

76. R. J. Gillespie, J. Chem. Ed. 47, 18 (1970).

77. L. Pauling, The Nature of the Chemical Bond, 3rd ed., Cornell University Press, Ithaca, N.Y. (1960).

78. P. E. Skakke and S. E. Rasmussen, Acta Chem. Scand. 24, 2634 (1970).

79. H. J. Whitefield, J. Chem. Soc. (A), 113 (1970).

80. H. J. Gysling, H. R. Luss and D. L. Smith, Inorg. Chem. 18, 2696 (1979).

81. M. S. Bennet, F. A. Cotton and D. L. Weaver, Nature 212, 286 (1966).

82. L. Pazdernik, F. Brisse and R. Rivest, Acta Cryst. Sec. B, 33, 1780 (1977).

83. E. R. Corey, J. Y. Corey and W. F. Paton, Acta Cryst. Sec. B, 33, 1254 (1977).

84. R. K. Chadha and J. E. Drake, J. Organomet. Chem. (1984), in press.

PART FOUR

AB INITIO STUDIES OF COMPLEXES BETWEEN SiF_4 AND NH_3

CHAPTER VIII

AB INITIO STUDIES OF COMPLEXES BETWEEN SiF_4 AND NH_3

VIII.1 Molecular orbital calculations

Molecular orbital calculations are so well documented that there is hardly any need to go into details or mathematical derivations. Some excellent books have been written on the subject[1-6] discussing development, applications and approximations. The Roothaan[7,8] equations developed from Hartree-Fock[9,10] equations form the basis of ab initio calculations through which a number of integrals are evaluated by an algebraic self consistent method in order to calculate a wave function.

All the commonly used molecular orbital approximations begin with the Roothaan form of the Self Consistent Field (SCF) equations. Inherently, these approximations are semiempirical in the sense that the aim is to interpret relationships and trends in experimental data. The CNDO/2 (complete neglect of differential overlap) method[3,11-13] is the most widely used. As the name suggests, this method neglects all two-electron integrals which depend on the overlapping of different atomic orbitals. There are other less known semiempirical approximations such as INDO[14] and MINDO[15] which differ in the extent of parametrization. The Hückel[16] approximation is the most drastic, but is nevertheless widely used among organic chemists.

Chemists are already familiar with various approximations of the molecular orbital theory. Until recently, ab

initio calculations have been monopolized by theoretical chemists. The great advances in computer technology and the increase in the availability of computer programs have practically put every molecule within the capability of the non-theoretical chemist. Now, an inorganic chemist can obtain an ab initio wavefunction programme which can be used as a black box. This trend is expected to accelerate with computer development which, in turn, contributes to a decrease in computation time.

VIII.2 Introduction

Complexes of the type $MX_4.nL$, where M = a group IV metal (Si, Ge, Sn or Pb), X = halogen, L = uni- or bidentate ligands such as Me_3N, Me_3P, NH_3, bipy, etc., and n = 1 or 2 have been known for a long time. The synthesis of the complex $SiF_4.2NH_3$ was first reported by Davy in 1812[17] and various chemical and physical properties of the complex were reported in several early studies.[18-21] For the 1:1 adducts, $MX_4.L$, there are two plausible geometrical isomers with the ligand L in the axial or equatorial positions. (Henceforth, a complex will be labeled according to the position of the ligand; a for axial and e for equatorial). Likewise, the octahedral 1:2 adducts, $MX_4.2L$, may have either cis or trans geometrical isomers.

The few studies on complexes of the type $SiF_4.L$,

where L is NH_3 [22] or Me_3N[23,24], were in agreement that the axial configuration is the favoured isomer. For the 1:2 adduct, $MX_4.2L$, the results are more contentious. Muetterties[25] reported on the ^{19}F n.m.r. spectra of some soluble octahedral $SiF_4.2L$ complexes. A single resonance line was observed in each case, strongly indicative of the trans arrangement. Furthermore, several group IV complexes have been shown by X-ray diffraction to favour the trans form in the solid state. These include $SiF_4.py$ [26], $GeCl_4.2py$[27], $SnCl_4.2HMPT$ and $SnBr_4.2HMPT$[28]. $SiF_4.2Me_3N$ was also claimed[23,24] to be trans from spectroscopic analysis.

By contrast, Aggarwal and Onyszchuk[29] concluded from their study of the infra red spectra of $SiF_4.2NH_3$ that it is in the cis form. They assigned the doublet, at 905 and 935 cm^{-1}, to the Si-N stretching and a peak centered on 725 cm^{-1} which is broad because of coupling among four bands attributable to the Si-F stretching modes. This apparently conflicting experimental result, if correct, suggests that the geometrical preferences of the complexes may depend on such factors as difference in electronegativities and/or bulkiness of the ligands. This, in turn, suggests that the two possible geometrical isomers may not differ greatly in total energy so that the tendency of one to form rather than the other could change under suitable conditions. It is also possible that the reaction pathways to 1:2 adducts

lead to one form which subsequently transforms into the other as conditions change. To clarify these questions, the electronic structures of five complexes are calculated: cis and trans isomers of $SiF_4.2NH_3$ and the a, e, and square pyramidal forms of $SiF_4.NH_3$.

Recently, a similar calculation for four different geometries of the 1:1 adduct appeared in the literature.[30] Our results agree well with the conclusion that the axial form is the more stable. However, the total energies do differ. The difference in the basis sets and the inclusion of configuration interaction could be responsible for the discrepancies in the total energy obtained by both calculations.

VIII.3 Calculations and Results

A QCPE (Quantum Chemistry Program Exchange) program[31] based on the minimal basis set ab initio MO theory, GAUSSIAN 70, was used in this work. In all cases optimal geometries were first determined by using basis set STO-3G. Molecular parameters of primary importance in these complexes are r_{Si-N}, <F-Si-N and <F-Si-F', followed by r_{Si-F} and for cis-$SiF_4.2NH_3$ the angle <N-Si-N' also belongs to the first group. The least crucial parameters are the orientation of ammonia molecular and r_{N-H}. The <F-Si-N and <F-Si-F' were first varied for several values of r_{Si-N} with the geometry of NH_3 frozen at its isolated state and

r_{Si-F} about 5-10% longer than in SiF_4. After the primary group was optimized, r_{Si-F} was optimized and the same procedure was repeated once. The same procedure was then applied to the third and last group. The geometries so generated were then used as the input for the optimization with the STO-6G option. Since the total energies of these complexes are in the high hundreds of atomic units, optimization was terminated when the total energy had converged to the fourth decimal place, 0.0001. Optimal geometries determined by STO-6G are generally not significantly different from those from STO-3G. Figure VIII.1 gives sketches of these molecules and their primary bond lengths and angles. Energies and charge distributions are given in Table VIII.1. For ease of comparison, SiF_4 and NH_3 are also included.

VIII.4. Discussion

A. Energy and Molecular Geometry

From Table VIII.1 it is obvious that, relative to the dissociation limit of $SiF_4 + NH_3$, the most stable of the 1:1 adducts is the axial form. This is in agreement with the concensus shown by experimental observations[22-24] and recently by theoretical calculations.[30] The equatorial form is 1.343 eV above the axial. Although this energy difference is not large considering all the internal

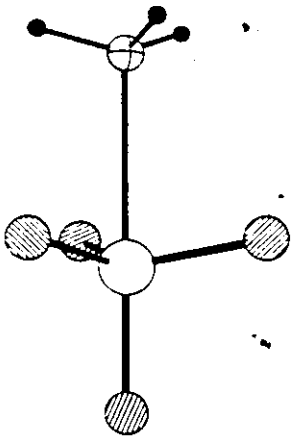

(a)

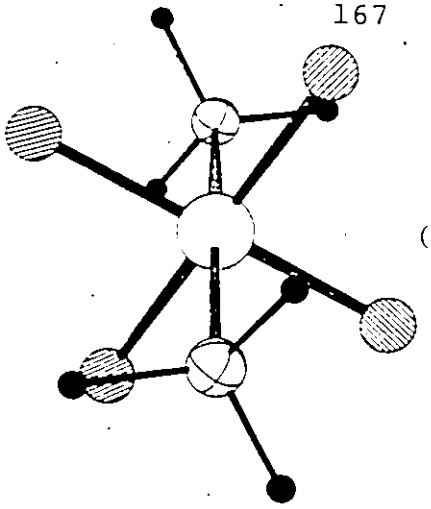

(d)

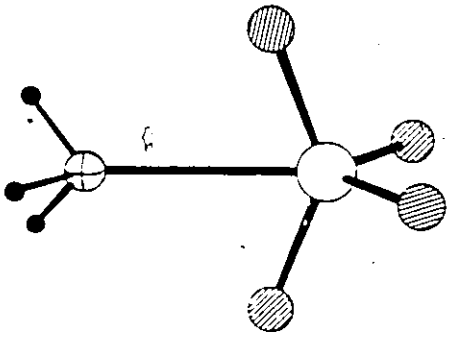

(b)

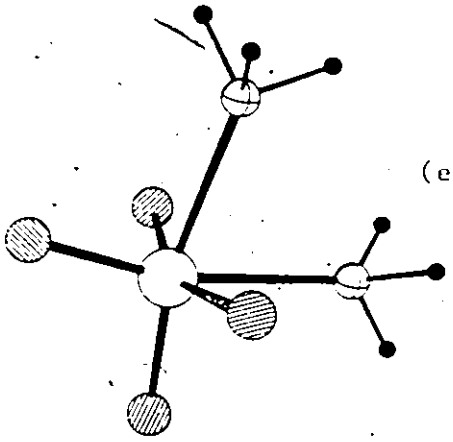

(e)

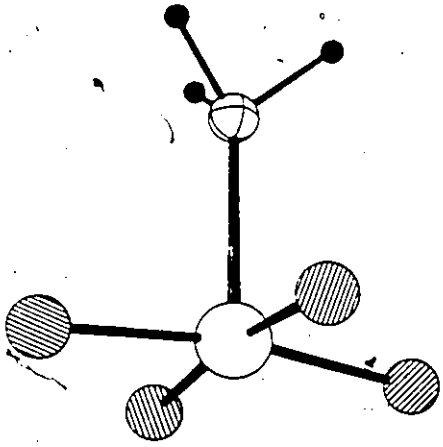

(c)

Fig. VIII$_{\delta}$1 (a) Axial $SiF_4.NH_3$. Bond lengths (Å): Si-N, 2.392; N-H, 1.007; Si-F_e, 1.573; Si-F_a, 1.621. Bond angles (deg): N-Si-F_e, 78.5; F_a-Si-F_e, 101.5; F_e,-Si-F_e, 116.1. (b) Equatorial $SiF_4.NH_3$. Bond lengths (Å): Si-N, 2.439; Si-F_e, 1.609; Si-F_a, 1.604; N-H, 1.008. Bond angles (deg): N-Si-Fe 109.9; N-Si-F_a, 69.4; F_a-Si-F_a, 101.6. (c) Square pyrimidal $SiF_4.NH_3$. Bond lengths (Å): Si-N, 2.012; Si-F, 1.619; N-H, 1.007. Bond angles (deg): N-Si-F,95.3; F-Si-F, 89.5. (d) trans-$SiF_4.2NH_3$. Bond lengths (Å): Si-N, 2.041; N-H, 1.008; Si-F, 1.632. (e) cis-$SiF_4.2NH_3$. Bond lengths (Å) Si-N, 2.112; N-H, 1.007; Si-F_e, 1.638; Si-F_a, 1.640. Bond angles (deg): N_e-Si-F_e, 79.6; N-Si-F_e, 89.3; N-Si-N, 76.5.

O, Si; ⓿, N; ●, F; ●, H.

Table VIII.1. Calculated total energy, dissociation energy, charge distributions, charge transfer, and dipole moment of $SiF_4.nNH_3$, n = 1,2.

Molecule	E_T(a.u.)	ΔE(eV)[a]	Charge Distributions[b]					C.T.[c]	μ_{el}(D)
			Si	N	F_a	F_e	H		
$SiF_4.NH_3$									
Axial	-739.8365	0.433	1.470	-0.531	-0.397	-0.385	0.205	0.084	4.19
Equatorial	-739.7872	-0.910	1.433	-0.496	-0.365	-0.380	0.185	0.057	4.81
Square pyramidal	-739.7508	-1.90	1.456	-0.519	-0.415		0.241	0.204	6.19
$SiF_4.2NH_3$									
Trans	-795.8187	0.359	1.463	-0.533	-0.463		0.243	0.196	0.0
Cis	-795.7620	-1.184	1.450	-0.467	-0.428	-0.421	0.197	0.124	8.94
SiF_4	-683.8357		1.434		-0.358				0.0
NH_3	-44.9849			-0.509			0.169		1.52

a. ΔE is the difference between E_T and the energies of appropriate component molecules.

b. F_a and F_e refer, respectively, to F atoms on the axial and equatorial positions.

c. C.T. stands for charge transfer per NH_3.

degrees of freedom of a complex of this size, the 1:1 adduct is stable only at low temperature and it is not likely that the complex would exist in an equilibrium between the axial and equatorial forms. There has been no report of the experimental observation of e-$SiF_4.NH_3$.

Various bond lengths in the two isomers are very close and the charge distributions are also within a few percent of each other. It is shown below that the net electrostatic interactions in these two isomers are the same and their Si-N bond orders are also very similar. Hence, other factors must be involved to explain why the axial is more stable. Repulsion between two covalent bonds is a concept well accepted at all levels of chemistry. From Figs. VIII.1 (a) and (b) it can be seen that Si-F bonds fall into two categories. One is perpendicular to, and the other parallel with the lone pair of ammonia. Obviously they exert different repulsion against the lone pair. The axial form has three Si-F bonds roughly perpendicular to, and one Si-F bond colinear with the lone pair. In the equatorial form, two Si-F bonds are at 70° to the lone pair and two are in the equatorial plane. The difference may explain the relative stabilities of these two isomers.

It is interesting to look at the molecular geometries

of these isomers from the viewpoint of perturbation to the tetrahedral structure of SiF_4 due to the complex formation with NH_3. With respect to the N atoms, the four F atoms can be divided into two groups. Those F atoms on the same side of the Si atom as the N atom are the primary neighbours, F_p, of N, while those on the opposite side are the secondary neighbours, F_s. For example, all three F atoms on the equatorial position of the axial form, Fig. 1(a), are F_p and the only axial F atom is the sole F_s. It can be seen in Fig. 1 that the angle $<F_s\text{-Si-}F_s$ is hardly perturbed from the tetrahedral angle of 109°28'. On the other hand, $<F_p\text{-Si-}F_s$ of both axial and equatorial and $<F_p\text{-Si-}F_p$ of the axial show deviations of approximately -8° and +7° respectively. Thus formation of a complex with NH_3 does not cause very large changes to the geometry of SiF_4 except in the sp-isomer. A more severe deviation from the tetrahedral structure is accompanied by a higher energy.

In these complexes the Si-N bond between SiF_4 and NH_3 is a coordinate covalent bond which can be considered as essentially a lone pair of N pointed towards the positively charged Si atom because of an electrostatic attraction. Optimal geometries of the axial and equatorial forms show the angle between a coordinate covalent bond and an ordinary covalent bond, $<F_p\text{-Si-N}$, to be smaller than the

angle between two covalent bonds, $<F_p\text{-}Si\text{-}F_s$. Since repulsion between two bonds is an important factor in determining the bond angle, this can be construed as an indication of a weaker repulsion exerted by a lone pair. This observation agrees with the notion that a coordinate covalent bond is not a full-fledged covalent bond.

Of the two isomers of $SiF_4.2NH_3$ the trans form is found to be energetically lower than the cis by 1.54 eV. Complexes with ligands bulkier than NH_3 are shown experimentally to be trans.[23-28] The deduction that follows is that the steric effect is the dominating factor in the cis-trans question. However, our calculations clearly show this not to be the case. Table VIII.1 shows that while the total energy of trans-$SiF_4.2NH_3$ is 0.359 eV lower than the total dissociation products, $SiF_4 + 2NH_3$, the following equations are also true:

$$a - SiF_4.NH_3 + NH_3 \rightarrow \text{trans-}SiF_4.2NH_3 \qquad -0.074 \text{ eV}$$

$$e - SiF_4.NH_3 + NH_3 \rightarrow \text{cis-}SiF_4.2NH_3 \qquad -0.274 \text{ eV}$$

In both cases the total energy of the 1:2 adduct is higher by a smaller amount than that of the reactants.

The inclusion of configuration interaction and probably 3d atomic orbitals on Si are likely to lower the calculated energy of the 1:2 adducts more than that of

the 1:1, making the former energetically more stable since the differences are so small. In any event, the possibility that the 1:1 adduct, upon formation, then is rapidly converted to its 1:2 counterpart cannot be ruled out. Thus, 1:1 and 1:2 adducts may establish an equilibrium unless other factors interfere. Complexes $SiF_4.L$ with a highly electronegative ligand are known[23,24] to exist in equilibrium with the 1:2 adducts but for those of other ligands, e.g., NH_3, 1:1 adducts are chemically stable only at low temperatures and under specific conditions.[29] Our calculations generally agree with these observations.

B. Charge Distributions

A glance at Table VIII.1 from left to right, shows that the very substantial positive charge on the Si atoms in these complexes changes very little from the value of 1.434 in SiF_4. It is interesting to notice, however, that in all cases but the equatorial, the Si atom becomes even more positive, although only slightly, upon formation of complexes with NH_3. The negative charge on N varies more widely in terms of % change. The proximity of two ammonia molecules in the cis arrangement may account for the fact that the charge in the cis isomer is significantly smaller than in all other complexes and also than in free ammonia. There are two groups of F atoms

with respect to charges. Those of axial and equatorial adducts are ca 0.385, or about 10% higher than in SiF_4. F atoms of the sp-SiF_4.NH_3 have a considerably larger negative charge and belong to the second group along with the 1:2 adducts where the charges range up to 30% greater than in SiF_4. The large negative charges on the N and F atoms are reflected in the positive charge on the H atoms. Although the 1:2 adduct has twice as many H atoms per SiF_4 compared to the 1:1 complexes, the positive charge of the H atoms in the trans isomer is nonetheless the largest of all, 0.243, or more than 40% larger than that of NH_3. Charge distributions in e-SiF_4.NH_3 come closest to component molecules.

The charge transfer from NH_3 to SiF_4 is of interest. Table VIII.2 shows the charge transfer (C.T.) in the axial and equatorial to be quite small. Thus, although these two complexes are strongly polar, as the charges on each atom indicate, they are hardly ionic and the polarity is strictly an internal property of the component molecules SiF_4 and NH_3. Conversely, sp-SiF_4.NH_3 and both 1:2 complexes have considerably more ionic character. The charge transfer of 0.196 and 0.124 for trans and cis-SiF_4.$2NH_3$, respectively, are values per NH_3 molecule. Undoubtedly the drastic distortions from the tetrahedral structure of

SiF_4 in these complexes led to this more extensive rearrangement of the electron density. Net electrostatic interactions between SiF_4 and the ligand show the degree of charge transfer. The values are -0.25 eV for both of a- and 3-$SiF_4.NH_3$, -0.56 eV for sp-SiF_4, NH_3, -1.13 eV and -0.80 eV, respectively, for trans and cis-$SiF_4.2NH_3$.

The exterior of these complexes could be basically viewed as an ellipsoid where the major axis is not much longer than the minor axes. Referring to Fig. 1 and Table 1 it becomes clear that in all complexes, except trans-$SiF_4.2NH_3$, one end of the ellipsoid is defined by the four negatively charged F atoms. Enveloped inside are the Si and N atoms. This overall exterior polarity enables these four complexes to form an ionic solid with a head-to-tail arrangement, providing a further stabilization. This facility is most pronounced in the cis 1:2 adduct due to the larger charges on the atoms and the higher number of H atoms compared to the 1:1 adducts. Thus, although the total energy of the isolated cis isomer is 1.543 eV higher than that of the trans, when all factors are considered, it is quite possible that the cis isomer becomes sufficiently stable in the solid phase to co-exist with the trans isomer or even become the favoured form. This is essentially the point Aggarwal and Onyszchuk[29]

made in explaining infra red spectra. The trans isomer is different. Because of its axial symmetry both ends of the ellipsoid are positively charged and only at the mid-section is a ring of negative charges composed of four F atoms. Despite its large charge transfer (0.196 per NH_3) and high internal polarity, its overall exterior charge arrangements cannot contribute to the additional stabilization mentioned above.

The answer to the cis or trans question seems to be a function of the physical state of the complex. In the solid phase it is conceivably in the cis form. By contrast, the trans arrangement should be favoured whenever the added stabilization from condensation is not in effect. This includes the gaseous and solution phases and when the complex is dispersed into solid matrices. This may explain the conflicting experimental observations on the 1:2 adducts:

C. Si-N Bonding

For molecular complexes, the mode whereby the component molecules are linked together is of interest. Bond angles are used above as circumstantial evidence to assert that the Si-N bond is not a full-fledged covalent bond. It is also shown that the net effect of electrostatic interaction is to hold the complexes together. In general, the severity of distortion from the tetrahedral shape of

SiF_4 and the magnitude of the net attraction are proportional. While the ionicity of the complexes increases from 1:1 to 1:2 adducts, the Si-N bond still has significant covalent character. For example, a-SiF_4.NH_3 has a bond energy of 0.433 eV but its net electrostatic effect is only -0.25 eV. Obviously, there must be covalency in the Si-N bond to account for the bond energy. Actually, the Si-N band accounts for more than the difference 0.183 eV (0.433-0.25) since the value of 0.433 eV is in reference to the neutral $SiF_4 + NH_3$ while -0.25 eV is in reference to $(SiF_4)^{-q} + (NH_3)^{+q}$, with $q = 0.084$.

The bond order is an approximate gauge of the covalency of a bond. In the 1:1 complexes, the Si-N bond has the bond orders of 0.22, 0.15, and -0.03 for the axial, equatorial and square pyramidal respectively. The small charge transfer in the axial and equatorial forms and their moderately low bond orders can be taken to indicate that the bonding between the ammonia lone pair and SiF_4 molecules is mainly electrostatic. While some measure of covalency is established in the bond its bond order is low, even in comparison with a highly polar bond such as C-O. Hence, it seems safe to say that no fundamental change has taken place at the lone pair of the ammonia molecule, despite complex formation. For the square pyramidal the lone pair is even less affected and the

bonding is exclusively electrostatic. The trans isomer has a bond order of 0.12 and the cis is moderately anti-bonding at -0.15.

REFERENCES

PART FOUR

1. J. C. Slater, Quantum Theory of Molecules and Solids, McGraw-Hill, New York (1963).

2. R. G. Parr, Quantum Theory of Molecular Electronic Structure, W. A. Benjamin, New York (1963).

3. J. A. Pople and D. L. Beveridge, Approximate Molecular Orbital Theory, McGraw-Hill, New York (1970).

4. W. G. Richards and J. A. Borsley, Ab initio Molecular Orbital Calculations for Chemists, Oxford University (1970).

5. S. Streitwiser, Molecular Orbital Theory for Organic Chemicals, John Wiley, New York (1961).

6. M.J.S. Dewar, The Molecular Orbital Theory of Organic Chemistry, McGraw-Hill, New York (1969).

7. C.C.J. Roothaan, Rev. Modern Phys., 23, 69 (1951).

8. C.C.J. Roothaan, Rev. Modern Phys., 32, 179 (1960).

9. D. R. Hartree, Proc. Cambridge Phil. Soc. 24, 89, 111, 426 (1928).

10. V. Fock, Z. Physik, 61, 126 (1930).

11. J. A. Pople and G. A. Segal, J. Chem. Phys. 43, 5129 (1965).

12. J. A. Pople and G. A. Segal, J. Chem. Phys. 44, 3289 (1966).

13. W. P. Santry and G. A. Segal, J. Chem. Phys. 47, 158 (1967).

14. J. A. Pople, D. L. Beveridge and P. A. Dobosh, J. Chem. Phys., 47, 2026 (1967).

15. N. C. Baird and M.J.S. Dewar, J. Chem. Phys. 50, 1262 (1969).

16. R. Hoffman, J. Chem. Phys. 39, 1397 (1963).

17. J. Davy, Philos. Trans. Roy. Soc. London, 352 (1812).

18. W. Mixter, Am. Chem. J. 2, 153 (1881).

19. J. Gierut, F. Sowa and J. Nieuland, J. Am. Chem. Soc. 58, 786 (1936).

20. T. S. Piper and E. G. Rochow, J. Am. Chem. Soc. 76, 4318 (1954).

21. D. M. Miller and H. H. Sisler, J. Am. Chem. Soc., 77, 4998 (1955).

22. B. Ault, Inorg. Chem. 20, 2817 (1981).

23. I. R. Beattie and G. A. Ozin, J. Chem. Soc. (A), 370 (1970).

24. J. E. Fergusson, D. K. Grant, K. Hickford and C. J. Wilkins, J. Chem. Soc., 99 (1959).

25. E. L. Muetterties, J. Am. Chem. Soc., 82, 1082 (1960).

26. E. L. Muetterties, Acta Cryst. B25, 156 (1969).

27. R. Hulme, G. J. Leigh and I. R. Beattie, J. Chem. Soc., 366 (1960).

28. R. Hulme, G. J. Leigh and I. R. Beattie, J. Organomet. Chem. 144, 39 (1978).

29. R. C. Aggarwal and M. Onyszchuk, Can. J. Chem. 41, 876 (1963).

30. C. Marsden, Inorg. Chem. 22, 3177 (1983).

31. W. J. Hehre, W. A. Lathan, R. Ditchfield, M. D. Newton and J. Pople, QCPE 11, 236 (1973).

VITA AUCTORIS

1955 Born in Beirut, Lebanon, May 25

1978 Received B.Sc. (General) University of Windsor, Windsor, Ontario

1979 Received B.Sc. (Honours) University of Windsor, Windsor, Ontario

1980 Married to Ehssan El Kalla, Dec. 27.

Awards: Best performance in Science Award, Notre Dame, Nelson, B.C. (1975).
University of Windsor Summer Research Scholarship (1982).
University of Windsor Post-graduate Scholarship (1983).

Publications

Ab initio molecular orbital studies of complexes between SiF_4 and ammonia. Canadian Journal of Chemistry 62(1), 27 (1984).

Crystal structures of three trimethyl arsine adducts with boron trihalides. Accepted for publication Journal of Crystallographic and Spectroscopic Research.

Spectroscopic investigation of methyl and dimethyl arsine adducts of boron trihalides. In preparation.

^{11}B nmr of trimethyl, dimethyl, and methyl arsine adducts of mixed and unmixed boron trihalides. In preparation.

Vibrational analysis of methyl phosphine (and deuterated analogs) adducts of boron trihalides. In preparation.

Synthesis and characterization of some Group IV-Selenium ligands. In preparation.

Synthesis and characterization of Palladium and Platinum compounds-Crystal structure of $Cl_2Pd(Me_3SiCH_2SeMe)_2$. In preparation.

This example is shown in Fig. E.1, the structure is composed of 4 modules, each is a CAS module shown in Fig. 5.7. An input is received by system on alternate cycle, and an output is produced on alternate cycle, too. The whole computation of this example takes 7 cycles, where a cycle is the time delay of the CAS module.

E.2 The MBFIR Structure

The modulo bit plane filter (MBFIR) is the basic computational module of the array proposed in 5.5. It is a FIR array with inputs as single bits. It is composed of 2-D systolic array and a modulo adder, the building block element of this array is shown in Fig. 5.17, the input/output bits of this element is as follows:

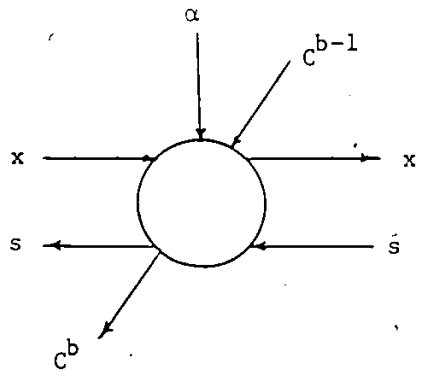

As an example consider B=4, N=5, K=5, m=5. Twenty computational elements are required arranged in 4 rows and 5 columns, a modulo 5 adder is used. If the coefficients and the input signals are as follows

$\alpha(0) = 2, \alpha(1) = 5, \alpha(2) = 1, \alpha(3) = 4, \alpha(4) = 6$

$x(0) = 1, x(1) = 0, x(2) = 1, x(3) = 1, x(4) = 1$

The first three steps are shown in Fig. E.2. Each step takes 2 time cycles, the output $|y(0)|_5 = 2$, $|y(1)|_5 = 0$ received in steps 1 and 3, respectively.

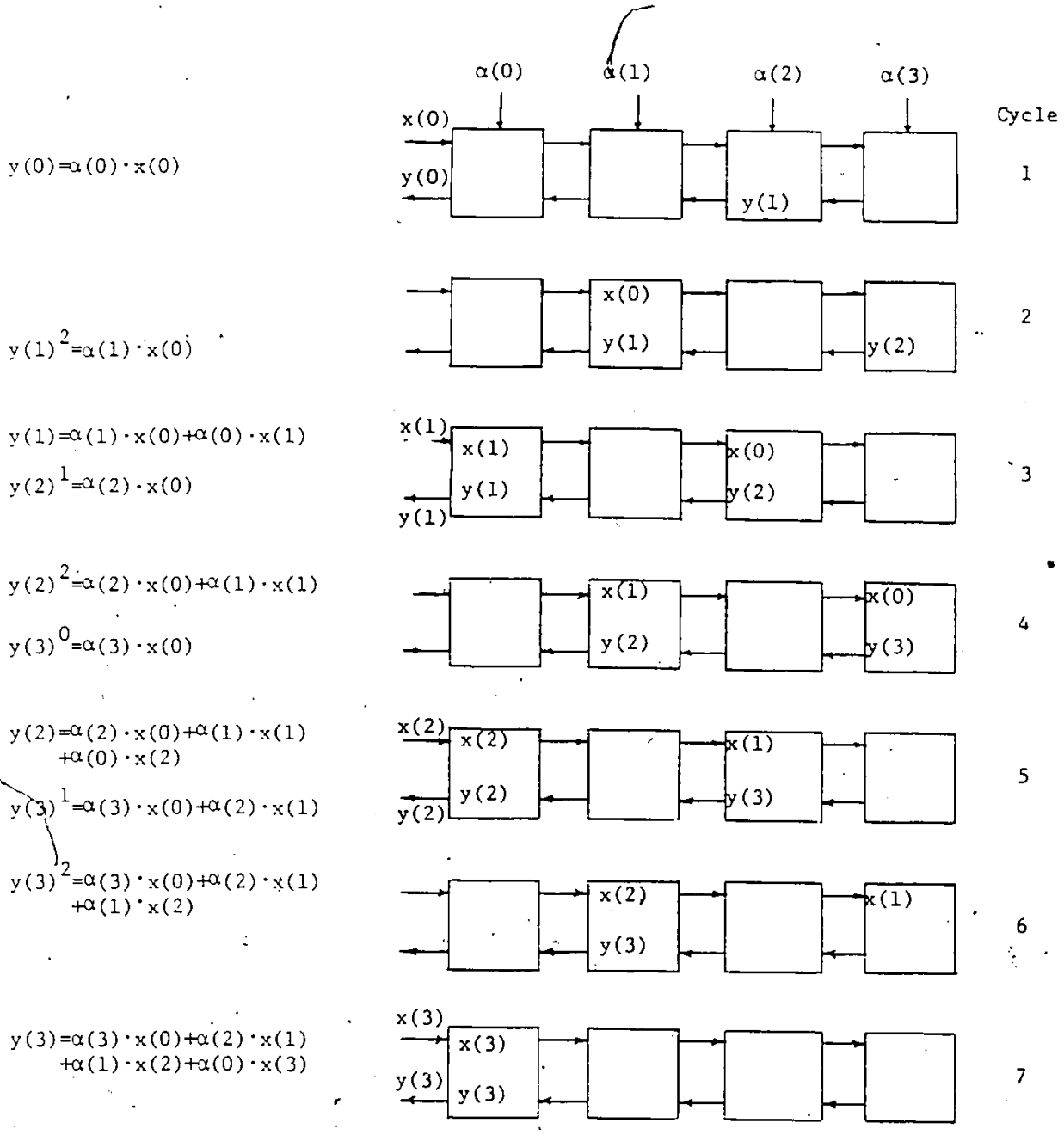

(all x's, y's, and α's are in residue representation)

Fig. E.1 The Data Flow Through the Word Level Structure

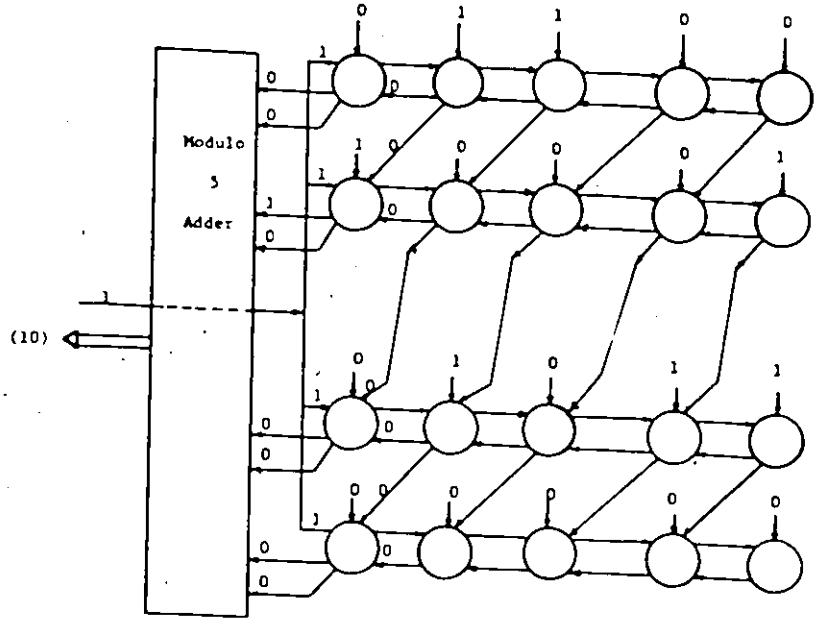

Step 1

Fig. E.2.a

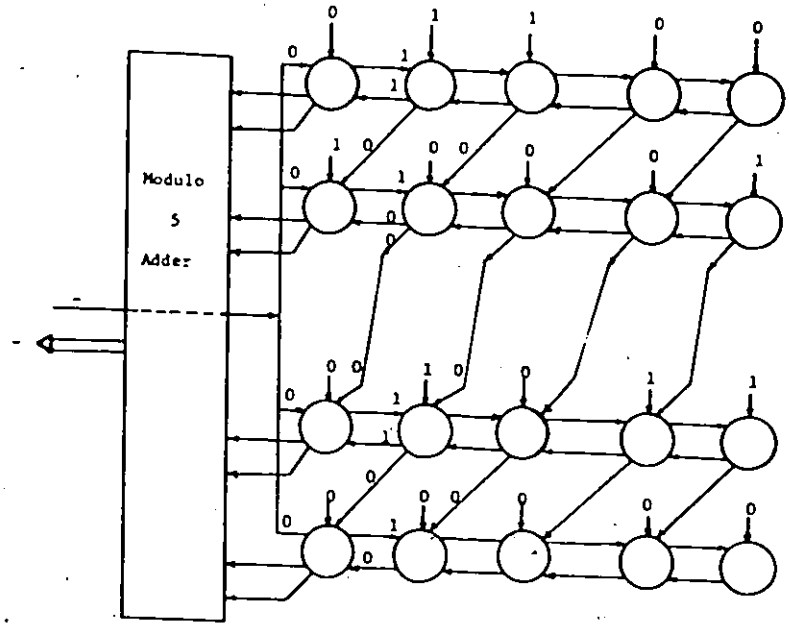

Step 2

Fig. E.2.b.

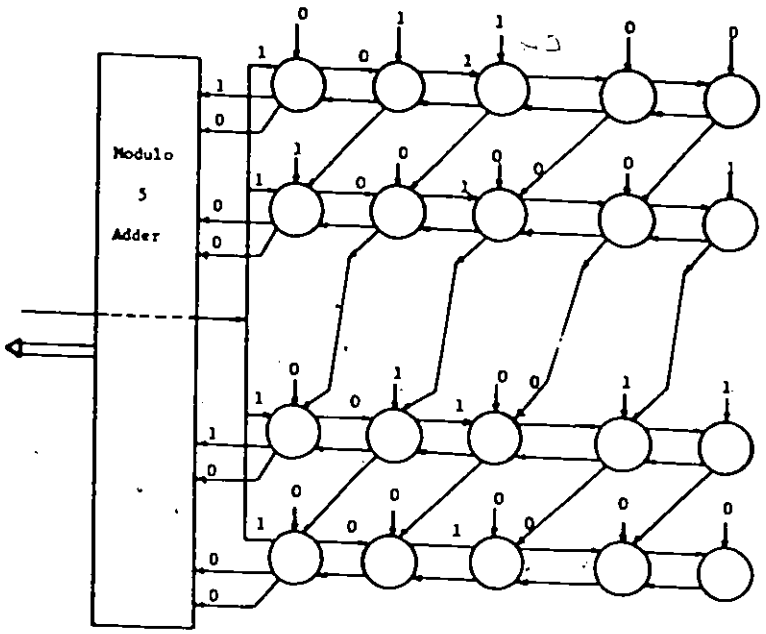

Step 3

Fig. E.2.c.

APPENDIX F

I/O Pins Requirements

The I/O and packaging constraints of monolothic VLSI chips have set limitations to the size of digital systems to be implemented in single chip. The improvement in packaging techniques does not match the growing number of devices to be accommodated in a chip, it is predicted that by late 80's, it will be possible to fabricate IC chips, each of which contains 10^7 or 10^8 individual transistors. On the other hand, it is very often that I/O dominates the speed of the computing structure as discussed in chapter 2.

The pin limitation problem has been investigated in early 70's. Landmeen and Russo [102] discussed how to achieve sufficient high circuit to pin ratio (CP) by partitioning the logic graph of a circuit in an efficient way. Russo [103] recognized this problem as a key factor in the effective use of LSI chips. He suggested several techniques to increase (CP); first is serialization of the transfer of information between chips which might lower performance. The second technique is based on encoding the bits of information to be transferred; e.g. instead of sending a signal and its complement, only the signal to be sent and an inverter to be included instead of sending the complement. The third approach is to use decentralization control to avoid sending control signals among chips of the same system. Recently, this problem has been considered on the abstract level. Wei and Kung [105] have studied the balance between input/output and computation, and have developed a lower bound for I/O requirements. They used the pebble game formulation to derive these bounds. Kedem and Zorat [106] have discussed the bounds

for different kinds of I/O schedules. Aggarwal [107] has investigated the placement of I/O pins and its effect on the area time complexity.

F.1 I/O Requirements for RNS Based Chips

Given an RNS based system having the following parameters:

L: the number of moduli

m_i: the i'th modulus ($i \in 1, L$)

I: the number of system inputs

O: the number of system outputs

to be implemented based on parallel inputs and outputs. We require the following number of pins P, (ignoring power, ground, and control pins):

$$P = \sum_{i=1}^{L} (I + O) \lceil \log m_i \rceil \qquad (1)$$

Table F.1 shows the required number of pins for different moduli sets. Assuming that all the moduli are in the same range of a value m, equation (1) can be written as follows:

$$P = L (I + O) \lceil \log m \rceil \qquad (2)$$

Table F.2 shows the required number of pins for some moduli ranges. Tables F.1 and F.2 show that for large moduli, P becomes very large and cannot be implemented in one chip. Two approaches can be followed to overcome this difficulty. The first approach is to decompose the system into several subsystems to be implemented in several chips, each having the maximum realizable number of pins. The second approach is to transfer the input and output data in serial rather than in parallel which takes a fewer number of chips but slows down the operation.

TABLE F.1 The Required Number of Pins for Some Moduli Set

Moduli Set	P Pins					
	I+O=3	4	5	10	15	24
{7, 9, 13, 19, 23}	63	84	105	210	315	504
{11, 17, 29, 33, 37}	78	104	130	260	390	624
{61, 79, 83, 85, 131}	105	140	175	350	525	840
{128, 217, 319, 449}	99	132	165	330	495	792
{457, 595, 613, 977}	117	156	195	390	585	936

F.2 The Parallel Approach

In this approach each pin is devoted to transfer a specific bit, for implementation, this number of pins will be distributed among several chips. The system can be decomposed in three ways: the layout decomposition, the function decomposition, or the hybrid decomposition.

F.2.1 The Layout Decomposition

In this decomposition, the system is dealt with as one functional module. Generally, the decomposition can take place in two ways, Fig. F.1. First, decomposition in two directions, which is very general and complicated. It may involve redesigning the system and modifying the data routing to fit the form of the layout. Second, decomposition in one direction, it is simpler and involves fewer modifications. Each subsystem is implemented by a chip having the maximum allowed number of pins.

F.2.1.1 Two-Direction Decomposition

This approach represents the worst case situation for a large moduli set and a complicated algorithm. For an input to be processed, the signal may have to travel through several chips in both directions. We

TABLE F.2 The Required Number of Pins for Different Moduli's Sizes

Range of m(bits)	L \ P	P Pins 3	4	5	10	15	24
3	4	36	48	60	120	180	288
	5	45	60	75	150	225	360
	6	54	72	90	180	180	432
4	4	48	64	80	160	240	384
	5	60	80	100	200	300	480
	6	72	96	120	240	360	576
5	4	60	80	100	200	300	480
	5	75	100	125	150	375	600
	6	90	120	150	300	450	720
6	4	72	96	120	240	360	576
	5	90	120	150	300	450	720
	6	108	144	180	360	540	864
7	3	63	84	105	210	315	504
	4	84	112	140	280	420	672
	5	105	140	175	350	495	840
8	3	72	96	120	240	360	576
	4	96	128	160	320	480	768
	5	120	160	200	400	600	960
9	3	81	108	135	270	405	648
	4	108	144	180	360	540	864
	5	135	180	225	450	675	1080
10	3	90	120	150	300	450	720
	4	120	160	200	400	600	960
	5	150	200	250	500	750	1200

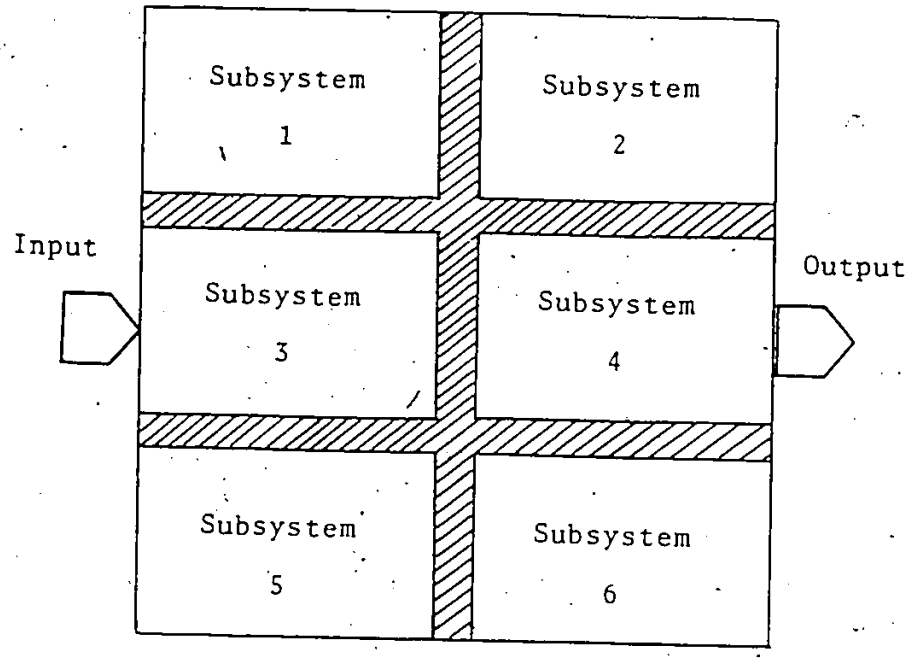

(a) Two Direction Decomposition

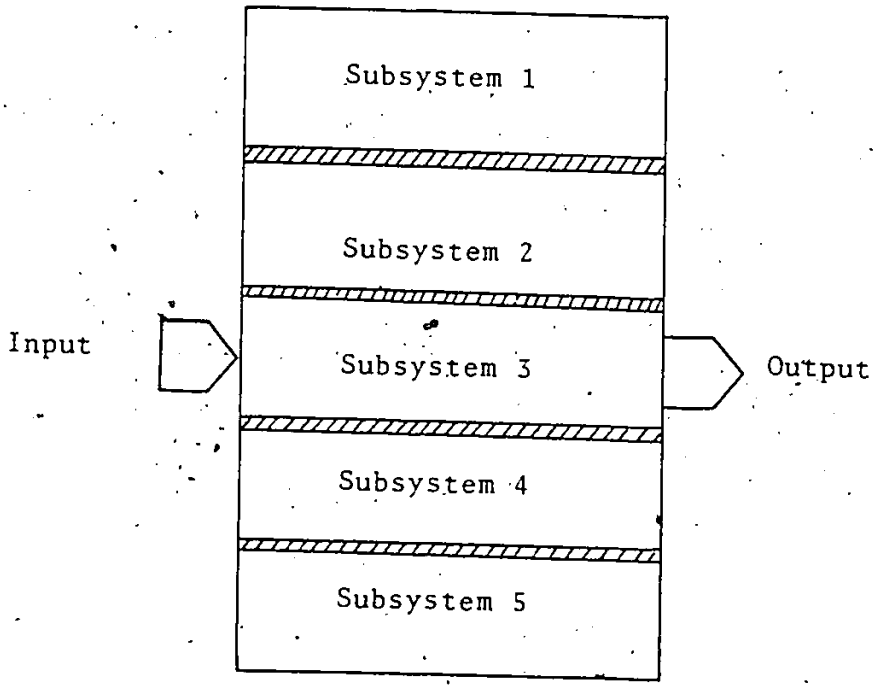

(b) One Direction Decomposition

Fig.F.1 The Layout Decomposition

assume that each chip of those implementing the subsystems has the following parameters:

p: the total number of pins

p_o: the number of pins required for control and communication among subsystems

b: the number of pins allocated for data

$$p = b + p_o \tag{3}$$

and we assume that $p_o = \delta b$, where δ is a constant ($0 < \delta < 1$). The value of δ depends on the scheme by which chips are communicating together. If the pins are distributed equally at two sides (although distributing the pins at 4 sides is possible, but having them at two sides is the common practice according to the state-of-the-art of packaging technology), the number of pins at each side p' allocated for data is:

$$p' = P/2\ (1 + \delta) \tag{4}$$

The number of the required chips in the vertical direction n' is:

$$n' = \text{Max}\ (LI\ \lceil \log m \rceil / p',\ LO\ \lceil \log m \rceil / p') \tag{5}$$

The number of levels (in the horizontal direction) is much dependent on the function performed by the system besides the number of pins per chip. If it is assumed that the number of levels is k, the total number of chips n is:

$$n = n' \cdot k^{\emptyset} \tag{6}$$

To calculate the time delay for a signal to propagate from the system input to the system output, two types of time delay have to be con-

sidered. The first, is the average time delay of each chip through which the signal has to travel, the second is the time delay due to the interconnection among chips due to pin drivers. The overall time delay T is given as follows:

$$T = \eta\, t_{ch} + (\eta - 1)\, t_{ich} \tag{7}$$

where

t_{ch}: the average time delay of a single chip

t_{ich}: the average time delay due to pin drivers and interconnection between two chips

η: the number of chips through which the signal has to travel.

The value of η depends on the function performed by each chip and the functional relation among all chips. The minimum value of η is k, which can be realized most of the time; the minimum time delay will therefore be

$$T_{min} = k\, t_{ch} + (k - 1)\, t_{ich} \tag{8}$$

As an average value, η can be considered to be $(n'/2 + k)$. Equation (8) can be rewritten as follows:

$$T = (n'/2 + k)\, t_{ch} + (n'/2 + k - 1)\, t_{ich} \tag{9}$$

F.2.1.2 One-Direction Decomposition

This is considered a special case of the two-direction decomposition. The chips are only arranged in the vertical direction; k = 1. The number of the required chips n is

$$n = L\ (I + O)\ [\log m]\ (1 + \delta)\ /\ p \qquad (10)$$

where δ is the number of pins devoted for data communication among chips, it is relatively large compared to the two-direction decomposition. The time delay for this structure is expressed as follows:

$$T = n/2\ t_{ch} + (n/2 - 1)\ t_{ich} \qquad (11)$$

F.2.2 The Functional Decomposition

In this approach, the system is decomposed into subsystems to be implemented by several chips based on the performed function by each subsystem. For RNS based system, an apparent way is to implement each modulo circuit using a single chip, with an extra chip for the scaling circuit. The number of the moduli in the system determines the number of the required chips as follows:

$$n = L + 1 \qquad (12)$$

The size of the circuit and of the modulus is controlled by the maximum allowed number of pins per chip, as follows:

$$p = (I + O)\ [\log m]\ (1 + \delta) \tag{13}$$

Table F.3 shows the maximum size of a modulus at certain values of $(I + O)$ and δ.

The time delay is calculated using a similar method to that used in the previous section:

$$T = T_{chm} + t_{ich} + t_{chs} \tag{14}$$

where t_{chm}: is the average delay of each chip associated with a modulus of the moduli set.

t_{ich}: is the time delay due to the interconnection between the moduli set chips and the scaling chip, it is related mainly to the pin drivers.

t_{chs}: is the average delay of the scaling chip.

F.2.3 The Hybrid Decomposition

This decomposition combines between the previous two decomposition methods. The system is decomposed according to the moduli set, but the scaling circuit is not implemented separately, it is sliced among the chips of the moduli set, Fig. F.2. The number of required chips is L. The maximum size of the circuit and of the moduli are smaller than the values in the functional decomposition, as follows :

$$p = (I + O)\ [\log m]\ \ (1 + \delta)\ (1 + k) \tag{15}$$

where δ is as defined before and k is a constant expressing the fraction of the chip devoted to the scaling circuit, $0 < k < 1$.

The time delay of the system is

$$T = t'_{chm} + t'_{ich} \tag{16}$$

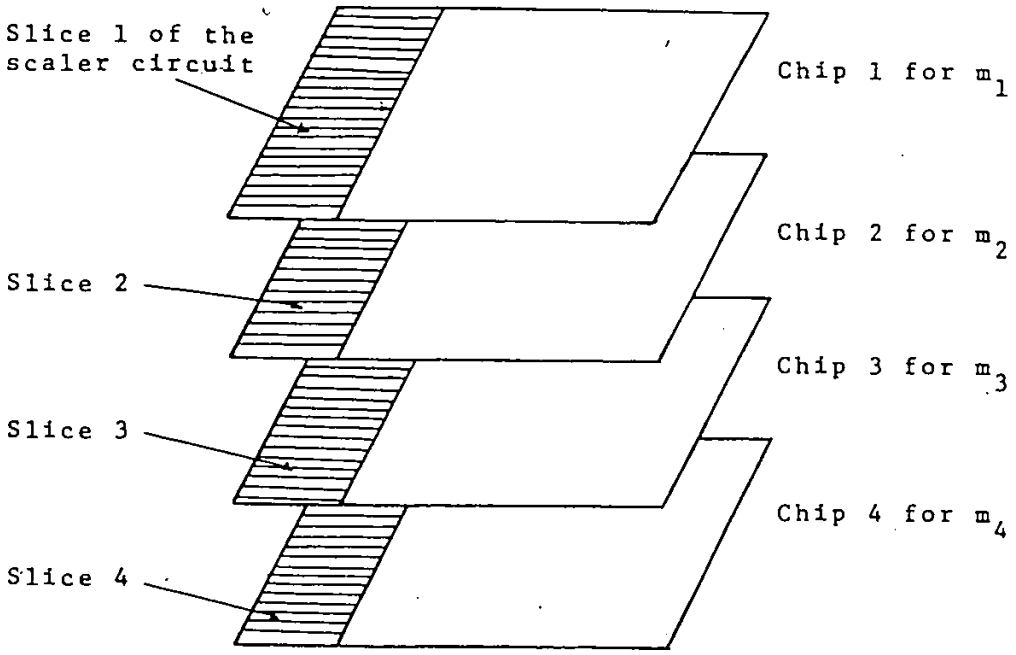

Fig. F.2 The System Implementation Based on the Hybrid Decomposition

TABLE F.3 The Size of Moduli Implied by Number of Pins

P	(I+0)	m in bits δ=0	δ=1/8
60	3	20	18
	4	15	13
	10	6	5
	15	4	3
	20	3	2
	30	2	–
80	3	26	23
	4	20	17
	10	8	7
	15	5	4
	20	4	3
	30	2	–
100	5	20	17
	6	16	14
	7	14	12
	10	10	8
	15	6	5
	20	5	4
	30	3	2
160	8	20	17
	9	17	15
	10	16	14
	15	10	8
	20	8	7
	30	5	4

where t'_{chm}: is similar to t_{chm}, but includes the time delay due to the scaling portion.

t'_{ich}: is the time delay due to the communication among the scaling part of each chip.

F.3 The Serial Approach

In this approach, each pin is used to transfer a group of bits in serial fashion. This strategy involves using serial-to-parallel demultiplexer circuits and parallel-to-serial multiplexer circuits to arrange the bits for each modulus. These associated circuits should be fast enough to avoid any data transfer bottleneck. In this approach, the whole system can be implemented in a single chip. Assuming that each pin handles ρ [log m], where $0 < \rho < 1$. When $\rho = 1$, this means that all the bits representing one modulus are transferred through one pin. The value of ρ depends on the size of the circuit and the number of moduli as follows:

$$p = L\ (I + O)/\ \rho \tag{17}$$

The total time delay includes the time delay due to demultiplexing and multiplexing, as follows:

$$T = t_c + 2\ \rho\ [\log m]\ \ t_{iO} \tag{18}$$

where t_c: is the computation time through the chip

t_{iO}: is the time delay due to multiplexing or demultiplexing of one bit

Examples of the input and output circuits for this approach are given in [87, 108].

REFERENCES

[1] Hua Loo Keng, Introduction to Number Theory, Springer-Verlag, 1982.

[2] A. Svoboda, "Rational Numerical Systems of Residue Classes", Stroje Ha Zpracovni Informaci, Sbornik V, Prague, Czechoslovakia, 1957.

[3] N.S. Szabo and R.I. Tanaka, Residue Arithmetic and Its Applications to Computer Technology, McGraw-Hill, New York, 1967.

[4] W.K. Jenkins and B.J. Leon, "The Use of Residue Number Systems in the Design of Finite Impulse Response Digital Filters", IEEE Trans. Circuits and Systems, Vol. CAS-24, No. 4, pp. 191-201, April 1977.

[5] M.A. Soderstrand, "A High Speed Low-Cost Recursive Filter Using Residue Arithmetic", Proc. IEEE, Vol. 65, No. 7, pp. 1065-1067, July 1977.

[6] G.A. Jullien, "Residue Number Scaling and Other Operations Using ROM Arrays", IEEE Trans. Comput., Vol. C-27, No. 4, pp. 325-337, April 1978.

[7] B. Tseng, G.A. Jullien, and W.C. Miller, "Implementation of FFT Structures Using the Residue Number System", IEEE Trans. on Computers, Vol. C-28, No. 11, pp. 831-844, Nov. 1979.

[8] W.K. Jenkins,"Recent Advances in Residue Number Techniques for Recursive Digital Filtering", IEEE Trans. on Acoustics, Speech, and Signal Processing, Vol. ASSP-27, No. 1, pp. 19-30, Feb. 1979.

[9] C.H. Huang, D.G. Peterson, H.E. Rauch, J.W. Teague, and D.F. Frasher, "Implementation of Fast Digital Processor Using the Residue Number System," IEEE Trans. Circuits and Systems, Vol. CAS-28, No. 1, pp. 32-38, Jan. 1981.

[10] H.K. Nagpal, G.A. Jullien, W.C. Miller, "Processor Architectures for Two-Dimensional Convolvers Using a Single Multiplexed Processor Element", IEEE Trans. on Computers, Vol. C-32, No. 11, pp. 989-1000, Nov. 1983.

[11] A.Z. Baraniecka and G.A. Jullien, "Residue Number System Implementations of Number Theoretic Transforms in Complex Residue Rings," IEEE Trans. on Acoustics, Speech, and Signal Processing, Vol. ASSP-28, No. 3, pp. 285-291, June 1980.

[12] F.J. Taylor, "Large Moduli Multipliers for Signal Processing," IEEE Trans. Circuits and Systems,Vol. CAS-28, No. 7, pp. 731-736, July 1981.

[13] M.A. Soderstrand and E.L. Fields, "Multipliers For Residue Number Arithmetic Digital Filters", Electronics Letters, Vol. 13, No. 6, pp. 164-166, March 1977.

[14] W.K. Jenkins, "The Design of Error-Checkers for Self-Checking Residue Number Arithmetic," IEEE Transactions on Computers, Vol. C-32, No. 4, pp. 388-396, April 1983.

[15] M.H. Etzel and W.K. Jenkins, "The Design of Specialized Residue Classes for Efficient Recursive Digital Filter Realization", IEEE Trans. Acoust. Speech and Signal Processing, Vol. ASSP-30, No. 3, pp. 370-380, June 1982.

[16] F.J. Taylor and H. Huang, "An Autoscale Residue Multiplier", IEEE Trans. on Comput., Vol. C. 31, No. 4, pp. 321-325, April 1982.

[17] W.K. Jenkins, "Techniques for Residue-to-Analog Conversion for Residue Encoded Digital Filters", IEEE Trans. Circuits and Systems, Vol. CAS-25, No. 7, pp. 555-562, July 1978.

[18] A. Baraniecka and G.A. Jullien, "On Decoding Techniques for Residue Number System Realizations of Digital Signal Processing Hardware," IEEE Trans. Circuits and Systems, Vol. CAS-25, No. 11, pp. 935-936, Nov. 1978.

[19] D.K. Banerji, "A Novel Implementation Method for Addition and Subtraction in Residue Number Systems", IEEE Trans. on Computers, Vol. C-23, No. 1, pp. 106-109, Jan. 1974.

[20] S. You and J. Chung, "On the Design of Modulo Arithmetic Units Based on Cyclic Groups," IEEE Trans. on Computers, Vol. C-25, No. 11, pp. 1057-1067, Nov. 1976.

[21] A.S. Ramnarayan, "Practical Realization of Mod p Prime Multiplier", Electronics Letters, Vol. 16, No. 12, pp. 466-467, June 1980.

[22] G.A. Jullien, "Implementation of Multiplication, Modulo a Prime Number, with Applications to Number Theoretic Transforms", IEEE Trans. on Computers, Vol. C-29, No. 10, pp. 899-905, Oct. 1980.

[23] W.K. Jenkins, "Techniques for High Precision Digital Filtering with Multiple Microprocessors", Proc. 20th Midwest Symp. on Circuits and Systems, Lubbock, TX, pp. 58-62, Aug. 1977.

[24] M.A. Bayoumi and G.A. Jullien, "Analysis of Microprocessor Based Digital Filters", Proc. of 21st International Symposium on Mini and Microcomputers and their Applications, San Francisco, pp. 57-60, May 1983.

[25] W.K. Jenkins, "A Highly Efficient Residue-Combinatorial Architecture for Digital Filters", Proc. of the IEEE, Vol. 66, No. 6, pp. 700-702, June 1978.

[26] F. Taylor, "A VLSI Residue Arithmetic Multiplier", IEEE Trans. on Computers, Vol. C-31, No. 6, pp. 540-546, June 1982.

[27] W.K. Jenkins, "A Technique for the Efficient Generation of Projections for Error Correcting Residue Codes", IEEE Trans. on Circuits and Systems, Vol. CAS-31, No. 2, pp. 223-226, Feb. 1984.

[28] Ferruccio Barsi and Piero Maestrini, "Error Correcting Properties of Redundant Residue Number Systems," IEEE Trans. on Computers, Vol. C-22, No. 3, pp. 307-315, March 1973.

[29] Time Magazine,

(a) R.T. Grieves, "Short-Circuiting Reference Books," pp. 74-75, June 13, 1983

(b) J. Cocks, "Sing a Song of Seeing," pp. 50-56, December 26, 1983.

(c) C.P. Alexander, "The New Economy," pp. 60-72, May 30, 1983.

(d) P.E. Dewit, "An Olympic Showcase of High Tech," pp. 52, July 9, 1984.

[30] L.A. Conway et al., "MPC79: A Large-Scale Demonstration of a New Way to Create Systems in Silicon," LAMBDA, pp. 10-19, Second Quarter, 1980.

[31] G. Moore, "VLSI: Some Fundamental Challenges," IEEE Spectrum, Vol. 16, No. 4, pp. 30-37, Apr. 1979.

[32] E.P. Farrel et al., "A Concurrent Computer Architecture and a Ring Based Implementation," Proc. Sixth Intl. Symp. Computer Architecture, pp. 1-11, April 1979.

[33] P.C. Treleaven, "VLSI Processor Architecture," IEEE Computer Magazine, Vol. 15, No. 6, pp. 33-45, June 1982.

[34] D.A. Patterson and C.H. Sequin, "Design Considerations for Single Chip Computers of the Future," IEEE Trans. on Computers, Vol. C-29, No. 2, pp. 108-116, February 1980.

[35] I.E. Sutherland and C.A. Mead, "Microelectronics and Computer Science," Scientific American, Vol.237,pp. 210-228, Sept. 1977.

[36] Kouichi Wada, "Area-Time Optimal Fast Implementation of Several Functions in a VLSI Model," IEEE Trans. on Computers, Vol. C-33 No. 5, pp. 455-462, May 1984.

[37] J. Allen, "Computer Architectures for Signal Processing," Proc. IEEE, Vol. 63, No.4, pp. 624-633, April 1975.

[38] F. Mintzer et al.,"The Real-Time Signal Processor," IEEE Trans. on Acoustics, Speech, and Signal Processing, Vol. ASSP-31, No. 1, pp. 83-95, February 1983.

[39] G. Culler et al., "A High Performance VLSI CMOS Arithmetic Processor Chip," Proc. IEEE International Conference on Acoustics, Speech and Signal Processing, pp. 1053-1056, 1982.

[40] J.M. Glass, "A Programmable Signal Processing Architecture," Proc. IEEE International Conference on Acoustics, Speech and Signal Processing, pp. 702-705, 1979.

[41] F. Mintzer and A. Peled, "The Architecture of the Real-Time Signal Processor," Proc. IEEE International Conference on Acoustics, Speech and Signal Processing, pp. 1049-1052, 1982.

[42] P.H. Sperry, "A Microprogrammed Signal Processing," Proc. IEEE International Conference on Acoustics, Speech and Signal Processing, pp. 579-582, 1981.

[43] R. Geppert, "Novel Structure of a User-Programmable Integrated Digital Signal Processing," Proc. IEEE International Conference on Acoustics, Speech and Signal Processing, pp. 691-694, 1982.

[44] A. Kanemasa et al., "An LSI Chip Set for DSP Hardware Implementation," Proc. IEEE International Conference on Acoustics, Speech and Signal Processing, pp. 644-647, 1981.

[45] M.J. Fosters and H.T. Kung, "The Design of Special Purpose VLSI Chips," Computer Magazine, Vol. 13, No. 1, pp. 26-40, Jan. 1980.

[46] C.T. Mullis and R.A. Roberts, "Digital Processing Structure for VLSI Implementation," Proc. IEEE International Conference on Acoustics, Speech and Signal Processing, pp. 8.8.1-8.8.3, 1984.

[47] F. Faggin, "How VLSI Impacts Computer Architecture," Spectrum, Vol. 15, No. 5, pp. 28-31, May 1978.

[48] B.R. Mears, "A Modular Method for Design Custom Signal Processing Integrated Circuits," Proc. IEEE International Conference on Acoustics, Speech and Signal Processing, pp. 8.7.1-8.7.4, 1984.

[49] D.I. Moldovan, "On the Design of Algorithms for VLSI Systems," Proc. of IEEE, Vol. 71, No. 1, pp. 113-120, January 1983.

[50] C.A. Mead and M. Rem, "Cost and Performance of VLSI Computing Structures," IEEE J. Solid-State Circuits, Vol. SC.14, No. 4, pp. 455-462, April 1979.

[51] C.D. Thompson, "Area-Time Complexity for VLSI," Proc. 17th Annual ACM Symp. on Theory of Computing, pp. 81-89, 1979.

[52] A. Yao, "The Entropic Limitations on VLSI Computations," Proc. 13th Annual ACM Symp. on Theory of Computing, pp. 308-311, 1981.

[53] H. Abelson and P. Andeae, "Information Transfer and Area-Time Tradeoffs for VLSI-Multiplication," CACM, Vol. 23, No. 1, pp. 20-23, January 1980.

[54] R.P. Brent and H.T. Kung, "The Area-Time Complexity of Binary Multiplications," JACM, Vol. 28, No. 3, pp. 521-534, July 1981.

[55] B. Chazelle and L. Monier, "A Model of Computation for VLSI with Related Complexity Results," Proc. 13th Ann. Symp. on Theory of Computing, pp. 318-325, 1981.

[56] C.E. Leiserson, "Area Efficient Graph Algorithms (for VLSI)," Proc. 21st Annual IEEE Symposium on Foundations of Computer Science, pp. 270-280, 1980.

[57] J.E. Savage, "Area-Time Tradeoffs for Matrix Multiplication and Related Problems in VLSI Models," J. of Compu. and Sys. Science, Vol. 20, No. 3, pp. 230-242, March 1981.

[58] R.J. Lipton and R. Sedgewick, "Lower Bounds for VLSI," Proc. 13th Ann. ACM Symposium on Theory of Computing, pp. 300-307, 1981.

[59] J. Vuillemin, "A Combinatorial Limit to the Computing Power of VLSI Circuits," Proc. 21st Annual Symposium on Theory of Computing, pp. 294-300, 1980.

[60] M.A. Bayoumi, G.A. Jullien, and W.C. Miller, "A VLSI Implementation of Memory Intensive Residue Number System Architecture," Proc. 20th Annual Allerton Conf., pp. 150-152, October 1982.

[61] C.A. Mead and L.A. Conway, Introduction to VLSI Systems, Addison Wesley, 1979.

[62] G. Kissin, "Measuring Energy Consumption in VLSI Circuits: A Foundation," Proc. 14th Annual ACM Symposium on the Theory of Computing, pp. 99-104, 1982.

[63] R.P. Brent and L.M. Goldschlager, "Some Area-Time Tradeoffs for VLSI," SIAM J. Computing, Vol. 11, No. 4, pp. 737-747, 1982.

[64] R.P. Brent and H.T. Kung, "The Chip Complexity of Binary Arithmetic," 12th Annual ACM Symposium on Theory of Computing, pp. 190-200, 1980.

[65] R.B. Johnson, "The Complexity of a VLSI Adder," Information Processing Letters, Vol. 11, No. 2, pp. 92-93, 20 October 1980.

[66] R.W. Keyes, "The Evolution of Digital Electronics Towards VLSI," IEEE J. Solid-State Circuits, Vol. SC-14, No. 4, pp. 193-201, April 1979.

[67] M.A. Bayoumi, G.A. Jullien, and W.C. Miller, "A VLSI Model for Residue Number System Architectures," Integration. The VLSI Journal (In Print).

[68] _____, "The Area-Time Complexity of a VLSI Residue Number System Arithmetic Unit," Proc. the 7th Conference on Information Sciences and Systems, pp. 6-9, 1983.

[69] G. Alia, F. Barsi and E. Martinelli, "A Fast VLSI Conversion Between Binary and Residue Systems," Information Processing Letters, Vol. 18, pp. 141-145, 30 March 1984.

[70] M.A. Bayoumi, G.A. Jullien, and W.C. Miller, "Multi Look-Up Table Module for RNS Systems Implementation," Electronic Letters, Vol. 20, No. 2, pp. 94-95, January 1984.

[71] _____, "Models for VLSI Implementation of Residue Number System Arithmetic Modules," Proc. 6th Symposium on Computer Arithmetic, pp. 174-182, Denmark, June 1983.

[72] M. Bayoumi, G.A. Jullien, and W.C. Miller, "RNS Modules for VLSI Implementation of Digital Filters," Proc. the 26th Midwest Symposium on Circuits and Systems, pp. 403-407, August, 1983.

[73] A.M. Mohsen and C.A. Mead, "Delay-Time Optimization for Driving and Sensing of Signals on High-Capacitance Paths of VLSI Systems," IEEE Trans. on Electron Devices, Vol. ED-26, No. 4, pp. 542-548, April 1979.

[74] S. Winograd, "On the Time Required to Perform Addition," J.ACM, Vol. 12, pp. 277-285, 1965.

[75] R.P. Brent, "On the Addition of Binary Numbers," IEEE Trans. on Comp., C-19, pp. 758-759, 1970.

[76] D.J. Kuck, "The Structure of Computers and Computations," Vol. 1, John Wiley & Sons, New York, 1978.

[77] J. Sklansky, "An Evaluation of Several Two Summand Binary Adders," IRE Trans. on Electronic Computers, Vol. 9, No. 2, pp. 213-226, June 1960.

[78] H.T. Kung, A VLSI Keynote Address And Panel Discussion, 1983 ACM Computer Science Conference, February 1983.

[79] M.A. Bayoumi, G.A. Jullien, and W.C. Miller, "An Area-Time Efficient NMOS Adder," Integration, The VLSI Journal, Vol. 1, No. 4, pp. 317-334, 1983.

[80] R.P. Brent and H.T. Kung, "The Chip Complexity of Binary Arithmetic," Proc. 12th Annual ACM Symp. Theory of Comput., pp. 190-200, April 1980.

[81] S. Waser, "State of the Art in High Speed Arithmetic Integrated Circuits," Computer Design, Vol. 17, No. 7, July 1978, pp. 67-75.

[82] R.P. Brent and H.T. Kung, "A Regular Layout for Parallel Adders," IEEE Trans. on Computers, Vol. 31, No. 3, March 1982, pp. 260-264.

[83] K. Hwang, "Computer Arithmetic: Principles, Architecture and Design," New York, Wiley, 1979.

[84] M.A. Bayoumi, G.A. Jullien and W.C. Miller, "A High Speed VLSI Adder," Proc. International Electrical, Electronics Conference, pp. 300-303, Toronto, Septe. 1983.

[85] M.A. Bayoumi, G.A. Jullien, and W.C. Miller, "An Array Implementation of Digital Filters," Proc. 1984 IEEE International Symposium on Circuits and Systems, pp. 1268-1271, May 1984.

[86] A. Peled and B. Liu, "A New Realization of Digital Filters," IEEE Trans. on Acoustics, Speech, and Signal Processing, Vol. ASSP-22, pp. 456-462, Dec. 1974.

[87] M.A. Bayoumi, G.A. Jullien, and W.C. Miller, "A Modular Implementation of Digital Signal Processing Architectures Using RNS," Proc. the 15th Annual Pittsburgh Conference on Modeling and Simulation, April 1984 (in print).

[88] _____ , "A VLSI Implementation of an NTT Multiplier Using RNS for Digital Signal Processing Applications," Proc. 2nd European Signal Processing Conference, pp. 837-841, Sept. 1983.

[89] _____ , "VLSI Implementation of RNS Modules and Their Proposed Applications," Proc. 21st Annual Allerton Conference pp. 1003-1013, October 1983.

[90] E.E. Swartzlander, Jr., "VLSI Technology for Signal Processing," 1978 Government Microcircuit Applications Conference Digest of Papers, Vol. 7, pp. 76-79, 1978.

[91] K.Y. Liu, "Architecture for VLSI Design of Reed-Solomon Decoders," IEEE Trans., Vol. C-33, No. 2, pp. 178-189, February 1984.

[92] H. Deman et al, "High-Speed NMOS Circuits for ROM-Accumulator and Multiplier Type Digital Filters," IEEE Journal of Solid-State Circuits, Vol. SC-13, #5, October 1978.

[93] E.A. Vopni et al, "A CMOS Time-Multiplexed Digital Filter for Vocoder Applications," Canadian Electrical Eng. J., Vol. 7, No. 1, pp. 30-35, 1982.

[94] M.A. Bayoumi, G.A. Jullien, and W.C. Miller, "A Systolic (VLSI) Array Using RNS For Digital Signal Processing Applications," Proceedings of the 1984 ACM Computer Science Conference, pp. 115-120, 1984.

[95] H.T. Kung, "Why Systolic Architectures"? Computer Magazine, Vol. 15, No. 1, pp. 37-46, Jan. 1982.

[96] L.R. Rabiner and B. Gold, Theory and Application of Digital Signal Processing, Prentice-Hall, 1975.

[97] Alan V. Oppenheim, Applications of Digital Signal Processor, Prentice-Hall, 1978.

[98] M.A. Bayoumi, G.A. Jullien, and W.C. Miller, "The Area-Time Complexity of a VLSI Digital Filter Using Residue Number Systems," Computers and Electrical Engineering, (An International Journal), (In print).

[99] M.A. Bayoumi, G.A. Jullien, and W.C. Miller, "A VLSI Implementation of Finite Impulse Response Digital Filters Using Residue Number Systems," Canadian Elect. Eng. J., (In print).

[100] _____, "Bit-Parallel Based Filters Using Residue Number System," Proc. of the 27th Midwest Symposium on Circuits and Systems, June 1984.

[101] Paul L. Mills, "The Design of Bit-Parallel Systolic Filter Algorithms," Proceedings of the 1984 ACM Computer Science Conference, pp. 121-130.

[102] B.S. Landman and R.L. Russo, "On a Pin Versus Block Relationship for Partitions of Logic Graphs," IEEE Trans. on Comp. C-20, pp. 1469-1479, 1971.

[103] R.L. Russo, "On the Tradeoff Between Logic Performances and Circuit-to-Pin Ratio for LSI," IEEE Trans. on Comp. C-21, pp. 147-153, 1972.

[104] K. Hwang and Y.H. Cheng, "VLSI Computing Structures for Solving Large-Scale Linear System of Equations," Proc. 1980 Int. Conf. on Parallel Processing, pp. 217-227, 1980.

[105] H. Jia-Wei and H.T. Kung, "I/O Complexity: The Red-Blue Pebble Game," Proc. of 13th Annual Symposium on the Theory of Computing, pp. 3263-333 , May 1981.

[106] Z.M. Kedem and A. Zorat, "On Relations Between Input and Communication Computation in VLSI," Proc. of 22nd Annual Symp. on the Foundations of Computer Science, pp. 37-44, October 1981.

[107] A. Aggarwal, "On I/O Placement in VLSI Circuits," Proc. of 21st Allerton Conference on Communication, Control, and Computing, pp. 236–245, October 1983.

[108] M.A. Bayoumi, G.A. Jullien, and W.C. Miller, "I/O Strategies for Residue Number System Architectures for Digital Signal Processing Applications," Proc. The 1984 IEEE International Symposium on Circuits and Systems, pp. 1069–1072, May 1984.